REDUCTION OF NO$_x$ AND SO$_2$ EMISSIONS FROM COAL BURNING PULSE COMBUSTORS

Final Report

E. A. Powell
B. T. Zinn
N. Miller
F. Chen

TABLE OF CONTENTS

LIST OF TABLES

LIST OF FIGURES

ABSTRACT

In this investigation, a Rijke pulse combustor was constructed, in which unpulverized coal was burned on a rotating bed where the presence of acoustic velocity oscillations resulted in bed fluidization and intensification of the combustion process. The objectives of this investigation were to determine (1) if the nitrogen oxides emissions of the experimental Rijke pulse combustor could be reduced by air staging the combustion process and (2) if the sulfur dioxide emissions of this pulse combustor could be reduced by the addition of sorbent materials such as limestone to the coal bed or to the gas stream above the bed.

A series of experiments was conducted without air staging or sorbent addition in order to determine the baseline emissions of NO_x and SO_2. A bituminous coal with about 1.5 percent nitrogen and about 1.3 percent sulfur was burned in all of the experiments. Under pulsating combustion conditions at a sound pressure level of about 160 dB and a frequency of about 65 Hz, NO_x emissions (3% oxygen basis) ranged from about 250 ppm for extremely fuel rich combustion ($\alpha = 0.6$) to about 700 ppm for large excess air conditions ($\alpha = 1.5$). Peak SO_2 emissions of about 1400 ppm were measured at about 10 percent excess air, with minimum emissions of about 850 ppm for fuel rich combustion and somewhat less than peak emissions (about 1200 ppm) for large excess air conditions.

Air staging experiments were conducted for total dimensionless air fuel ratios ranging from 1.0 to 1.4 and primary dimensionless air/fuel ratios ranging from 0.6 to 0.9. Injection heights ranged from 20 cm to 52 cm above the coal bed. Air staging was effective in reducing the nitrogen oxides emissions of coal burning Rijke type pulse combustors under the proper conditions. The largest reductions in NO_x emissions were obtained for primary dimensionless air/fuel ratios of about 0.7 with sufficient secondary air injection to yield total dimensionless air/fuel ratios between 1.1 and 1.4. For excess air values less than about 10 percent, air staging resulted in only small reductions in NO_x emissions. The injection point for best NO_x reduction was about 50 cm above the bed. Under optimum conditions, reductions in NO_x emissions of up to 56 percent were obtained.

Another series of experiments was conducted using sorbent addition to reduce sulfur dioxide emissions. In some of these experiments, pulverized dolomitic limestone was introduced along with the coal through the coal delivery tube just above the bed, while in the remainder of the experiments, the sorbent was dispersed in an air stream and injected at 15 cm or 23 cm above the coal bed. For sorbent introduced into the coal feed stream, sulfur dioxide reductions of only about 20 percent were obtained for pulsating combustion with about 20 percent excess air. For these experiments, there was a definite trend of decreasing SO_2 emissions with increases in excess air. Much higher SO_2 reductions were obtained when the sorbent was injected using the air entrainment system. In one experiment, conducted at a Ca/S ratio of 2.4 with sorbent particles having a mean diameter of about 40 μm, an SO_2 reduction of 83 percent was obtained.

INTRODUCTION

This final report summarizes the work accomplished under a research project entitled "Reduction of NO_x and SO_2 Emissions from Coal Burning Pulse Combustors" which was supported under DOE Grant No. DE-FG-88PC88918 during the period September 1, 1988 through August 31, 1990.

This project is a continuation of earlier work done at Georgia Institute of Technology [1] which demonstrated that both bituminous and subbituminous coals can be burned with efficiencies greater than 97 percent in Rijke type pulse combustors with only 10 percent excess air. In a Rijke pulse combustor, unpulverized coal is burned on a bed where the presence of acoustic velocity oscillations results in bed fluidization and intensification in the rates of mass, momentum, and heat transfer processes; phenomena which are apparently responsible for the superior performance of the pulse combustor. However, further studies with this combustor [2] showed that the emissions of nitrogen oxides and sulfur dioxide exceeded allowable emission standards. This project was, therefore, concerned with the reduction of sulfur dioxide and nitrogen oxides emissions from Rijke type coal burning pulse combustors by sorbent addition and combustion staging.

The first objective of this investigation was to determine if the nitrogen oxides emissions of an experimental Rijke pulse combustor could be reduced by air staging the combustion process. Most of the NO_x produced in coal combustors originates from the coal bound nitrogen, thus the control of this source of NO_x offers the greatest possibilities for NO_x reduction during coal combustion. Investigations of steady state coal burners have shown that staging the combustion process offers the greatest potential for NO_x reduction in coal combustors. In one form of combustion staging, known as air staging, the coal is burned in the first stage under fuel rich (gasification) conditions. In the absence of sufficient oxygen, the unstable nitrogen compounds released from the coal in the first stage (HCN and NH_3)

1

convert to harmless N_2 rather than NO_x. The fuel gases generated in the first stage are burned in the second stage with the secondary air which is introduced into the combustor downstream of the first stage. To reduce thermal NO_x generation in the second stage, it is desirable to operate the second stage at low temperatures and with the minimum amount of secondary air which will result in acceptable performance and low NO_x formation. Reduction of NO_x production in steady state coal burners is discussed in detail in Refs. [3], [4] and [5]. Reduction of NO_x in coal burning pulse combustors by means of combustion staging has not been previously investigated.

The second objective of this investigation was to determine if the sulfur dioxide emissions could be reduced by adding sorbent materials such as limestone or dolomite to the acoustically fluidized bed or to the flow of combustion gases above the bed. It is well known that combustion of a high sulfur coal in a fluidized bed of sorbent particles reduces SO_2 emissions. Naturally occurring limestone ($CaCO_3$) and dolomite ($CaCO_3:MgCO_3$) have been found to be good sorbents, with the former being better suited for atmospheric pressure fluidized beds and the latter more suited to pressurized fluidized beds. In atmospheric pressure fluidized beds, the limestone is first calcined in the endothermic reaction:

$$CaCO_3 = CaO + CO_2$$

which readily occurs at temperatures well below the bed temperature. The calcined limestone then reacts with the sulfur dioxide in the following reaction:

$$2CaO + 2SO_2 + O_2 = 2CaSO_4$$
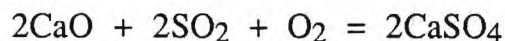
The calcination step has been found to result in a porous sorbent particle structure, which creates a large internal surface area which increases the rate of sulfation. The reaction product $CaSO_4$, obtained in the sulfation reaction, is bulkier that the reactant CaO, and it tends to choke the porous structure inhibiting further sulfation.

Consequently, the sorbent utilization is limited, thereby requiring excessively large quantities of sorbents to achieve compliance with national emission standards. Extensive studies at Argonne National Laboratory in the U. S. [6] and at CRE and BCURA in the U. K. [7] have examined in considerable detail the effect of various operating parameters and variables on the sulfation process.

The following work will be described in this report: (1) design, fabrication and assembly of the Rijke tube pulse combustor and the auxiliary systems, (2) baseline experiments to determine the NO_x and SO_2 emissions in the absence of sorbent addition or combustion staging, (3) air staging experiments to determine the effectiveness of substoichiometric primary coal combustion followed by secondary air injection above the bed in reducing the NO_x emissions, (4) non-pulsating experiments to determine the effect of pulsations on the NO_x emissions, and (5) sorbent addition experiments to determine the effectiveness of limestone or dolomite addition in reducing the SO_2 emissions. Finally a summary of the experimental results obtained under this project and the major conclusions will be given.

EXPERIMENTAL APPARATUS

RIJKE TUBE COAL COMBUSTOR

The Rijke pulse combustor basically consists of a vertical steel tube which is open at the upper end and connected to an acoustic decoupler at the lower end. The coal bed is located one quarter of the distance from the upstream (lower) end of the tube to the downstream (upper) end. The combustion process interacting with the mean flow through the tube excites the fundamental acoustic mode for an open-ended tube. For this mode the pressure oscillations are a maximum at the middle of the tube, while the acoustic velocity oscillations are a maximum at the ends of the tube. The open-ended boundary condition requires the pressure perturbations to be zero at the ends of the tube. The acoustic decoupler at the lower end is a section of pipe with a much greater cross-sectional area than the

Rijke tube itself. This preserves the open-ended boundary condition, while allowing control of the air flow through the combustor. The basic Rijke tube geometry along with the fundamental mode pressure and velocity profiles are shown in Figure 1.

The Rijke tube coal combustor was designed to allow operation at two different pulsation frequencies by changing the length of the tube, while maintaining the combustion at the quarter-length point. This was accomplished by means of a vertical insulated pipe section 183 cm long, which contains the coal bed, to which various horizontal pipe sections can be added. The two configurations are shown in Figure 2. In the short configuration, which has a total length of 3.05 m, a vertical section of uninsulated pipe is connected to the top of the insulated section. The bottom of the insulated section is connected to the decoupler by means of an elbow and a short horizontal pipe section. In the long configuration, which has a total length of 6.10 m, two additional lengths of horizontal pipe are added. At the bottom (decoupler) end of the system, a 76-cm pipe section is inserted between the elbow and the short pipe section connected to the decoupler. At the top (exhaust) end, the vertical pipe is replaced by an elbow and a 1.93 m horizontal section of pipe leading to the exhaust. In both configurations, the coal bed is located 12.7 cm above the lower end of the vertical insulated pipe section.

The Rijke tube pulse combustor in the short configuration is shown in more detail in Figure 3 along with the primary and secondary air supplies, the coal feed system, and the sorbent feed system. The vertical insulated combustion section of the Rijke tube is made from 25.4 cm I. D. carbon steel pipe lined with 5 cm thickness of a castable ceramic insulation (Babcock and Wilcox Kaocrete HDHS 98 RFT) leaving a central bore diameter of 15 cm. This section is provided with three quartz viewing windows and is instrumented with several chromel-alumel (Type K) thermocouples and a piezoelectric pressure transducer at the middle of the combustor. A gas sampling port is located in the exhaust section attached to the upper end of the combustion section. Coal is fed continuously into the

Amplitude Distributions
along the Combustor

p' ~ Acoustic Pressure
u' ~ Acoustic Velocity
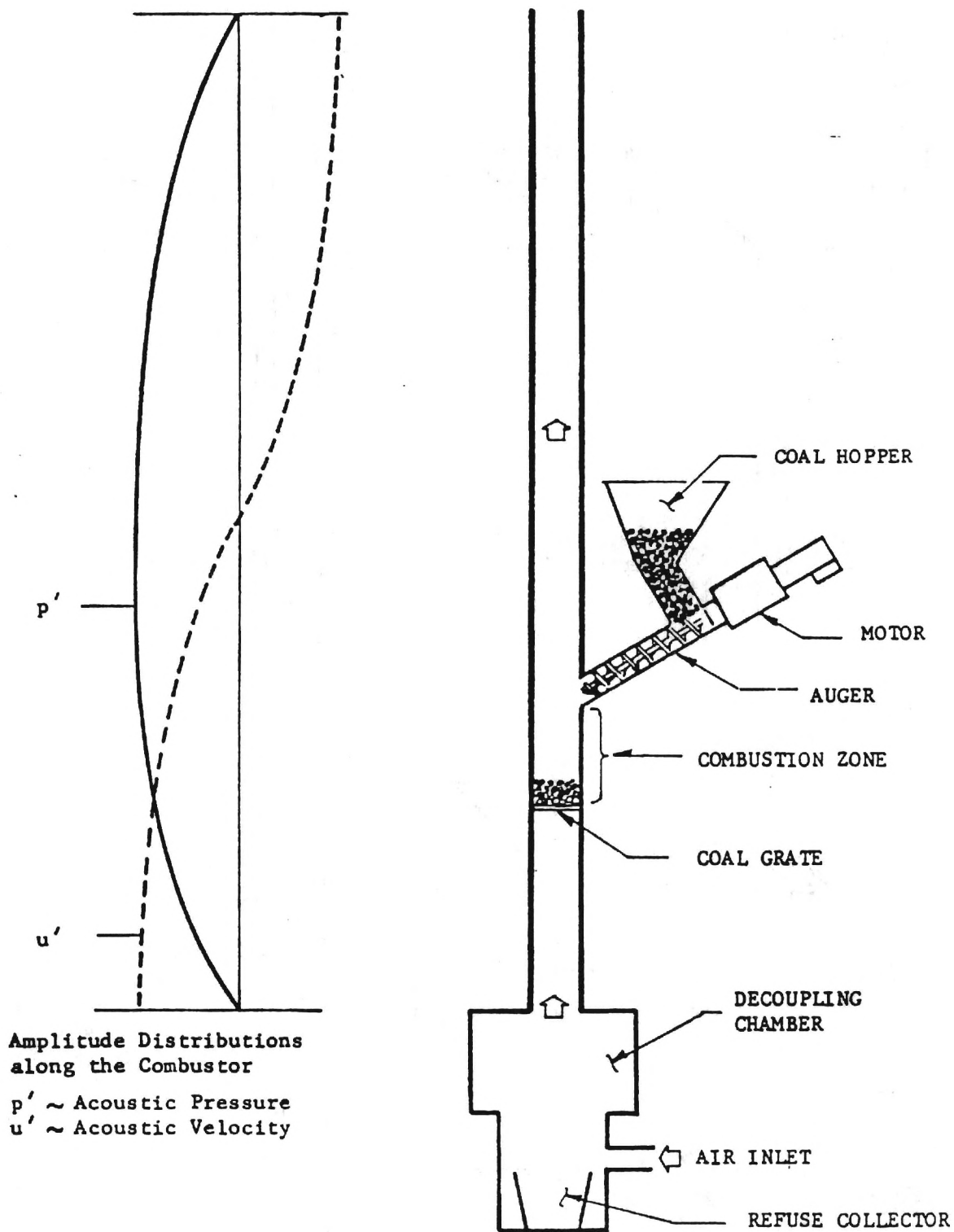
Figure 1. A Schematic of the Coal Burning Rijke Tube
Pulsating Combustor Developed at Georgia
Tech and Its Acoustic Wave Structure.

Upper Horizontal Extension
for Long Configuration
193 cm

Exhaust
Section
for Short
Configuration
58 cm

Insulated Combustion
Section, 183 cm

Decoupler for
Long Configuration

Decoupler for
Short
Configuration

Coal Bed

Lower Adapter
Elbow

Decoupler Pipe
18 cm

Decoupler Extension for
Long Configuration, 76 cm
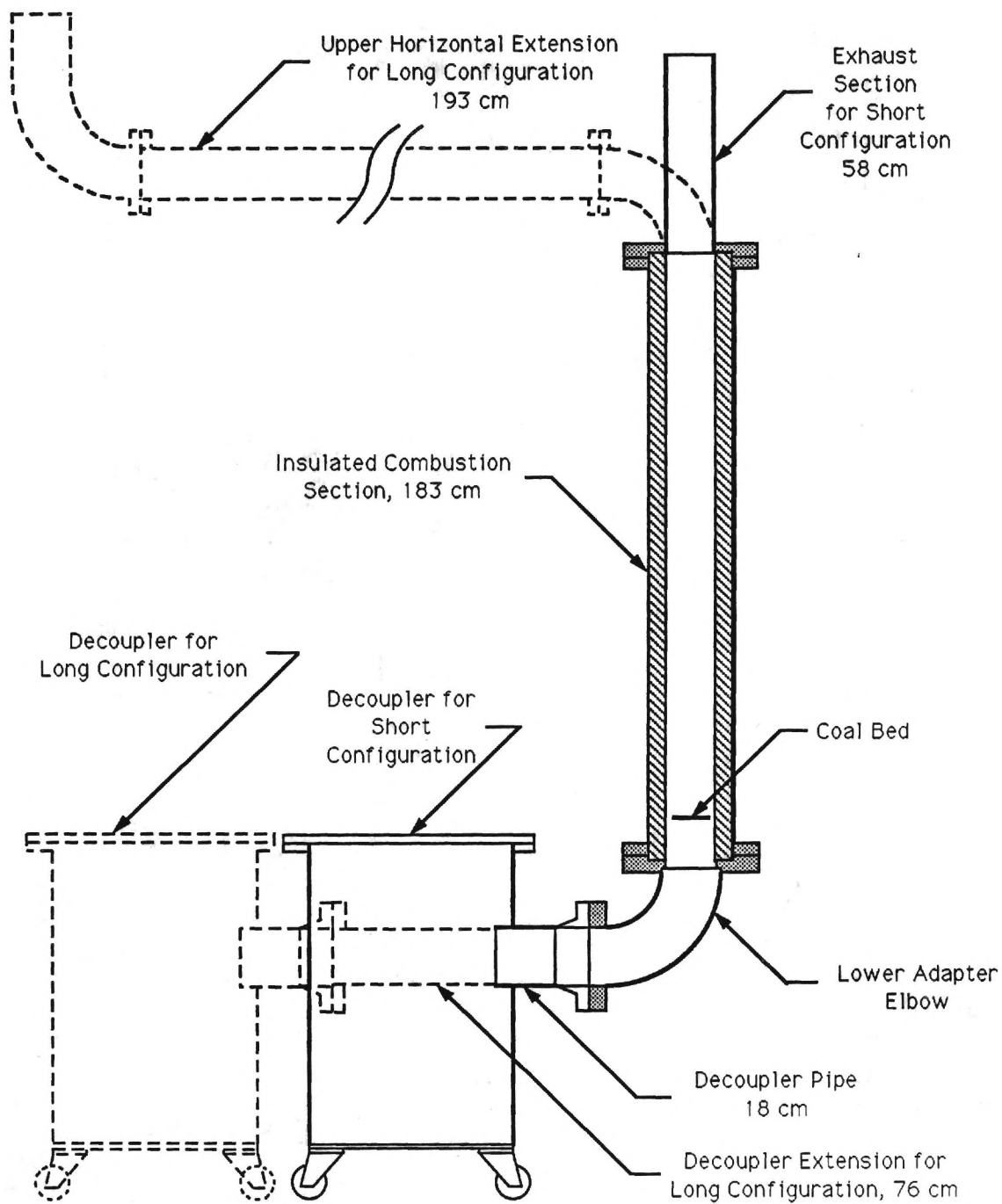
Figure 2. Rijke Pulse Combustor Configurations
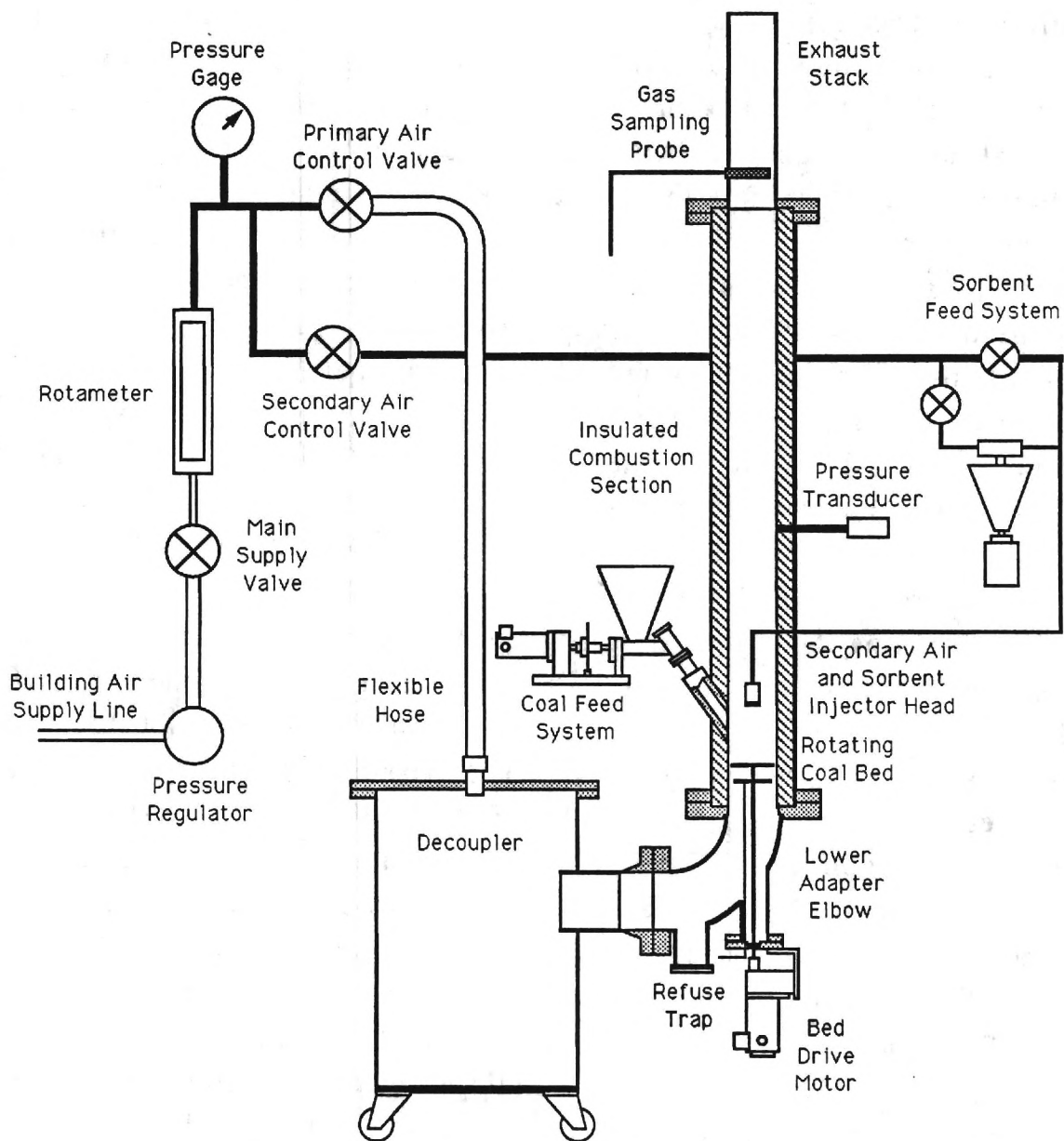
Figure 3. Rijke Pulse Combustor and Auxiliary Systems

combustion tube by a motor driven auger supplied by a hopper. The coal is supported by a motor driven rotating bed, which gives uniform distribution of coal on the bed. Bed rotation also grinds the ash particles down to sufficiently small sizes that they can continuously fall through the bed grid, thus preventing accumulation of coal and ash on the bed. During combustor operation, ash and unburned coal which fall through the bed accumulate in a refuse trap at the bottom of the lower adapter elbow which can be emptied periodically. The primary combustion air enters the combustor from the decoupler and passes vertically through the coal bed. The coal is ignited by a propane burner located just below the bed. For combustion staging experiments, a secondary air system delivers air through a radial injector located at the axis of the combustor above the bed. The injector height above the bed can be varied.

The rotating bed assembly is shown in Figure 4. The support for the rotating bed grid is a spoked wheel fabricated from carbon steel which fits closely within a stationary ring of the same material. The ring is attached to the refractory lining of the combustor and provides a seal preventing air from bypassing the bed around its periphery. The bed grid is made of #6 mesh stainless steel grid which will retain coal particles larger than about 3 mm in diameter. The bed grid is spot welded to the rotating support wheel. The support wheel is connected by two screws to a 65 cm long 1.2 cm diameter shaft which passes through two ball bearings at the lower end. The bearings are supported by a bearing house flange which is attached to the flanged pipe extending downward from the lower adapter elbow. The rotating bed is driven by a variable-speed DC geared motor.

A detailed view of one of the observation windows is shown in Figure 5. The three quartz windows measure 30.5 cm long by 6.4 cm wide by 1.9 cm thick. These are located at the bed level, the center, and the upper end of the combustion section. About a third of the length of the bed level window extends below the bed to allow viewing the ignition/preheating system and the underside of the bed
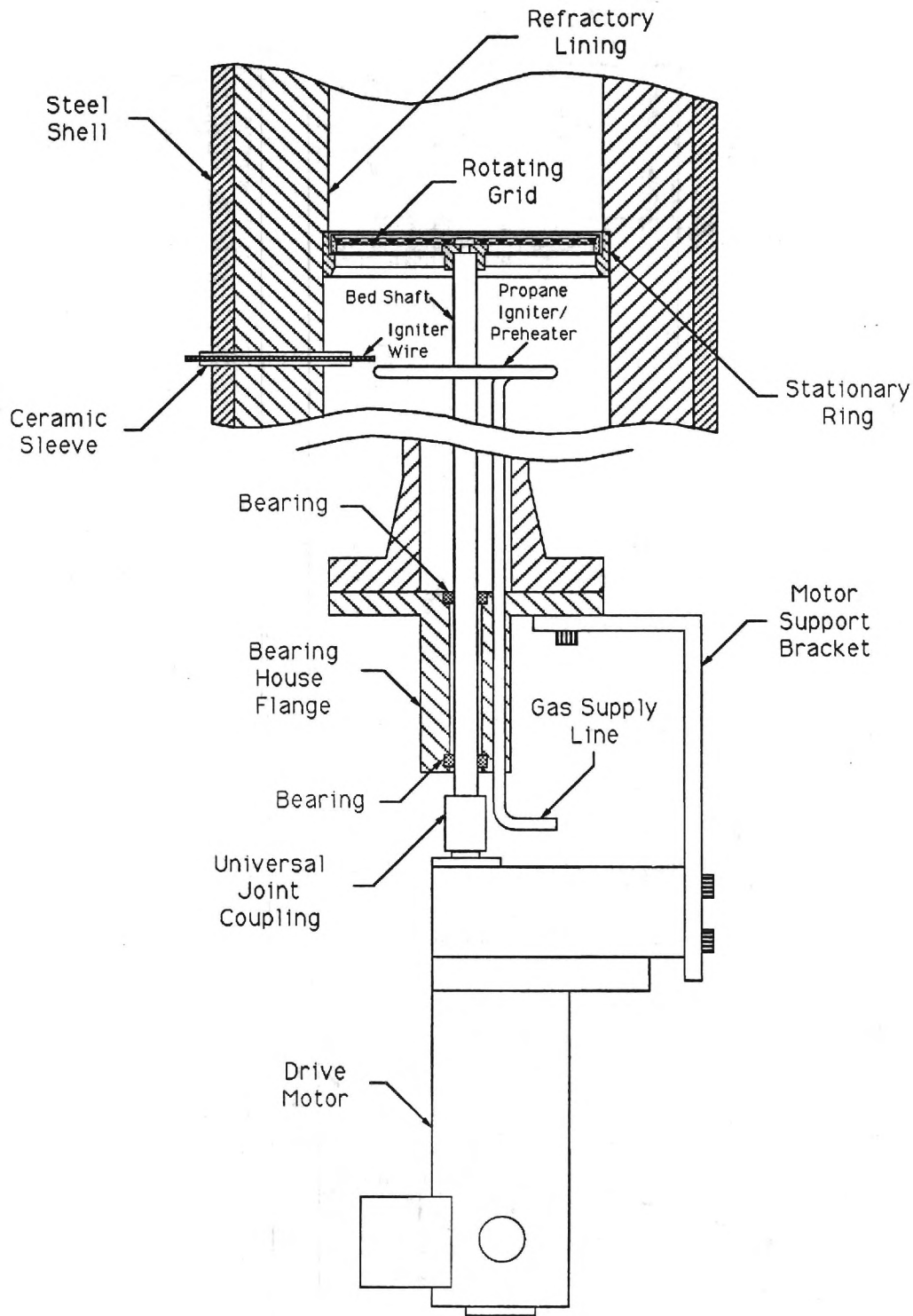
Figure 4.   Rotating Bed Assembly.
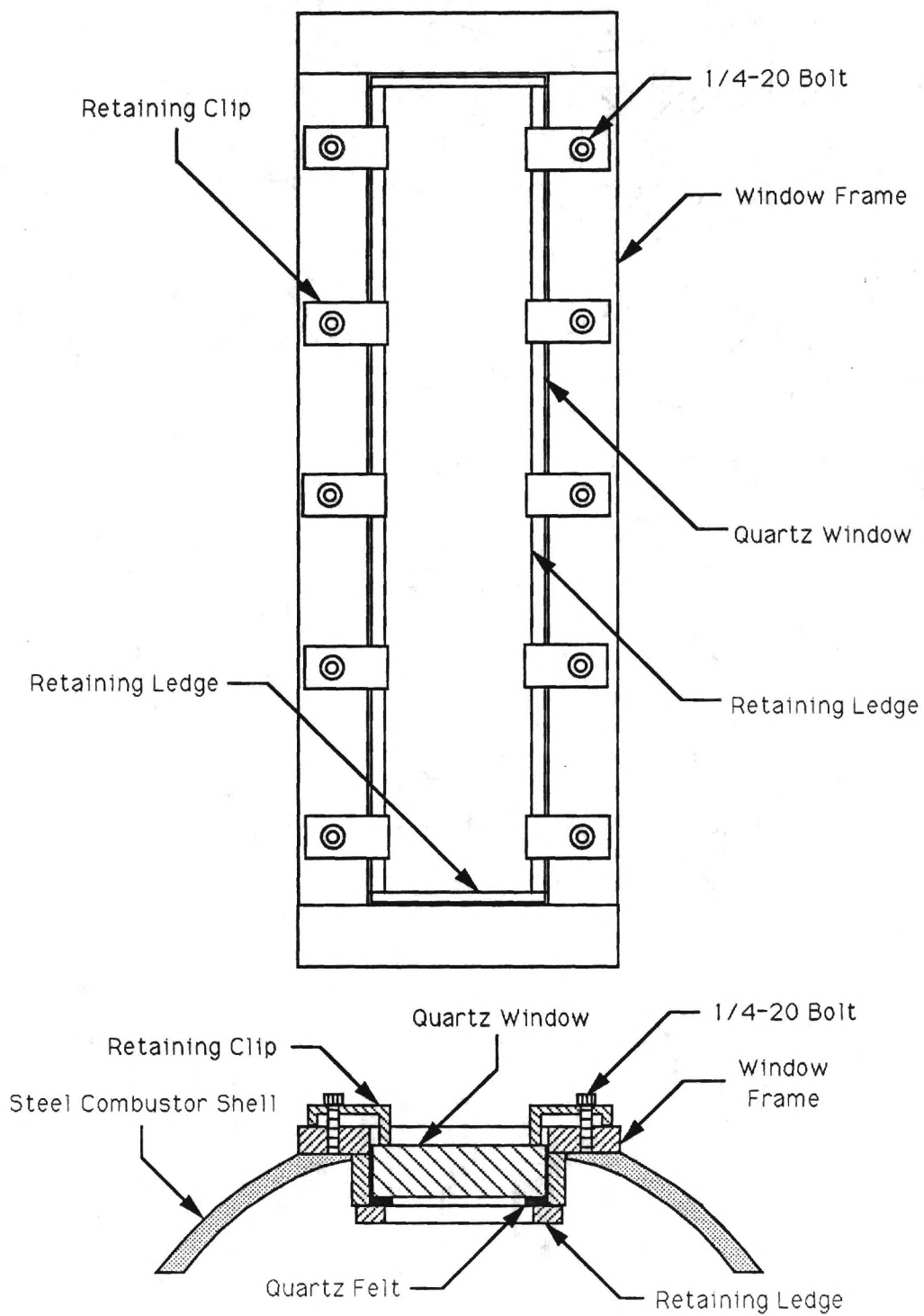
Figure 5. Combustor Observation Window

during combustor operation. Each window is seated in a stainless steel frame which was welded into a hole cut in the steel combustor shell. Quartz felt strips were installed around the perimeter of each window frame and cemented in place using a high temperature RTV compound. These provide a buffer between the quartz window and the steel window frame and serve as a seal against gas leaks. Each window is held in place using ten bolt-mounted clips. The bed level window required special provisions to close the gap between the forward edge of the coal bed and the inner surface of the quartz window. This was necessary to prevent air from bypassing the bed and to prevent coal and ash particles from falling through this gap. A removable ceramic block mounted on a horizontal stainless steel plate was fabricated to fit in the gap between the bed and the window. This block is supported by two notches in the vertical edges of the window frame.

AIR SUPPLY SYSTEM

The air supply system is shown in Figure 3. This system supplies the main combustion air and also auxiliary air for either the sorbent injection system or the secondary combustion air. Air from the 850 kPa building air supply passes through a pressure regulator set at 340 kPa to a 3.8 cm diameter flexible hose (rated at 1030 kPa) which is connected to a control valve on the control panel. The flowrate into the combustor is controlled and monitored by means of a rotameter. The air pressure is measured just downstream of the rotameter. The line from the rotameter is split into primary and secondary lines, each with a control valve. The primary line is connected to the decoupler by a 3.8 cm diameter flexible hose. The secondary air passes through 0.95 cm diameter copper tubing to a port in the combustor wall located a short distance above the desired secondary air injection point. A sidebranch in the secondary air line contains the sorbent feed and entrainment system. Within the combustion section, a length of 0.95 cm diameter stainless steel tubing leads downward from the port in the combustor wall to the injector head on the combustor axis. The injector head, which is used

11

for both secondary air injection and sorbent injection, is described in detail in the discussion of the sorbent feed system.

IGNITION/PREHEATING SYSTEM

The ignition/preheating system is shown in Figures 4 and 6. Propane from a supply tank flows through 1.27 cm diameter copper tubing to a shut-off valve on the control panel (Figure 6). This is followed by a solenoid valve, a control valve, and a rotameter. The solenoid valve is controlled by an ultraviolet flame detector mounted outside the lower combustor window. The solenoid valve automatically shuts off the flow of propane to the combustor if the flame detector does not sense a flame in the combustor. An "override" system allows the solenoid valve to be opened, independently of the flame detector, to permit igniting the burner. The control valve is used to adjust the propane flow rate as measured by the rotameter. The propane then flows through a 0.64 cm diameter copper line which is connected to the stainless steel burner ring located below the coal bed (Figure 4). The burner ring is shown in detail in Figure 7. The propane burns as a diffusion flame in the air stream supplied to the combustor. The air/fuel ratio is controlled by adjusting the air and propane flow rates to the combustor. The gas is ignited by a spark ignition system using a 10 kV AC power supply. The switches controlling the spark ignition system are located on the main control panel.

COAL FEED SYSTEM

The coal feed system is shown in Figure 8. A horizontal auger 18 cm long and 3.8 cm in diameter delivers the coal from a hopper into an inclined water-cooled coal delivery tube leading into the combustor above the bed. The variable speed drive motor is coupled to the auger shaft by a universal joint in order to prevent problems due to any slight misalignment of the motor shaft and the auger shaft. The rectangular base of the hopper was welded directly to the auger tube with its long axis parallel to the axis of the auger. To

Flame
Detector
Electronics

Rotameter

Solenoid
Valve

Control Valve

Shut-Off
Valve

Natural Gas or
Propane Supply

Spark
Electrode

UV Flame
Detector

Quartz Window

Burner
Ring

Igniter Wire

Switch

10 KV

Spark Igniter
Power Supply
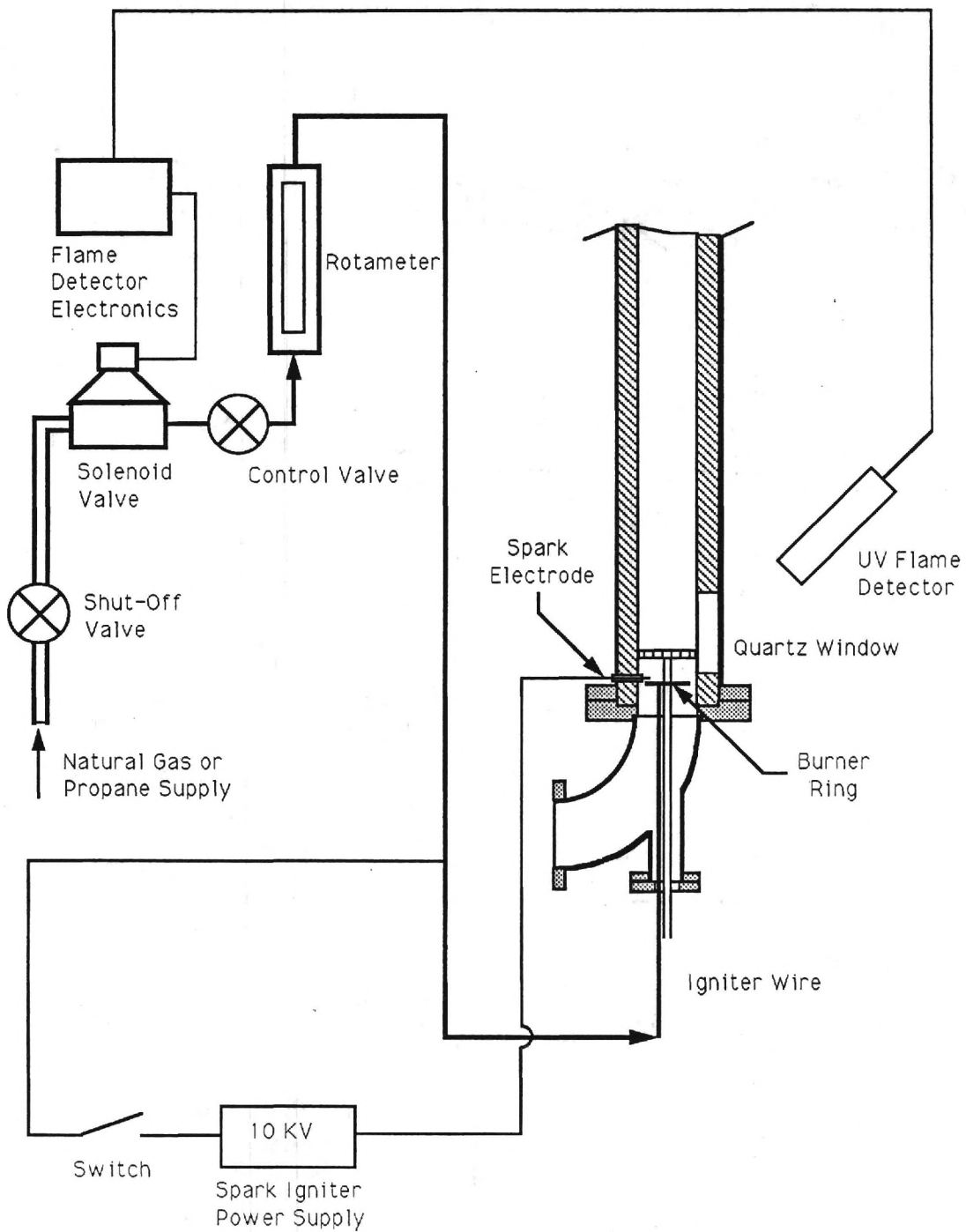
Figure 6. Rijke Combustor Ignition/Preheating System

1.6 mm Diameter
Holes approximately
12.5 mm apart

6.4 mm O.D.
Stainless Steel
Tubing

10 cm
Diameter
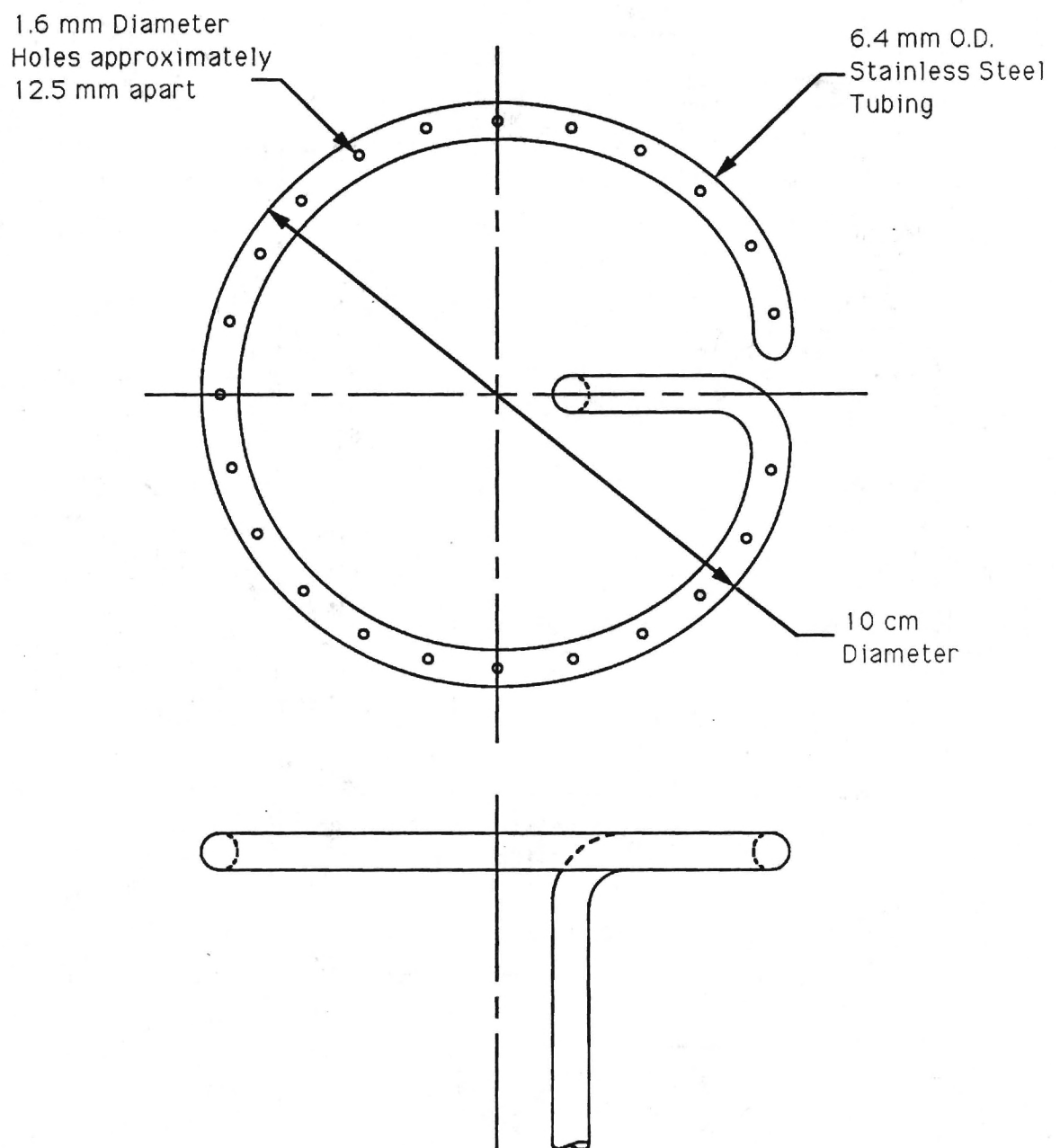
Figure 7. Igniter - Preheater Ring

14
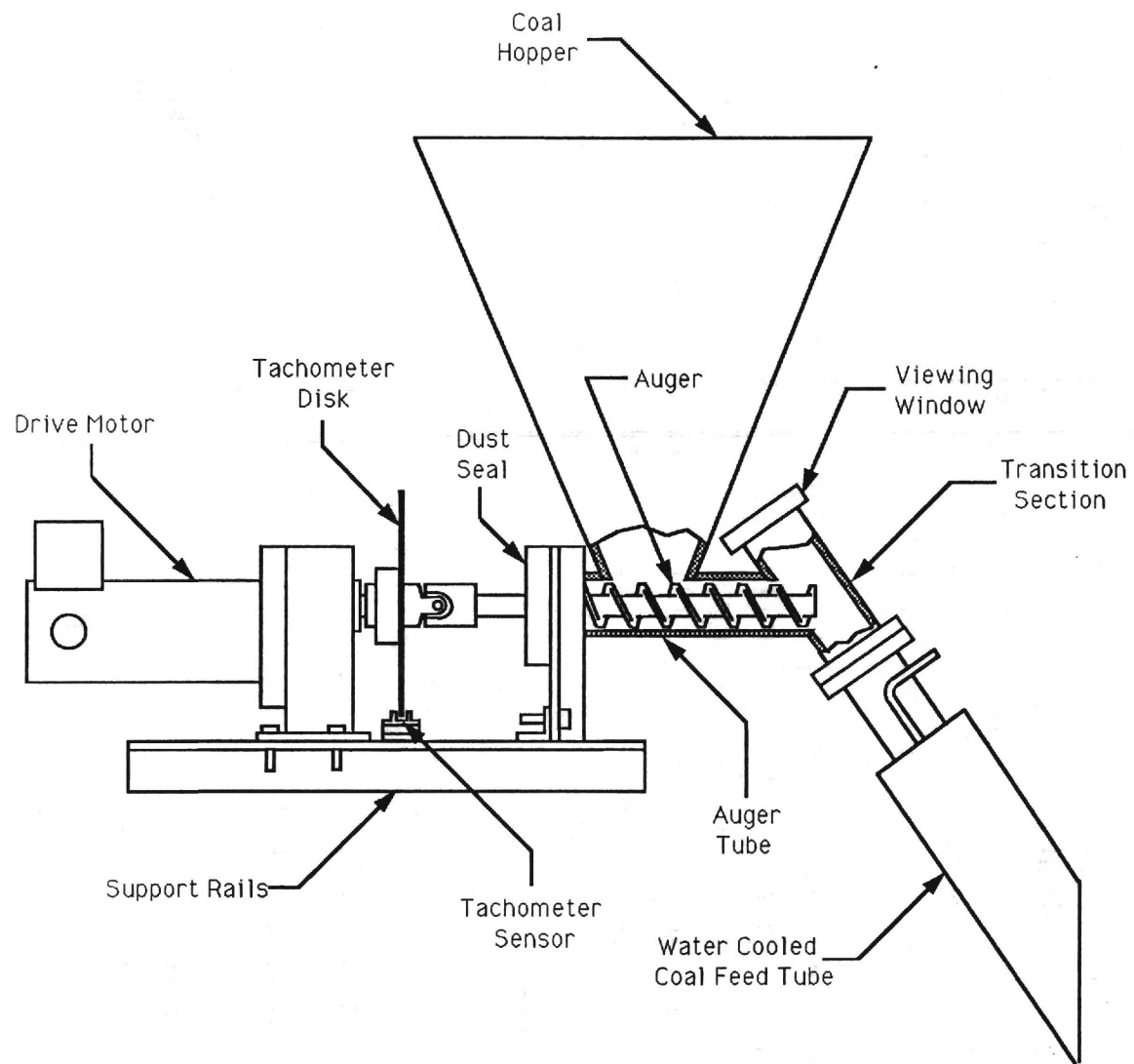
Figure 8.   Horizontal Coal Feed Auger.

facilitate disassembly, the auger tube was welded to a short flanged section of pipe which was then bolted to the coal delivery tube.

An opto-electronic tachometer was installed on the coal feed system in order to obtain instantaneous auger speed (RPM) measurements needed to determine the coal feed rate. A slotted disk was attached to the auger shaft such that it passes between a LED light source and a photodiode as shown in Figure 9. As the wheel rotates, it periodically interrupts the light beam giving a pulsed output which is read by a frequency meter. The disk has 60 slots, thus the frequency reading in Hz yields the auger speed directly in RPM. The maximum speed of the coal feed auger is about 20 RPM.

The inner pipe of the inclined coal delivery tube is the same diameter as the auger tube (4.25 cm I.D.), and the outer pipe forming the water jacket has an inside diameter of 6.32 cm. Water enters the cooling jacket through a 6.4 mm O.D. stainless steel tube extending nearly to the lowest (and hottest) end of the annular water cavity and exits through another stainless steel tube near the top on the opposite side. The water cooling is needed primarily to prevent the coal from sticking to the inside of the delivery tube and eventually blocking the tube. The coal delivery tube was also provided with a viewing window at its upper end to facilitate the determination of the cause of any failure of the auger to feed properly.

SORBENT FEED SYSTEM

The sorbent feed assembly consists of a drive motor, hopper and auger mounted on rails as shown in Figure 10, a sorbent entrainment venturi shown in Figure 11, and a sorbent injection nozzle shown in Figure 12.

In earlier sorbent feed system designs, two difficulties were encountered. First, after filling the hopper with limestone, the auger would feed for only about a minute before a cavity formed in the limestone around the entrance to the auger. This phenomenon,

16

Split Slotted Disk

Auger Shaft

Split Hub

Auger Shaft

Split Hub

Mounting Bracket

Optical Sensor

Slotted Disk

LED Source

Photodiode

Mounting Bracket

17
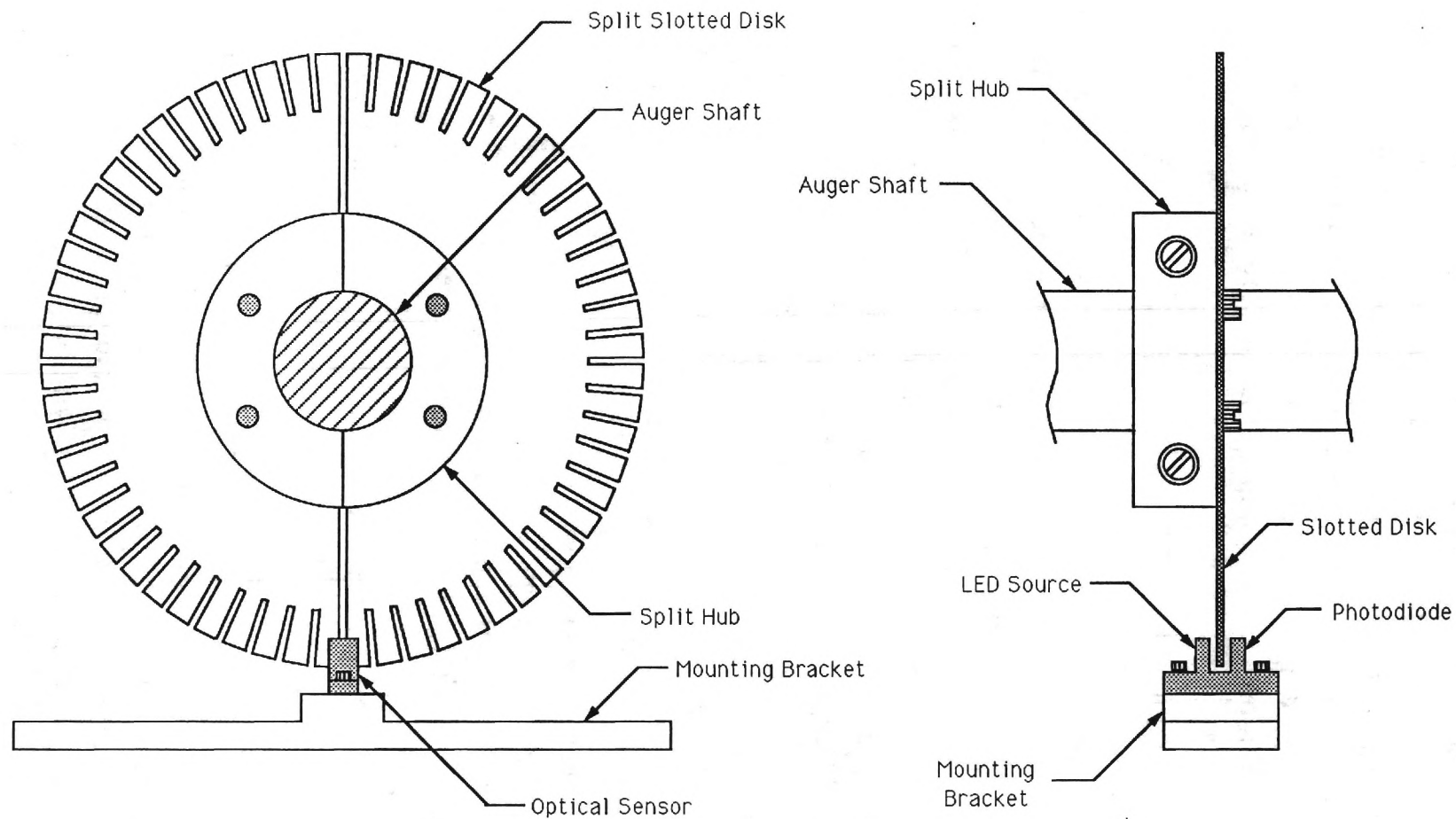
Figure 9. Opto-electronic Tachometer for Coal Feed Auger.

referred to as "bridging" or "rat-holing", is commonly encountered when attempting to transport finely pulverized materials. The second problem was that at the required air flow rates the pressure at the venturi throat was greater than atmospheric, resulting in air "blowback" through the auger and out through the hopper. Of course during blowback conditions, it was impossible to feed limestone into the venturi.

In order to overcome the "bridging" problem, the vertical auger configuration originally used was abandoned in favor of the horizontal auger configuration shown in Figure 10. Thus gravity would be more effective in maintaining flow to the auger and preventing bridging. However, tests with the horizontal auger revealed that bridging was still a serious problem. Since it is well known that mechanical vibration of similar feed systems may alleviate "bridging", a motor driven vibrator was mounted on one side of the sorbent hopper. The feed system was itself mounted on a separate stand so it is free to vibrate and to eliminate transmission of vibrations to the combustor and other components. This arrangement was found to successfully eliminate "bridging" and allow feeding of the pulverized sorbent material at a uniform rate.

The sorbent entrainment "venturi" shown in Figure 11 serves principally as a transition from circular cross-section tubing to a rectangular cross-section entrainment section and back to circular tubing again. The rectangular cross-section was needed in order to give a flush fit with the exit end of the auger. After encountering the blowback problem, it was discovered that the venturi throat area was too large, resulting in a throat pressure nearly equal to the pressure at the exit of the venturi, which was greater than atmospheric pressure due to downstream friction losses. (The pressure at the limestone injector orifice must be atmospheric for subsonic flow.) Thus the venturi was designed to have a variable throat area. To prevent the possibility of clogging, the minimum allowable throat height is about 0.8 mm with a width of 12.7 mm. Tests indicated that reducing the throat area reduced the throat pressure to below atmospheric pressure in the absence of sorbent

18
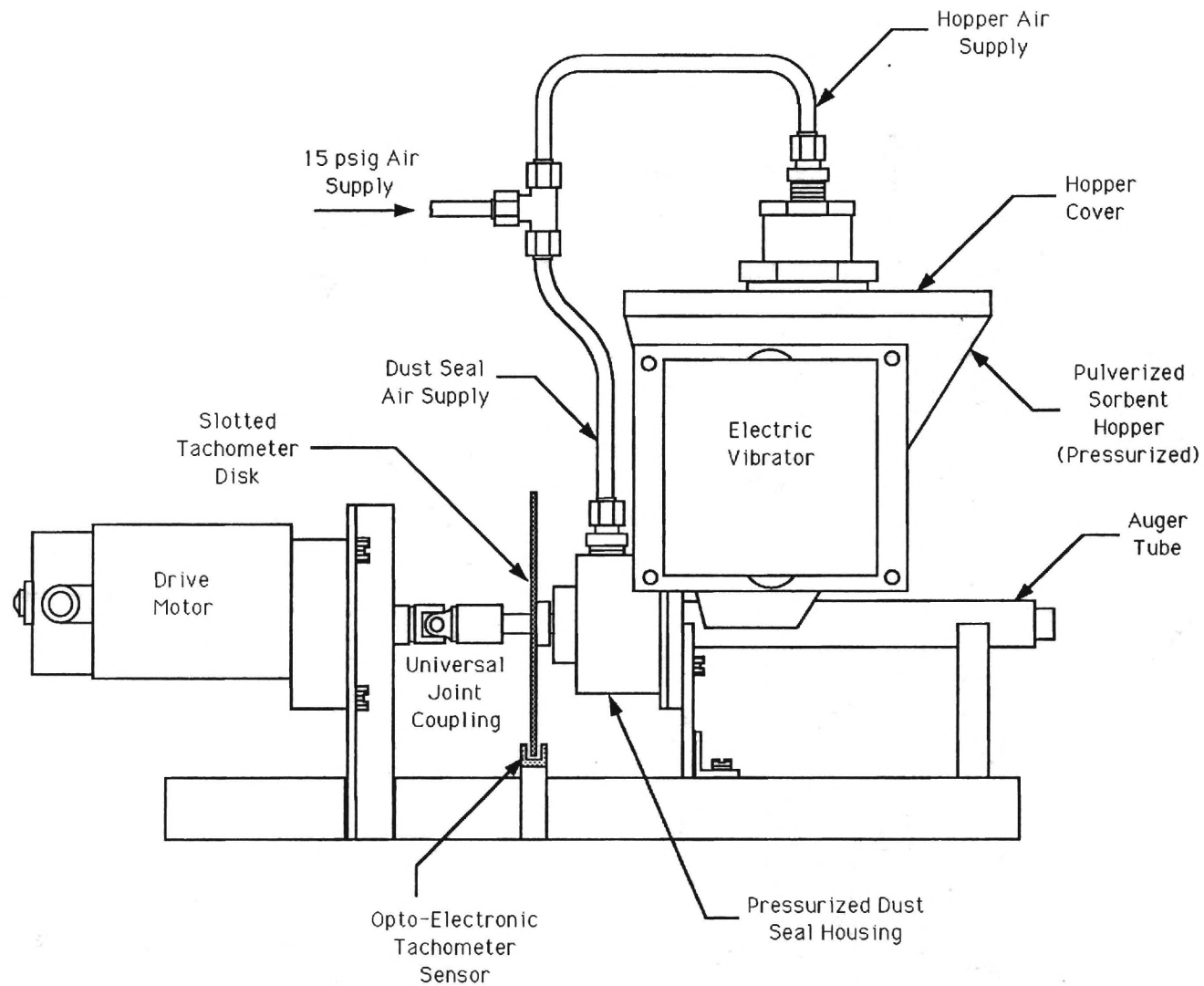
Figure 10. Modified Sorbent Feed System.
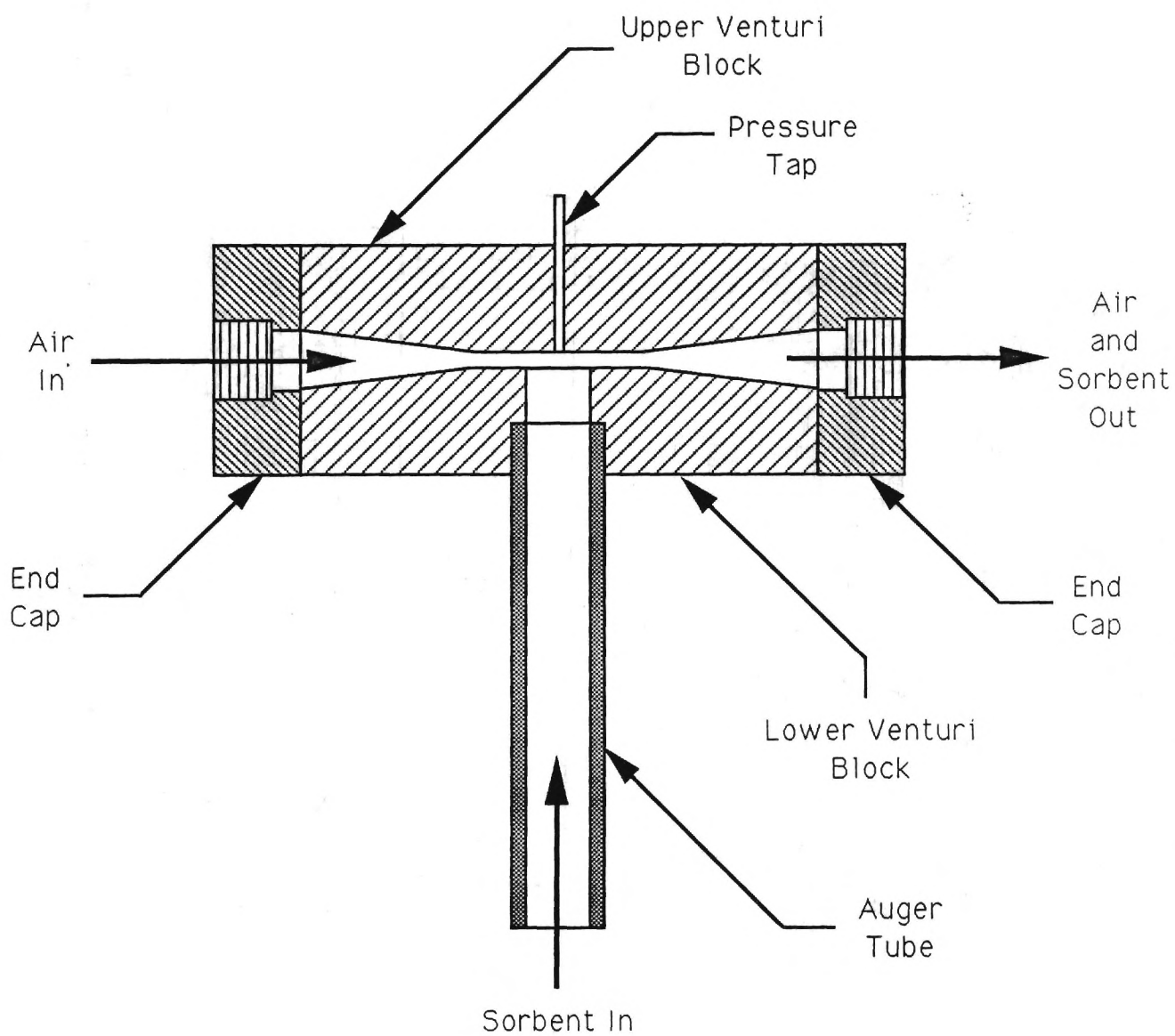
Figure 11. Pulverized Sorbent Entrainment Venturi.

20

material, but the throat pressure became greater than atmospheric pressure when sorbent was introduced into the venturi. This increased pressure, which again resulted in blowback through the auger and hopper, was due to the increased downstream resistance caused by the presence of the sorbent particles. To prevent blowback the hopper was modified so that it could be pressurized (Figure 10). A steel cover plate was welded to the top of the hopper. A threaded pipe connection allows filling of the hopper with pulverized sorbent, after which an air supply line is connected. A dust seal bearing at the base of the auger prevents dust blowback into the laboratory when the hopper is pressurized. Subsequent tests revealed that the blowback problem was successfully eliminated.

A tachometer system was also installed on the sorbent feed auger shaft to determine the instantaneous rotational speed of the auger which is needed in order to accurately measure the sorbent feed rate into the combustor. This tachometer is similar to the one installed on the coal feed system (Figure 10). A bracket mounted on the support rails holds an opto-electronic sensor whose signal is sent to the same electronic pulse counter used for the coal feed system.

A detail of the sorbent injector head is shown in Figure 12. The injector head consists of a conical nozzle section with a conical centerbody. This directs the axial flow in the delivery tube radially outwards into the combustion gases. The exit gap can be adjusted in order to obtain the optimum injection velocity for dispersing the sorbent particles over the cross-section of the Rijke tube.

INSTRUMENTATION

Eight thermocouples were installed to measure gas temperatures on the axis of the combustor at several distances above the coal bed. All thermocouples used were Type K (chromel-alumel) with 1.6 mm diameter Inconel sheaths. The thermocouples were connected to a multichannel sequential switching device which was connected to a digital temperature readout. The thermocouple

Air and Limestone

3/8" Stainless
Steel Tubing

Conical Nozzle
Section

Radial
Injection

Radial
Injection

30 Degree Conical
Centerbody
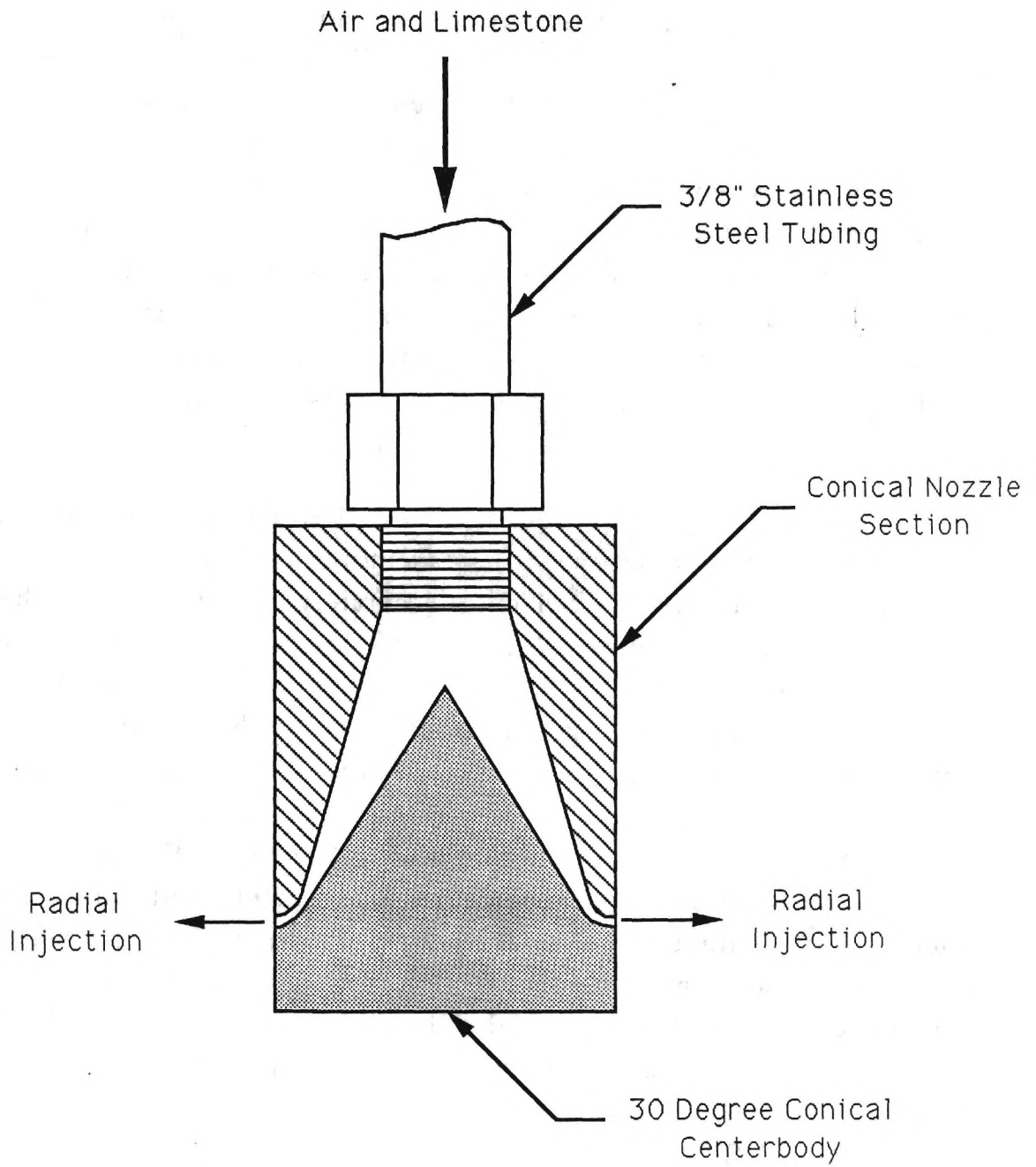
Figure 12.   Limestone Injector Head

22

voltages were also input to the computerized A/D data analysis system.

A low impedance piezoelectric pressure transducer (Kistler Model 211B5) was installed in the combustor to measure the dynamic pressure amplitude or sound pressure level during pulsating operation. The transducer was installed at the middle level where the pressure amplitude is the greatest. To protect the transducer from the high temperature environment, the transducer was located in the side branch of a tee fitting connected to the combustor by a length of 0.64 cm diameter stainless steel tubing. The opposite end of the tee was connected to a 10 m long coiled section of soft plastic tubing to prevent acoustic resonances from occurring in the stainless steel tubing (i. e., by damping out reflections from the open end). The acoustic losses in the stainless steel tubing were determined to be about 2 dB, which were taken into account in the transducer calibration procedures. The output from the transducer was amplified and measured on a voltmeter and frequency counter for determination of the amplitude and frequency of the pressure oscillations, respectively. The transducer output was displayed on an oscilloscope for general observation of the wave shape. A DC voltage signal proportional to the RMS amplitude of the transducer output was also generated and used as input to the computerized data acquisition system.

GAS ANALYSIS SYSTEM

During combustor operation the sampled exhaust gases are transferred through a heated stainless steel tube to the gas analyzer system. The concentrations of five chemical species in the exhaust gases are determined by the analyzer. The concentrations of carbon dioxide, carbon monoxide, and sulfur dioxide are determined by means of nondispersive infrared analyzers. A paramagnetic analyzer is used to determine the oxygen concentration, while the concentration of nitrogen oxides is determined by a chemiluminescent analyzer.

23

BASELINE EXPERIMENTS

EXPERIMENTAL PROCEDURE

A series of baseline experiments was conducted to determine the performance of the Rijke pulse combustor in the short configuration (3.05 m length) without combustion staging or sorbent addition. For these experiments the coal feed rate was 75 g/min and air/fuel ratios ranged from 0.6 to 1.5. These experiments were conducted according to the following procedure. Beginning with an empty bed, the combustor was preheated with propane for about five minutes under non-pulsating conditions. During the preheat phase, the propane flow rate was about 25 standard liters/min (SLM) and the air flow rate was about 1020 SLM. Next the bed rotation and coal feed were started while continuing to preheat with propane. After about two minutes, the coal was burning under non-pulsating conditions, and the primary air flow was adjusted for the desired air/fuel ratio and the propane was shut off. Immediately, pulsating operation began with pressure amplitudes of about 160 dB and a frequency of about 65 Hz. Oscilloscope traces of the acoustic pressure showed sinusoidal waveforms with little or no harmonic distortion. Pulsating operation was usually maintained for periods ranging from 15 to 25 minutes, but longer operating times were possible.

The onset of pulsating combustion is readily apparent from observations through the viewing windows. The flame height decreases drastically, the coal bed becomes fluidized and agitated by the acoustic velocity, and the intensity of the combustion increases as evidenced by the increased brightness of the combustion zone. A full view of the Rijke pulse combustor during a typical pulsating combustion experiment is shown in Figure 13. The three viewing windows in the vertical insulated combustion section are shown, where the lower window appears very bright due to the intense combustion zone extending above the coal bed. The coal feed system is to the left of the combustion section, while the decoupler is behind
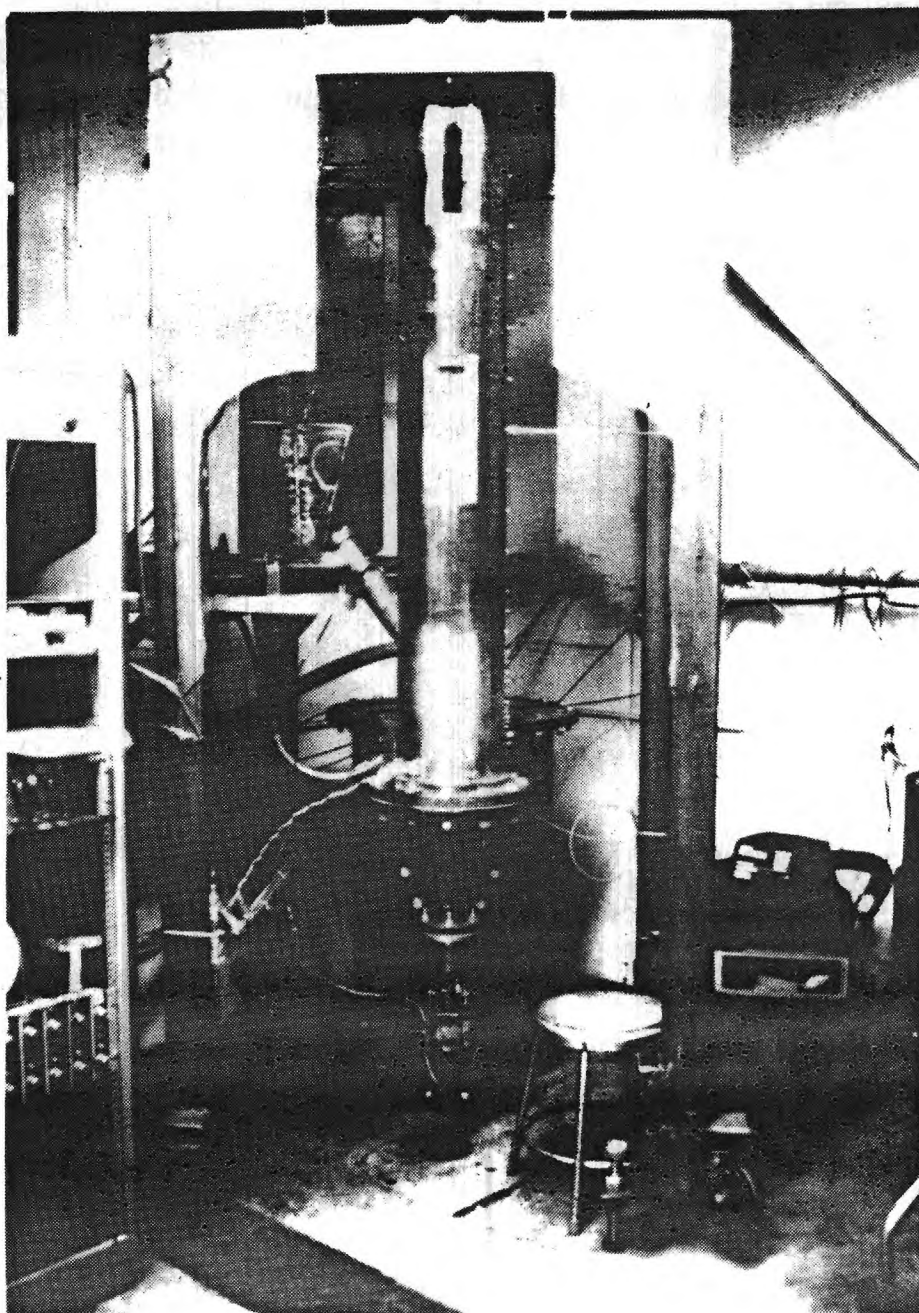
Figure 13. Photograph of Rijke Pulse Combustor During Pulsating Operation.

25

the combustor. The combustion section is suspended from a large steel frame with four legs with casters and leveling bolts, while the decoupler has its own set of casters. Figure 14 shows close-up views through the lower observation windows during nonpulsating (left) and pulsating (right) combustion of coal. In the pulsating case, pieces of coal and ash are visible several centimeters above the bed as a result of the extreme agitation caused by the large amplitude acoustic velocity oscillations through the bed. The acoustic velocity oscillations also caused flamelets to periodically extend below the coal bed grid during each oscillation cycle. These appear to be stationary to the eye since the flamelets oscillate at about 65 Hz. Figure 15 gives an oblique view upward through the lower part of the bed observation window showing these flamelets.

COAL PROPERTIES

The coal used in all of the experiments was a bituminous coal obtained from Georgia Power Company's Plant McDonough located near Atlanta. This coal was obtained from a large pile which had recently been delivered from a single trainload. The coal as received had a wide range of particle sizes, from coal dust (less than 0.1 mm) to large lumps several centimeters across.

A representative sample of the coal obtained from Plant McDonough was subjected to proximate and ultimate analysis. The proximate analysis was performed at the Central Test Laboratory of Georgia Power Company, while the ultimate analysis was performed by the General Test Laboratory of the Alabama Power Company. These analyses were obtained at no cost to the project. The results of the analyses are presented in Table I. In performing the proximate analysis, the sample as received was first air-dried for 12 hours at 40 C. An 8-mesh sample was extracted, and the remainder was ground to 60-mesh. The 60-mesh sample was heated for 1 hour at 104 C, while the 8-mesh sample was heated for 1.5 hours at the same temperature. This yielded a 60-mesh moisture content of 1.84 percent and an 8-mesh moisture content of 1.63 percent. The 60-
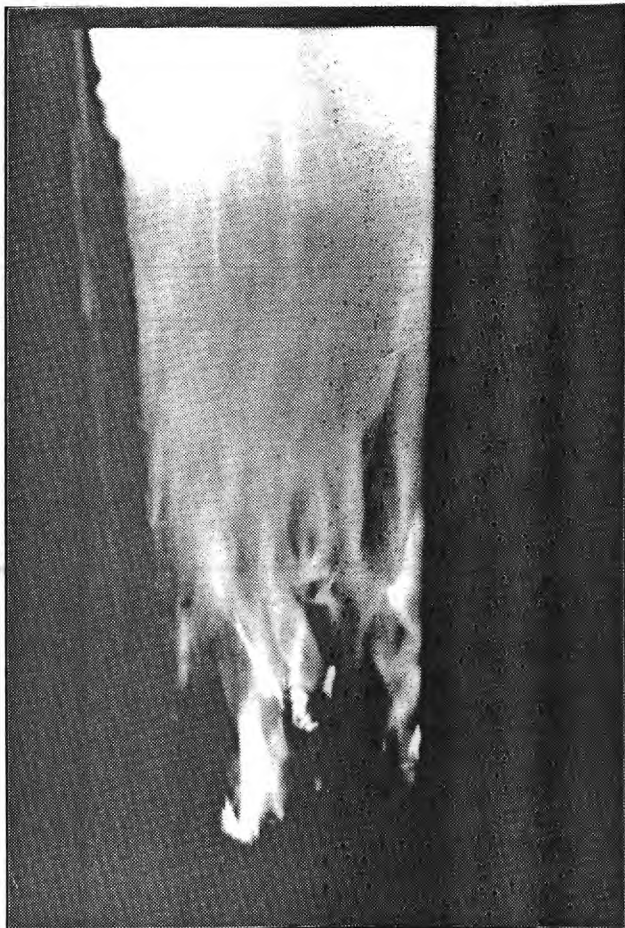
Preheating with Propane   Pulsating
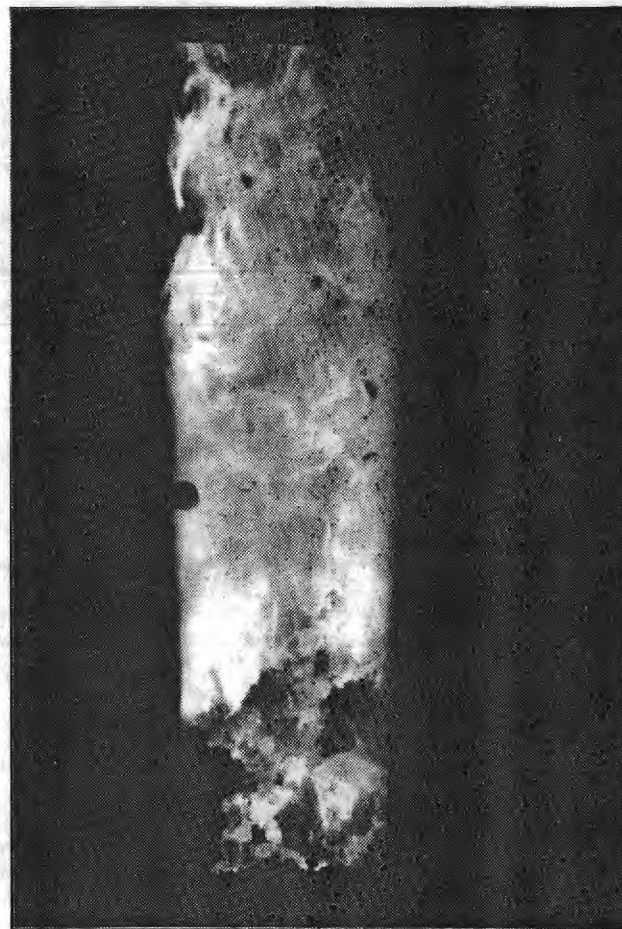
Figure 14. Photographs of Combustion Zone During Preheating and Pulsating Combustion of Coal.

Figure 15. Photograph of Oscillatory Flamelets Extending Below Bed
During Pulsating Combustion of Coal.

mesh sample was then subjected to proximate analysis to yield the "As Determined" values in Table I. The "As Received" values were calculated on the basis of the moisture loss during the preliminary air drying. The 8-mesh and 60-mesh moisture values were used in calculating the dry basis values. The heating value of the coal as received was 29,060 kJ/kg.

Table I. Coal Analysis

PROXIMATE ANALYSIS			
Analysis	As Determined	As Received	Dry
Moisture	2.05	5.60	-
Volatiles	33.19	31.98	33.88
Ash	11.08	10.68	11.31
Fixed Carbon	53.68	51.74	54.81
Sulfur	1.31	1.26	1.33

ULTIMATE ANALYSIS		
Analysis	As Determined	Dry
Carbon	72.20	73.85
Hydrogen	5.09	4.95
Nitrogen	1.48	1.51
Sulfur	1.31	1.33
Oxygen	6.60	7.03
Ash	11.08	11.33
Moisture (60 mesh)	2.24	-

In order to obtain consistency in the size distribution of the coal lumps burned in the Rijke pulse combustor, a large sieve was constructed for sizing the coal. This sieve consists of a wooden frame with a hinged lid. The bottom of the frame holds a hardware cloth screen to retain coal particles larger than about 6 mm in diameter.

The coarser screen on the lid retains coal lumps larger than about 12 mm in diameter. The sieve fits over the top of an empty 55-gallon drum which catches the fine particles which fall through the lower screen. The coarser lumps are retained on the upper screen and are stored separately for later crushing. The particles between the screens, which are between 6 mm and 12 mm in diameter, are then transferred to drying boards and later stored for use in the combustor.

BASELINE RESULTS

For each of the baseline tests, sound pressure levels, frequencies, exhaust gas compositions (CO_2, CO, O_2, NO_x and SO_2) and gas temperatures were measured as a function of the dimensionless air/fuel ratio (α) for a fixed coal feed rate of 75 g/min. Measurements were recorded every six seconds during a typical experiment lasting about 15 - 20 minutes. A total of 22 baseline experimental runs were conducted with at least two runs for each value of the dimensionless air/fuel ratio.

Plots of the measured sound pressure level and exhaust gas species concentration values as a function of elapsed time are shown in Figures 16, 17 and 18 for a typical baseline experiment with a dimensionless air/fuel ratio of 1.00 (stoichiometric combustion). The sound pressure levels shown in Figure 16 indicate that the pulsation amplitude was nearly constant during the entire experiment; the variation in amplitude was less than 0.7 dB above or below the mean amplitude of 159.8 dB. The concentrations of carbon dioxide, oxygen, and carbon monoxide in the exhaust gases during this experiment are shown in Figure 17. After an initial transient period of about five minutes, the concentrations of these gases attained nearly constant values for the remainder of the test. The concentration of carbon dioxide reached a steady value of 16.2 percent by volume, while the concentration of residual oxygen was reduced essentially to zero. This indicates nearly complete combustion of the coal during pulsating operation. The concentration of carbon monoxide averaged
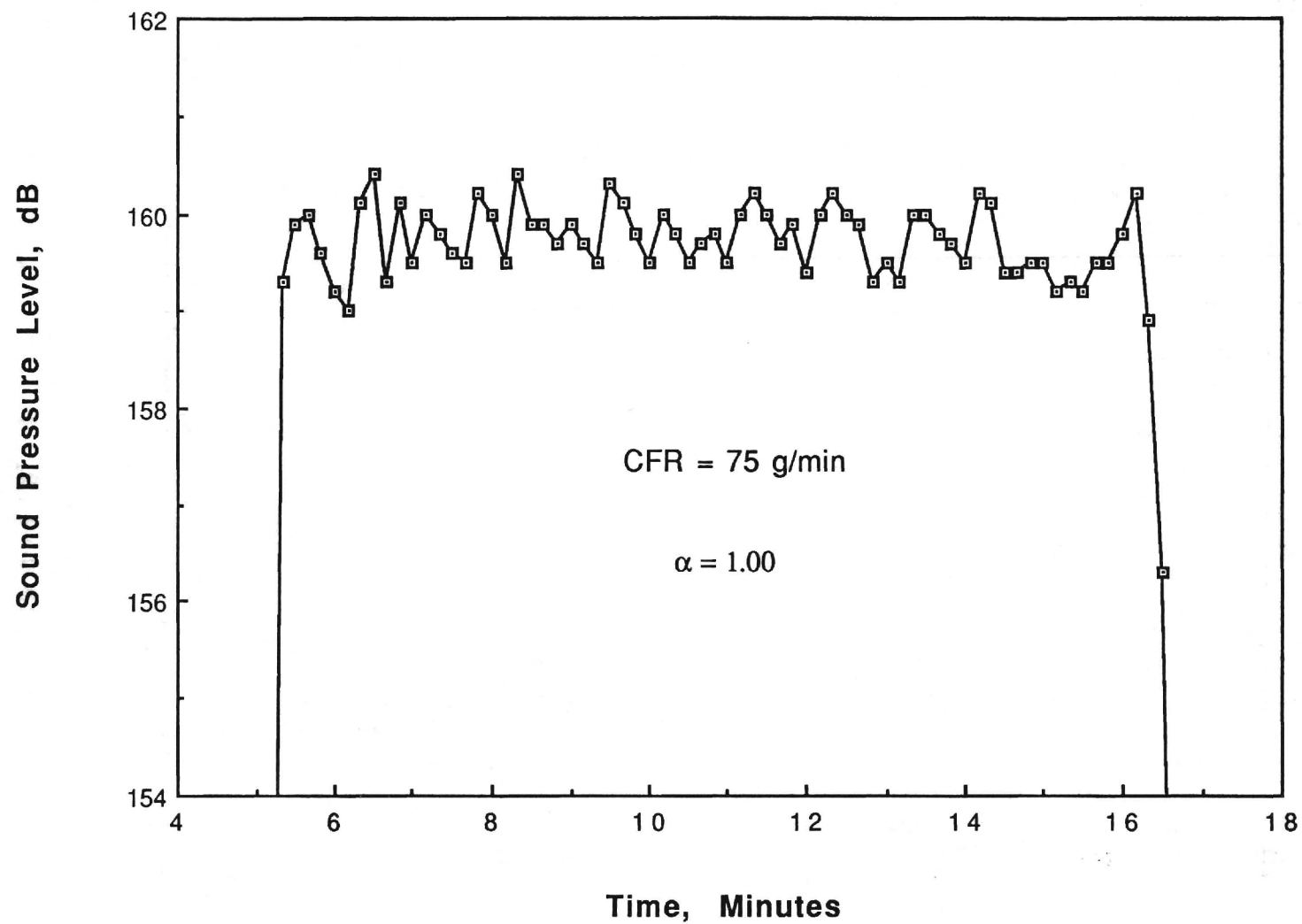
Figure 16.   Sound Pressure Levels for a Typical Baseline Experiment.
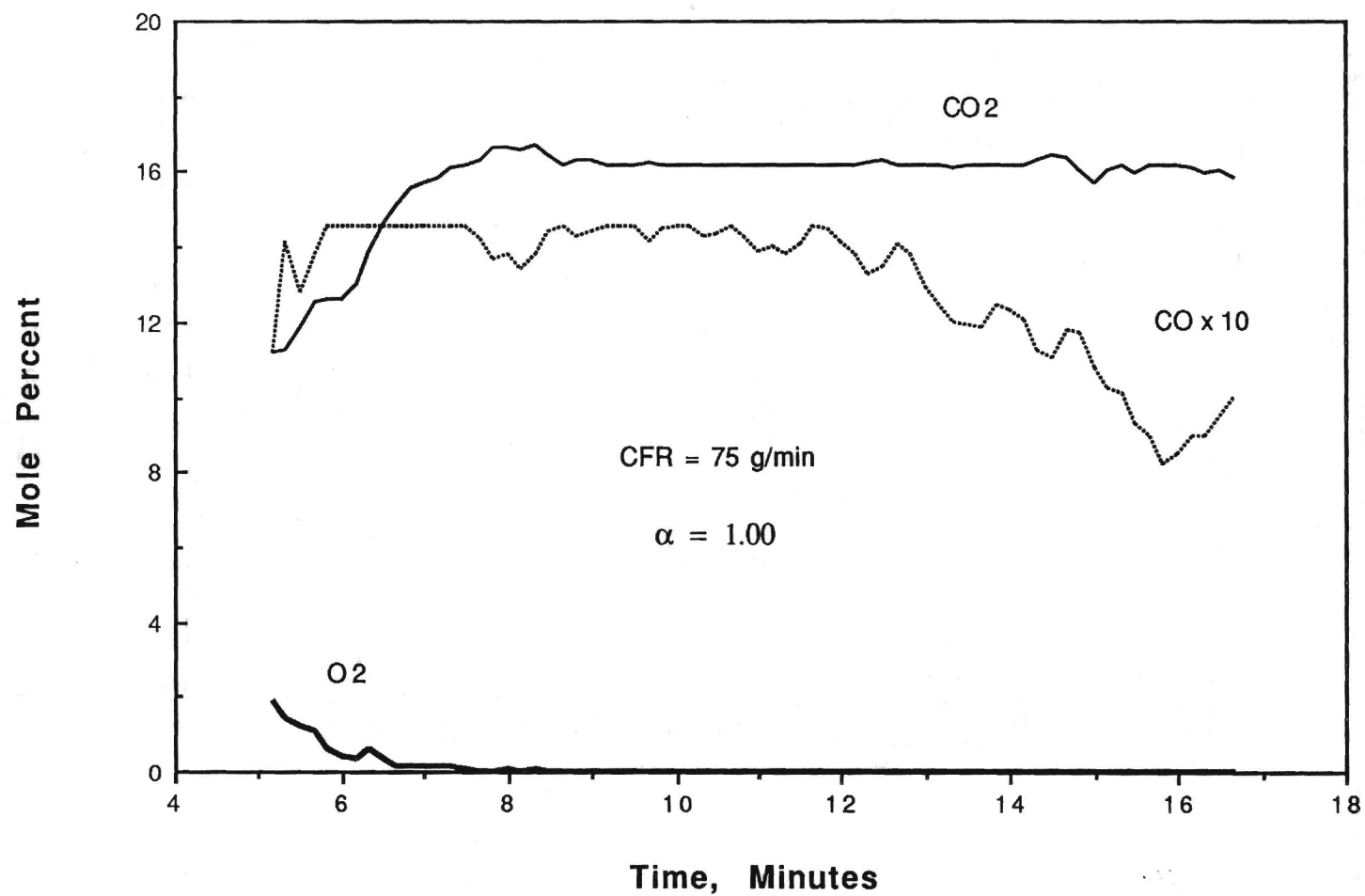
Figure 17. Exhaust Gas Carbon Dioxide, Oxygen, and Carbon Monoxide Concentrations for a Typical Baseline Experiment.

about 1.4 percent during the middle of the experiment, and it decreased significantly during the later stages of the test. The high levels of CO indicate that a small amount of excess air is needed for good combustion efficiency of this system. The emissions of nitrogen oxides and sulfur dioxide for this experiment are presented in Figure 18. Both NO_x and SO_2 concentrations exhibited sharp peaks during the transient period, but soon reached steady state values. The NO_x concentration averaged about 360 ppm by volume during the early phases of the run and gradually increased to about 425 ppm toward the end of the test. The SO_2 concentration fluctuated about a mean of about 1300 ppm during the experiment. During this experiment the agglomerates were continuously broken up by the action of the rotating bed, and the distribution of coal on the bed was very uniform. Furthermore, the ash particles were ground down to small enough sizes so that they continuously fell through the bed grid, thus preventing accumulation of coal and ash on the bed.

Since the measured quantities fluctuated with time during the 15-20 minute experiments, data was time averaged over two or three time periods (each lasting 3-5 minutes) for each test. Plots of the measured quantities as a function of time were used to determine which one of the time averages was more typical of the experiment. This procedure determined a representative value for each of the measured quantities for each experiment. For each dimensionless air/fuel ratio, the time averaged data from the appropriate experiments were then averaged and tabulated. The results of the baseline experiments are summarized in Table II. Plots were generated of each quantity as a function of α; these are given in Figures 19 through 21.

Sound pressure level and frequency as a function of α are shown in Figure 19. Sound pressure level was a maximum, about 160 dB, for stoichiometric conditions ($\alpha = 1.00$). The lowest amplitude recorded was 156 dB at dimensionless air/fuel ratios of 0.6 and 0.7. The pulsation frequency increased as the dimensionless air/fuel ratio was increased, ranging from about 64 Hz at $\alpha = 0.6$ to

33
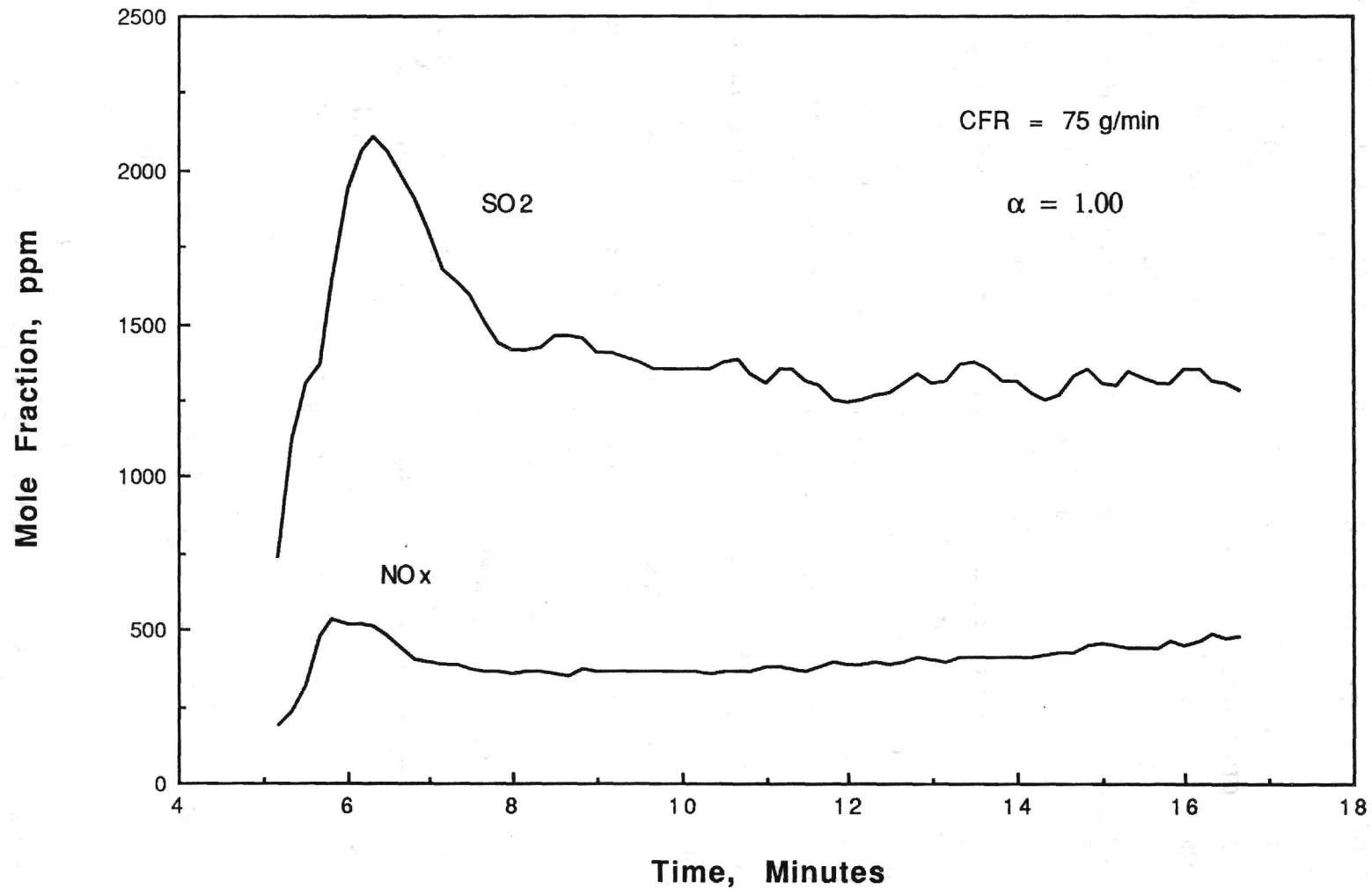
Figure 18.   Nitrogen Oxides and Sulfur Dioxide Emissions for a Typical Baseline Experiment.
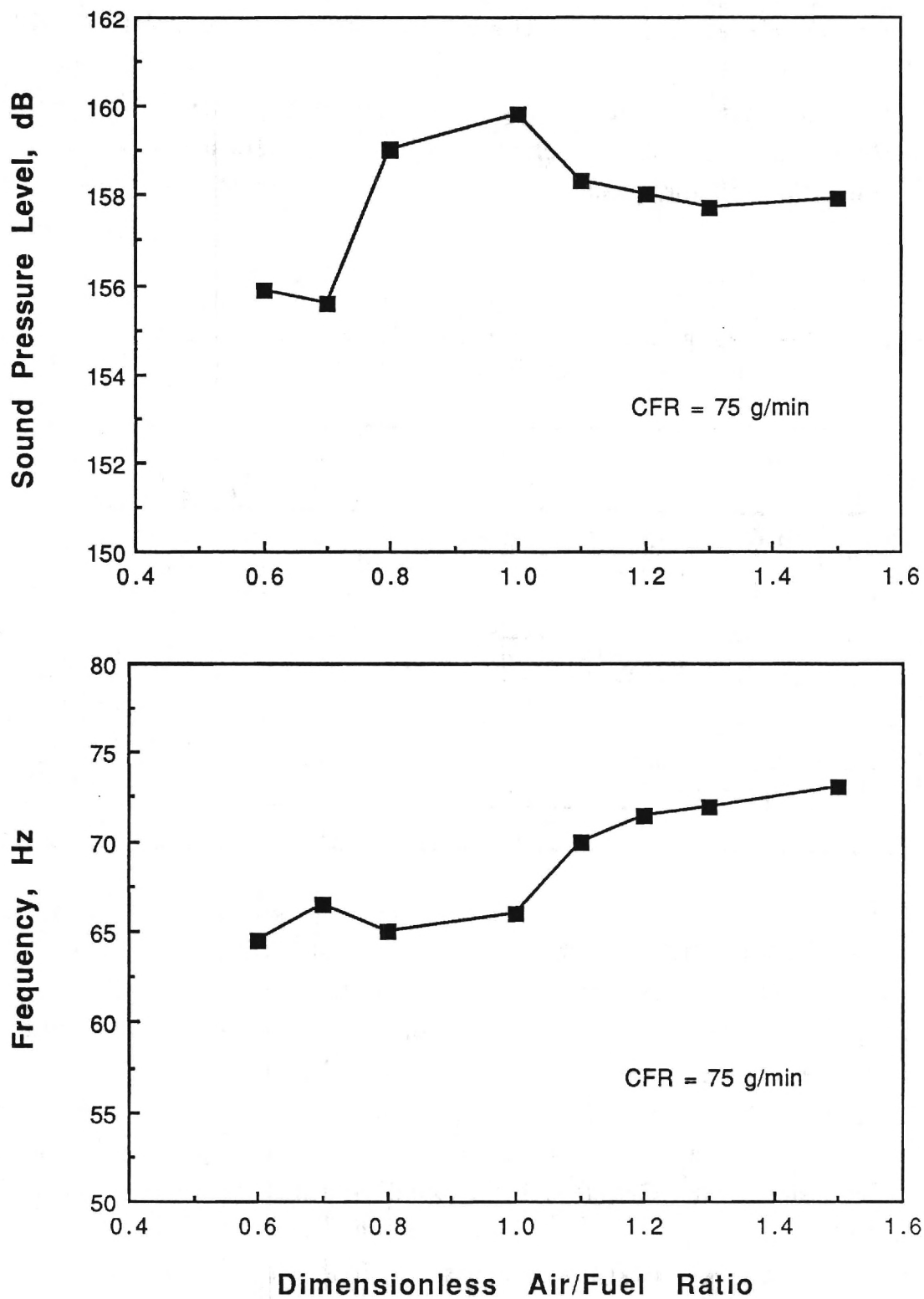
Figure 19. Dependence of Baseline Sound Pressure Levels and Frequencies on Dimensionless Air/Fuel Ratio.

about 73 Hz at $\alpha = 1.5$. These frequencies are consistent with the fundamental longitudinal acoustic mode of the open-ended Rijke tube combustor. The changes in frequency with dimensionless air/fuel ratio are due to changes in the temperature distribution and composition of the gases in the region between the coal bed and the exhaust outlet.

Table II. Averaged Sound Pressure Levels, Frequencies and Exhaust Compositions for Baseline Experiments.

No. of Tests	α	SPL (dB)	Freq (Hz)	CO_2 (%)	CO (%)	NO_x (ppm)	SO_2 (ppm)	O_2 (%)
2	0.6	155.9	64.5	15.4	1.12	484	NA	0.29
5	0.7	155.6	66.5	14.5	0.73	451	1420	1.36
2	0.8	159.0	65.0	16.2	1.01	398	1450	0.04
4	1.0	159.8	66.0	16.6	0.83	443	1420	0.65
2	1.1	158.3	70.0	16.5	0.42	502	1480	0.52
2	1.2	158.0	71.5	15.1	0.05	585	1270	3.16
2	1.3	157.7	72.0	10.5	0.02	592	1140	5.83
2	1.5	157.9	73.0	11.3	0.06	559	940	6.47

Carbon dioxide (CO_2), carbon monoxide (CO), and residual oxygen (O_2) concentrations are shown in Figure 20. Carbon dioxide levels were maximum (16.5 percent) for stoichiometric conditions, and they were above 16 percent for dimensionless air/fuel ratios between 0.8 and 1.1. Carbon monoxide concentrations ranged between 0.7 and 1.2 percent for stoichiometric and fuel rich combustion, but CO levels dropped sharply when excess air was added, becoming less than 0.06 percent for $\alpha = 1.2$ or greater. For dimensionless air/fuel ratios below 1.1, residual oxygen concentrations were small (less than one percent), but they increased sharply as excess air was increased, reaching 6 to 6.5 percent for dimensionless air/fuel ratios of 1.3 and above.

36
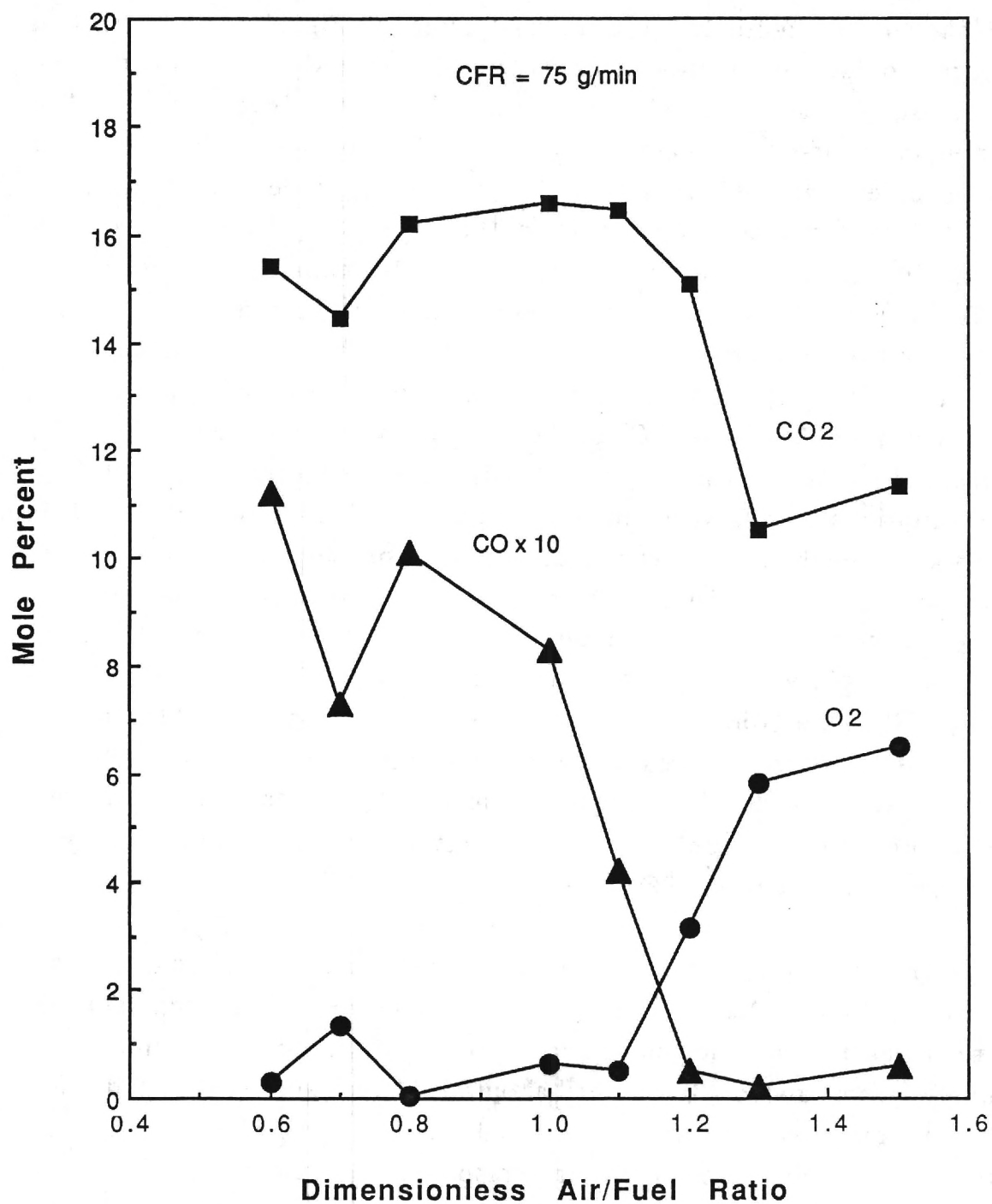
Figure 20. Effect of Dimensionless Air/Fuel Ratio on Baseline Exhaust Concentrations of Carbon Dioxide, Carbon Monoxide and Oxygen.

Nitrogen oxides (NO_x) and sulfur dioxide (SO_2) concentrations are shown in Figure 21. The upper graph in Figure 21 shows that nitrogen oxides production was between 400 and 600 ppm for the entire range of dimensionless air/fuel ratios investigated. The maximum concentration of NO_x (about 590 ppm) was obtained for dimensionless air/fuel ratios of 1.2 and 1.3, while minimum NO_x (about 400 ppm) occurred at $\alpha = 0.8$. This graph also shows that sulfur dioxide concentrations were near 1450 ppm for dimensionless air/fuel ratios below 1.1, and they decreased steadily for larger air/fuel ratios primarily due to the dilution effect of the excess air. To remove this dilution effect and allow comparison with other data, the measured NO_x and SO_2 concentrations were reduced to a 15% excess air (3% excess oxygen) basis. The reduced NO_x and SO_2 concentrations are shown in the lower graph of Figure 21. This reveals a much more pronounced effect of dimensionless air/fuel ratio on the NO_x emissions from the pulse combustor. The reduced NO_x concentrations were about 250 ppm for α below 0.8, they increased rapidly as α increased from 0.8 to 1.3, and they reached about 725 ppm for $\alpha = 1.5$. The reduced SO_2 concentrations exhibited a strong increase with increasing dimensionless air/fuel ratio for α less than 1.1, ranging from about 850 ppm to 1400 ppm. For higher dimensionless air/fuel ratios, there was a gradual decrease in the reduced SO_2 concentration.

The gas temperature profiles for the baseline experiments are shown in Figure 22. For most of the experiments, gas temperatures were measured at the combustor axis at four to seven locations, ranging from about 20 cm to about 155 cm above the bed. The highest temperatures were measured for a dimensionless air/fuel ratio of 1.1, with slightly lower temperatures obtained for the larger air/fuel ratios ($1.2 < \alpha < 1.5$). These temperatures decreased nearly linearly with increasing height above the bed, ranging from about 1000 C at 30 cm above the bed to about 800 C near the upper end of the combustion section (120 cm). This decline in temperature resulted from heat losses through the combustor walls. As the dimensionless air/fuel ratios were lowered below $\alpha = 1.1$, the gas
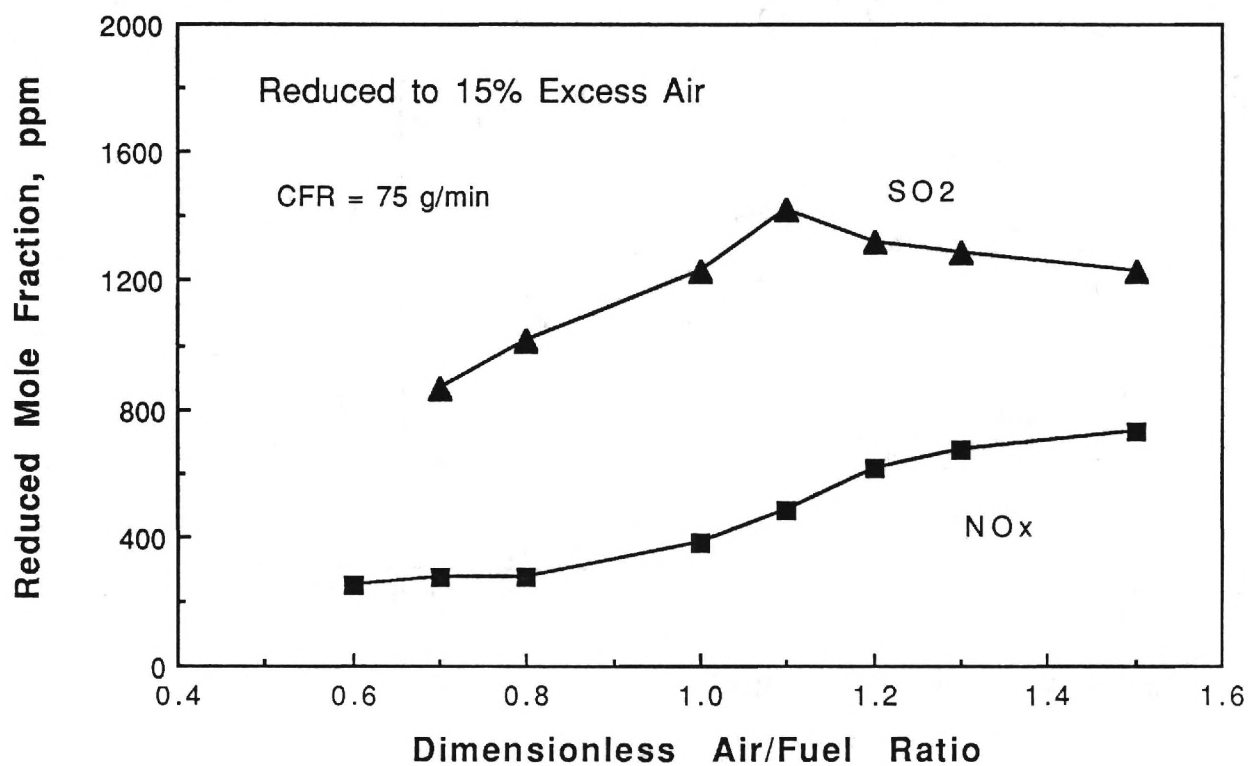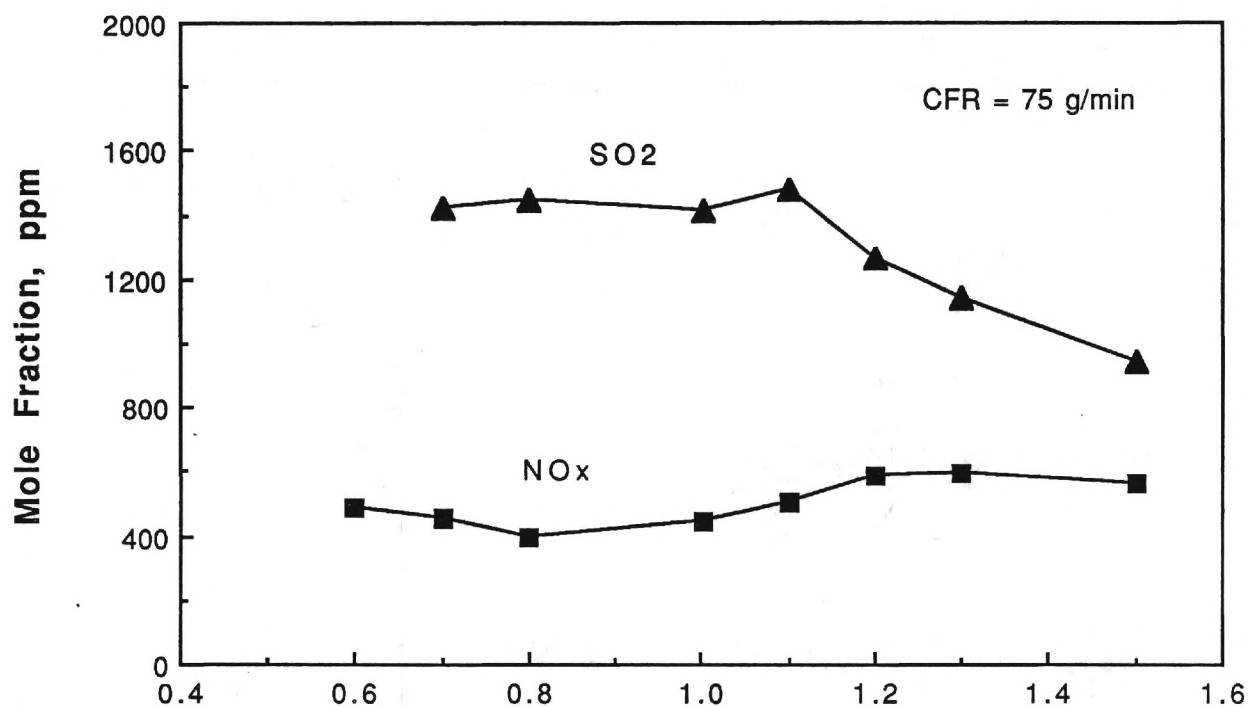
Figure 21. Effect of Dimensionless Air/Fuel Ratio on the Baseline Emissions of Nitrogen Oxides and Sulfur Dioxide.
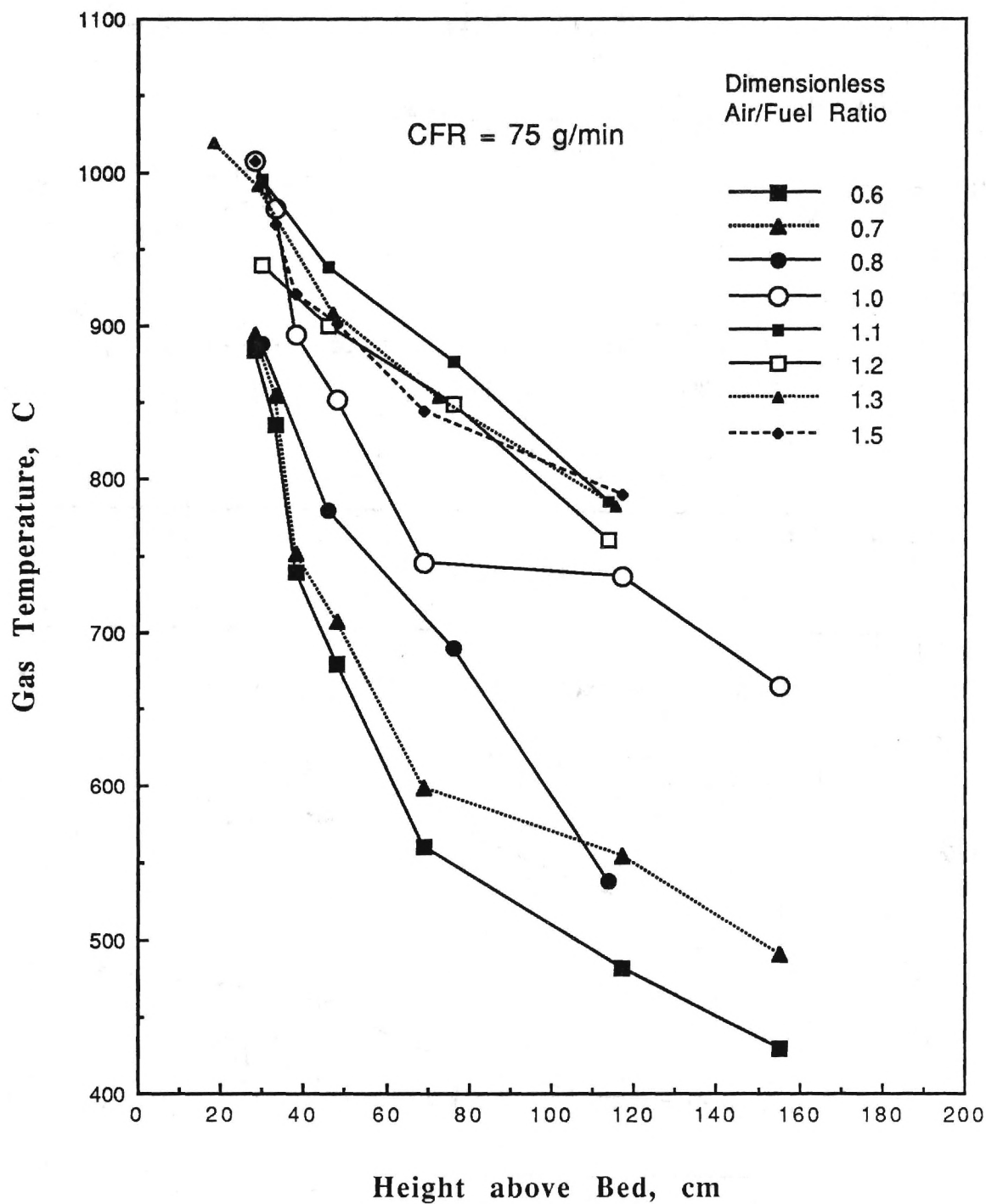
Figure 22. Baseline Gas Temperature Profiles.

temperatures at the lowest levels decreased by moderate amounts (about 100 C), while at higher levels levels the temperature decrease was much larger (about 200 to 300 C). For dimensionless air/fuel ratios in the range $0.6 < \alpha < 1.0$, the temperature profiles were nonlinear, being characterized by a much steeper decline in temperature in the lower half of the combustor and a more gradual decline in temperature in the upper half of the combustion section. The lowest gas temperatures were obtained for a dimensionless air/fuel ratio of 0.6; these ranged from about 900 C at 30 cm above the bed to about 425 C at the upper end of the combustion section (155 cm).

AIR STAGING EXPERIMENTS

Two groups of air staging experiments were conducted during this investigation. In these experiments the coal was burned in the primary combustion zone under fuel rich (gasification) conditions, and secondary air was introduced some distance above the bed (secondary combustion zone) to complete the combustion of the fuel gases (CO, CH_4, H_2, etc) produced by devolatilization processes in the primary combustion zone. The stoichiometry of the primary combustion zone was specified by the dimensionless primary air/fuel ratio, α_1, which was always less than unity. The overall stoichiometry of the entire air-staged combustion process was determined by the total dimensionless air/fuel ratio, α_t. In the first series of air staging experiments, the total air/fuel ratio, α_t, was equal to one. The second group of air staging experiments was conducted with total air/fuel ratios greater than one.

AIR STAGING EXPERIMENTS WITH α_t OF UNITY

In this series of air-staging tests, the secondary air was injected at three heights above the bed: 20 cm, 27 cm, and 37 cm. The secondary air supply system and injector are shown in Figure 3. In each experiment the total air/fuel ratio (α_t) was stoichiometric, that is, $\alpha_t = 1.00$. Each of these experiments were divided into three

segments lasting about five minutes each. In the first segment, a primary air/fuel ratio of 1.0 was used (no secondary air injection). The primary air/fuel ratio was then reduced to 0.7 in the second segment and to 0.5 in the third segment. Time averaged values of sound pressure levels, frequencies, exhaust gas compositions (CO_2, CO, O_2, NO_x and SO_2) and temperatures were obtained for each segment.

A total of nine air staging experiments were conducted in this series. Two experiments were conducted with secondary air injection at 37 cm above the bed, three experiments were run with air staging at 27 cm above the bed, and four experiments were conducted with air staging at 20 cm above the bed. For each secondary air injection height and each primary air/fuel ratio, α_1, the time averages of each of the measured quantities for the appropriate experiments were averaged. The resulting values were then tabulated and plotted as a function of the primary air/fuel ratio, α_1, for the three secondary injection heights above the bed. These data are presented in Table III and Figures 23 through 28.

Figure 23 shows that sound pressure levels increased nearly linearly from 154 dB at $\alpha_1 = 0.5$ to about 160 dB at $\alpha_1 = 1.0$. Secondary air injection height had very little affect on the amplitude and frequency of the pulsations.

Carbon dioxide concentrations for the air staging experiments are shown in Figure 24. Except for the lowest secondary air injection point (20 cm), the CO_2 concentration increased monotonically with increasing primary dimensionless air/fuel ratio. Carbon dioxide concentrations ranged between 12.5 percent and nearly 16 percent, with the lower values corresponding to $\alpha_1 = 0.5$. Except for the unexpected decrease in CO_2 concentration for secondary air injection at 20 cm, CO_2 concentrations increased only slightly between $\alpha_1 = 0.7$ and $\alpha_1 = 1.0$. The concentration of CO_2 also decreased significantly with increasing height of the secondary air injection point. Carbon dioxide concentrations measured in the air staging experiments at $\alpha_1 = 1.0$ were somewhat lower than those measured in the baseline

Figure 23. Effect of Dimensionless Primary Air/Fuel Ratio and Secondary Air Injection Height on Pulsation Amplitude.

43

Figure 24.   Effect of Dimensionless Primary Air/Fuel Ratio and Secondary Air
Injection Height on the Exhaust Carbon Dioxide Concentration.

44

experiments at stoichiometric combustion conditions. This was probably due to the dilution effect of a small amount of secondary air used to cool the injection head for the case of $\alpha_1 = 1.0$.

Table III. Averaged Sound Pressure Levels and Exhaust Gas Compositions for Air Staging Experiments with $\alpha_t = 1.00$.

Air Staging Location (cm)	α_1	SPL (dB)	CO_2 (%)	CO (%)	NO_x (ppm)	SO_2 (ppm)	O_2 (%)
20	0.4	151.3	12.7	0.05	597	1190	5.7
	0.5	154.1	14.5	0.20	555	1230	4.1
	0.7	156.3	15.8	0.15	535	1260	2.8
	1.0	159.9	14.1	0.58	505	1470	2.3
27	0.5	153.6	13.6	0.05	453	1170	4.5
	0.67	156.2	15.5	0.05	498	1300	3.1
	0.7	156.6	15.5	0.10	516	1210	2.7
	1.0	159.7	15.7	0.45	485	1310	1.8
37	0.5	153.8	12.7	0.10	429	1090	5.2
	0.7	155.7	15.0	0.15	454	1250	3.0
	1.0	159.2	15.3	0.35	471	1310	2.1

The measured carbon monoxide emissions for the air staging experiments are shown in Figure 25. Carbon monoxide concentration generally increased with increasing dimensionless primary air/fuel ratio. Carbon monoxide concentration varied between about 0.05 and 0.6 percent, with the higher values for $\alpha_1 = 1.0$ (no secondary air injection). Increasing the secondary air injection height generally reduced the amount of CO in the exhaust gases. The CO concentrations measured in the air staging tests for $\alpha_1 = 1.0$ were generally lower than those measured in the baseline experiments under stoichiometric combustion conditions.

Figure 25. Effect of Dimensionless Primary Air/Fuel Ratio and Secondary Air Injection Height on the Exhaust Carbon Monoxide Concentration.

Measured oxygen concentrations in the exhaust gases during the air staging experiments are shown in Figure 26. Residual oxygen levels were higher for lower values of the primary air/fuel ratio, with a maximum of 5.7 percent for $\alpha_1 = 0.4$ with secondary air injection at 20 cm above the primary combustion zone. For $\alpha_1 = 1.0$, residual oxygen was about 2 percent. Residual oxygen levels generally increased as the secondary air injection height was increased. These residual oxygen levels indicate that combustion of the coal gases by the secondary air injection was not complete, since the total air/fuel ratio was stoichiometric. Residual oxygen concentrations in the air staging tests for $\alpha_1 = 1.0$ were somewhat higher than those measured in the baseline experiments under stoichiometric combustion conditions.

The measured nitrogen oxides concentrations in the exhaust gases for the air staging experiments are shown in Figure 27. Nitrogen oxides emissions ranged between 400 ppm and 600 ppm with only moderate reductions due to air staging. For secondary air injection at 20 cm above the bed, decreasing α_1 increased the NO_x concentrations, but reducing α_1 yielded slight decreases in the NO_x emissions for the higher injection points. Increasing the height of the secondary air injection point resulted in decreased NO_x emissions, especially for the smaller primary air/fuel ratios.

Although the object of the air staging experiments was the reduction of NO_x emissions, the effect of air staging on sulfur dioxide emissions was also obtained. These results are shown in Figure 28. At the lowest secondary air injection point, sulfur dioxide emissions ranged from about 1200 ppm for $\alpha_1 = 0.4$ to nearly 1500 ppm for $\alpha_1 = 1.0$. Raising the secondary injection point clearly decreased SO_2 emissions for $\alpha_1 = 0.5$ but had little effect on SO_2 concentrations for $\alpha_1 = 0.7$.
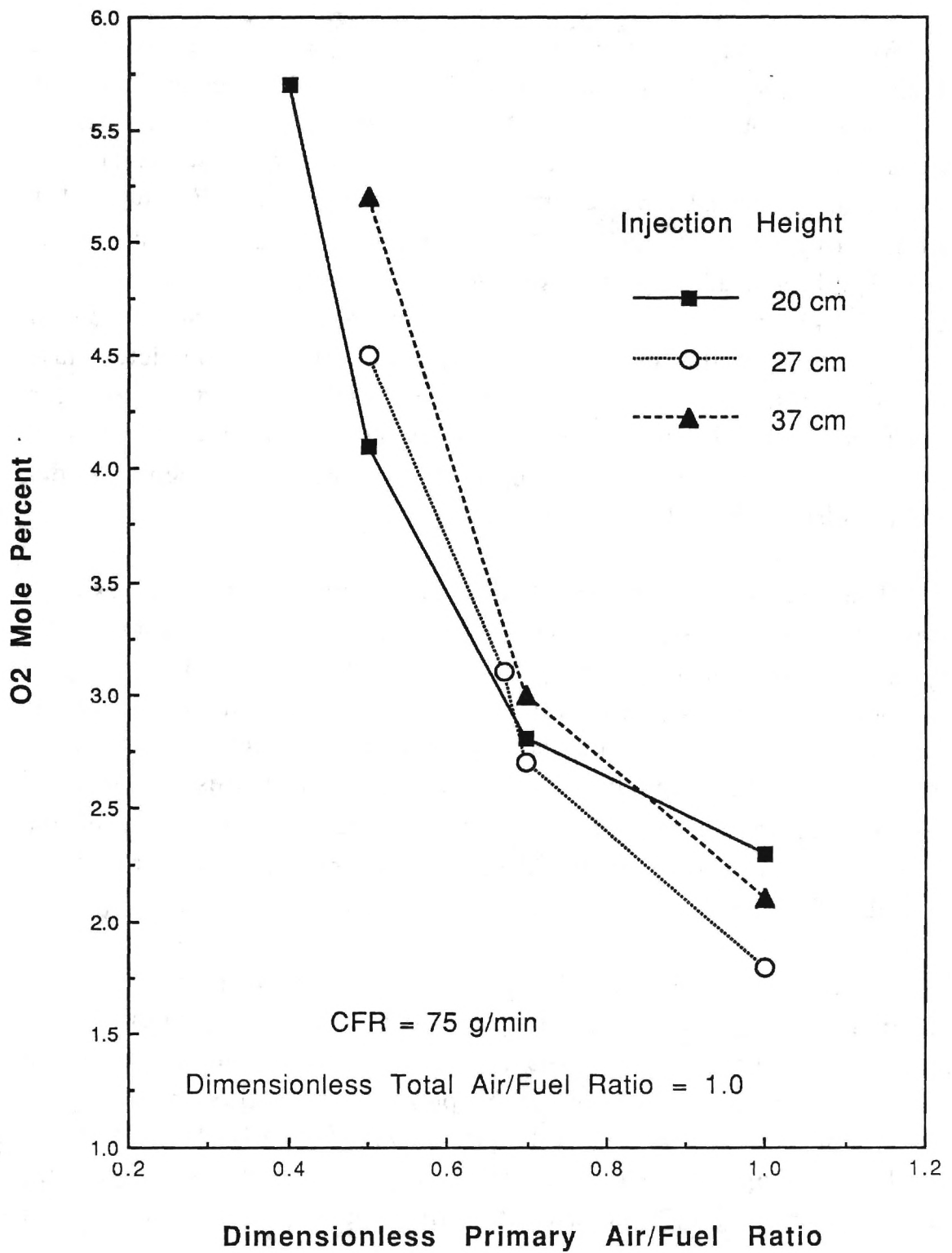
Figure 26. Effect of Dimensionless Primary Air/Fuel Ratio and Secondary Air Injection Height on the Exhaust Oxygen Concentration.
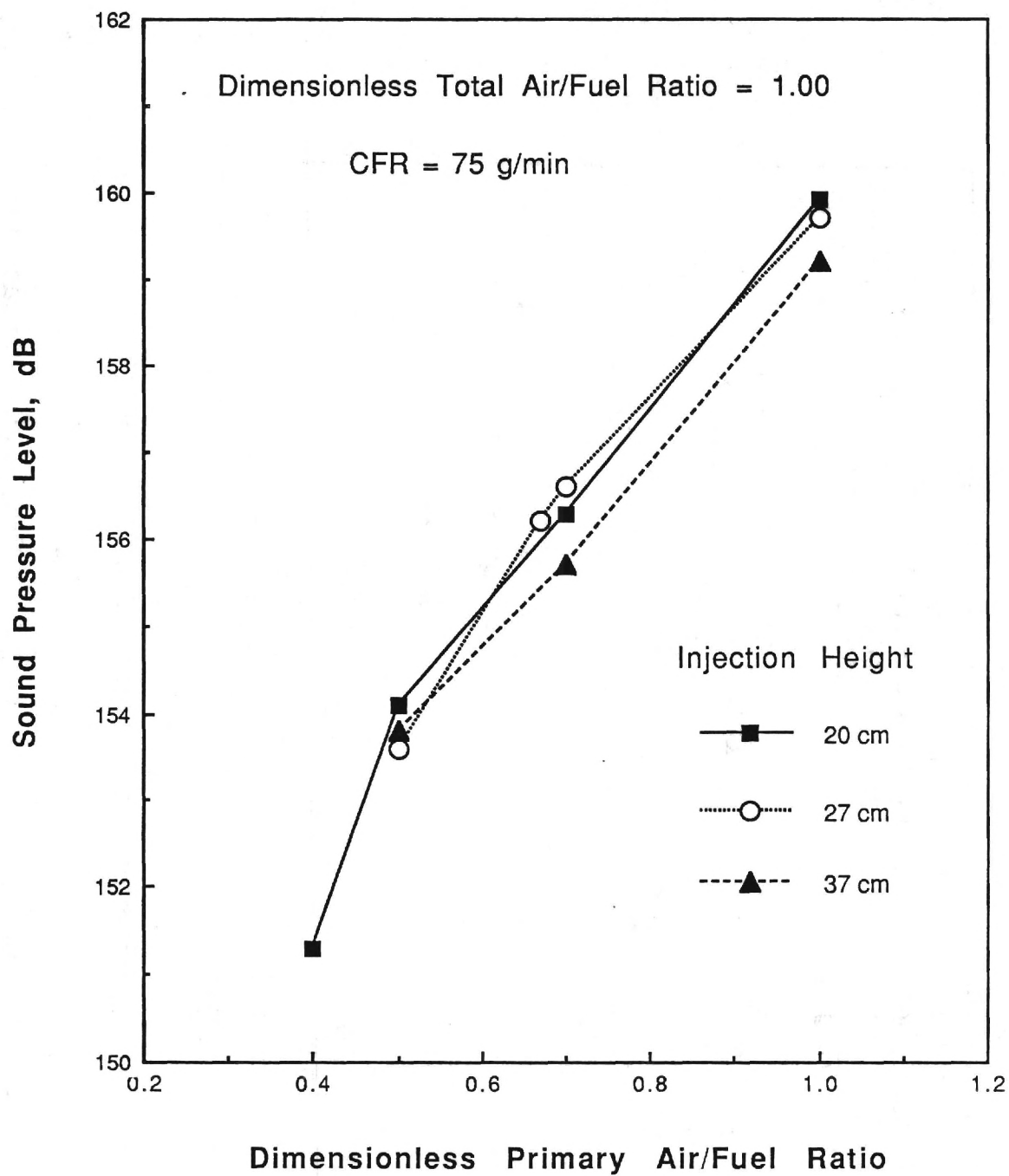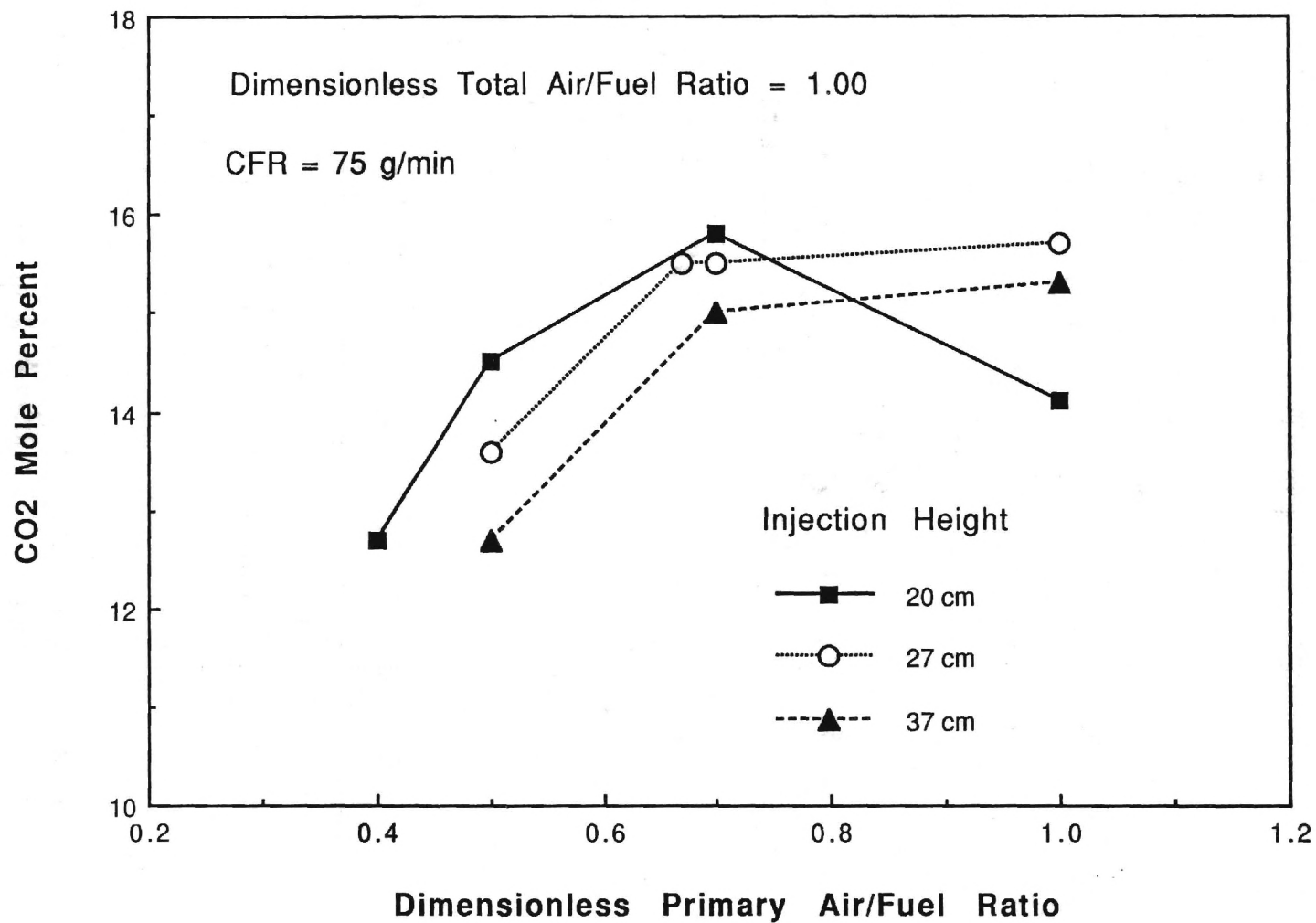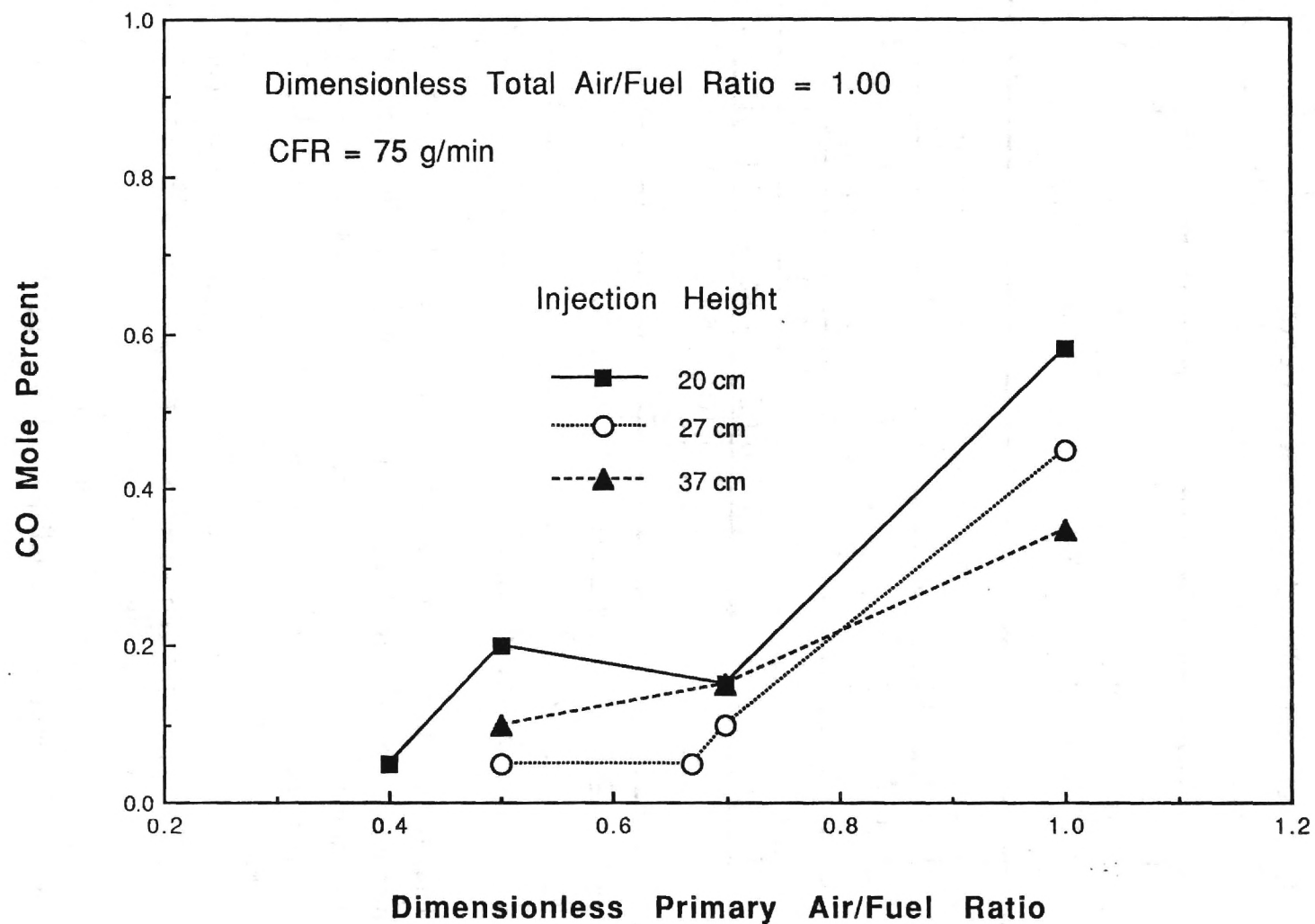
48
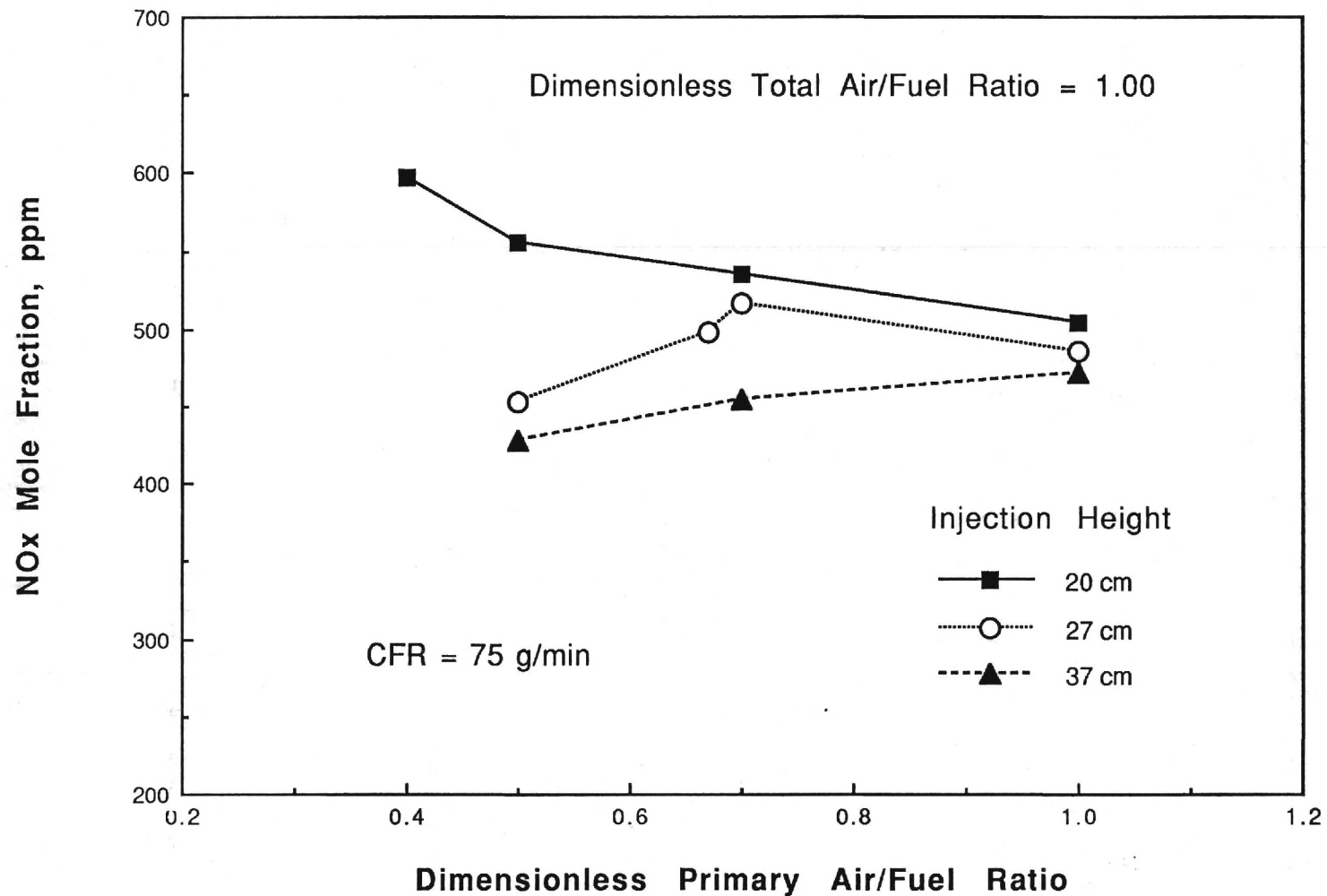
Figure 27. Effect of Dimensionless Primary Air/Fuel Ratio and Secondary Air Injection Height on Nitrogen Oxides Emissions.
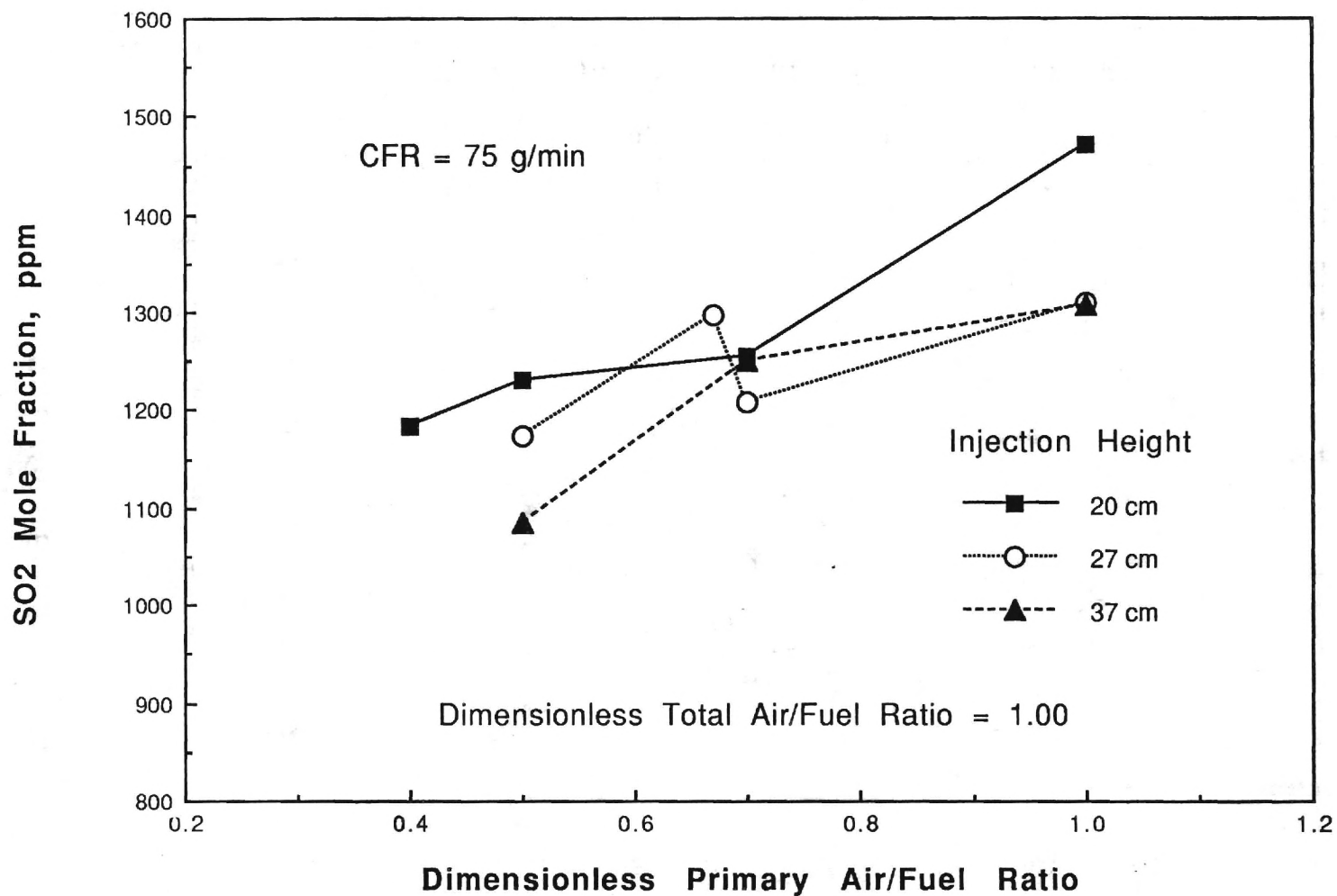
Figure 28. Effect of Dimensionless Primary Air/Fuel Ratio and Secondary Air Injection Height on Sulfur Dioxide Emissions.

The effect of air staging on the temperature distributions in the combustor downstream of the coal bed are shown in Figure 29. Here, temperature profiles are shown for secondary air injection at 37 cm above the bed for different primary air/fuel ratios. The curve for $\alpha_1 = 1.0$ represents stoichiometric burning without air staging, where the monotonic decrease in temperature with increasing height above the coal bed is due to heat losses through the combustor walls. For the two cases with secondary air injection, the heat release in the secondary combustion zone results in higher temperatures in this region (25 - 45 cm above the bed) than those obtained without air staging. For positions higher than 75 cm above the bed, the temperatures obtained with air staging are considerably lower than those obtained without secondary air. Since the total air/fuel ratio for all three cases is the same, this temperature deficit at the combustor exit is a further indication of the incomplete combustion and resultant smaller heat release obtained with air staging under pulsating combustion conditions.

AIR STAGING EXPERIMENTS WITH α_t GREATER THAN UNITY

The second group of air staging experiments was conducted with total dimensionless air/fuel ratios greater than one. The secondary air was also injected higher above the bed (52 cm) than in the first group of air staging experiments. This injection height was chosen based on data from the earlier experiments which indicated that NO_x emissions decreased with increasing injection height (see Fig. 24). In this series, as in the previous one, the coal feed rate was 75 g/min. A total of 16 experiments was conducted in this series, each consisting of four or five segments lasting about five minutes each. In each experiment the primary dimensionless air/fuel ratio was fixed, while the amount of secondary air and hence the total dimensionless air/fuel ratio was varied stepwise from 1.1 to 1.4. Experiments were conducted for primary air/fuel ratios of 0.9, 0.8, 0.7 and 0.6. As in the previous experiments, measurements of sound
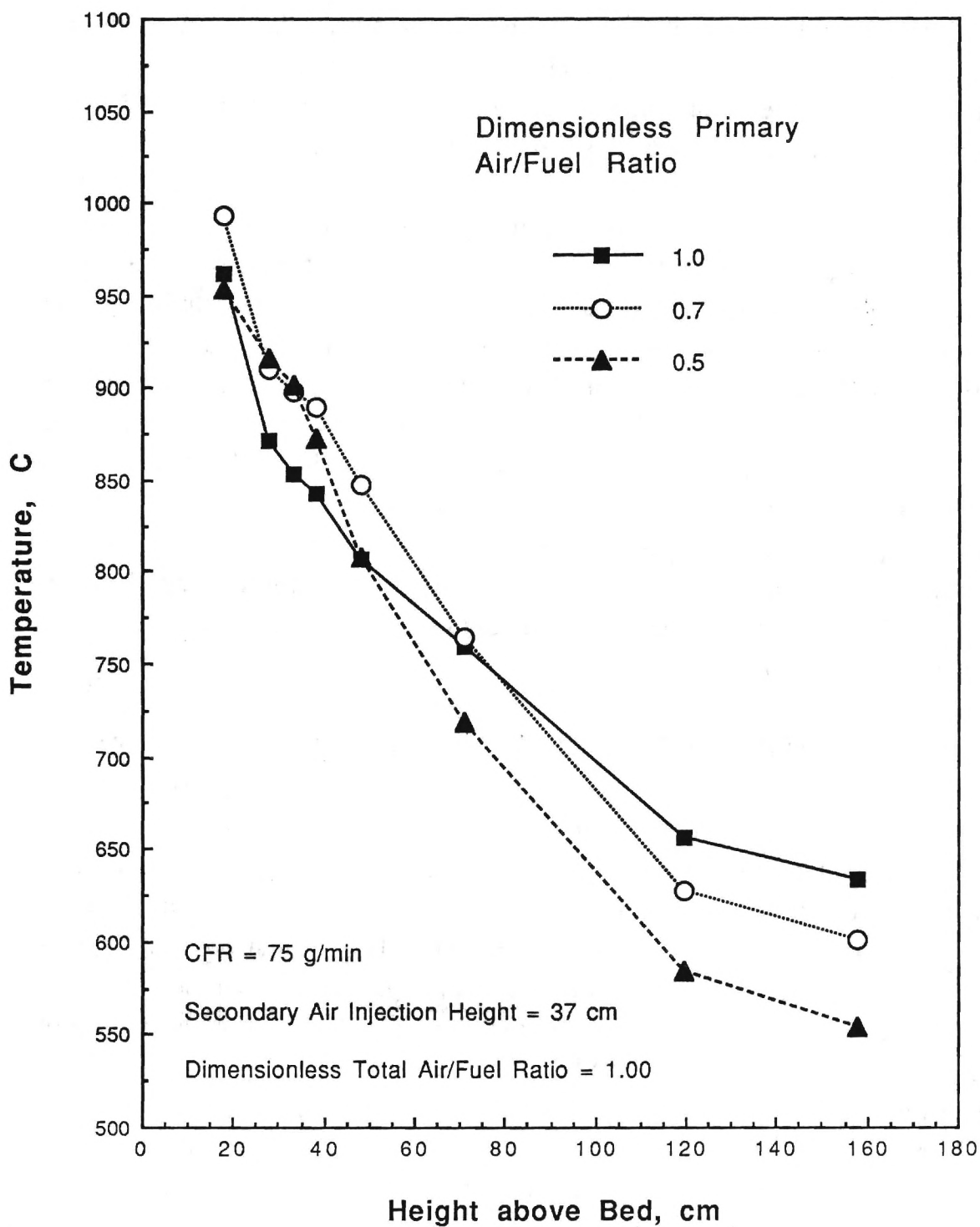
Figure 29. Effect of Air Staging on the Gas Temperature Distributions Downstream of the Coal Bed.

pressure levels, frequencies, and gas compositions (CO_2, CO, O_2, NO_x and SO_2) and gas temperatures were made. However the CO and SO_2 data are not relevant to the issue of NO_x reduction, and they are not included in the results presented herein.

The results of the air staging experiments for $\alpha_t > 1.0$ are summarized in Tables IV through VI and in Figures 30 through 33. The individual test data are given in Table IV for primary dimensionless air/fuel ratios of 0.9 and 0.8. Each set of values of sound pressure level (SPL), mole fractions of carbon dioxide (CO_2), oxygen (O_2), and nitrogen oxides (NO_x), and the combustion efficiencies presented in Table IV are the time averages over the appropriate test segment in a single air-staging experiment. For a given primary dimensionless air/fuel ratio, α_1, two to four test segments were conducted for each value of the total dimensionless air/fuel ratio, α_t. The corresponding time averages for primary dimensionless air/fuel ratios of 0.7 and 0.6 are given in Table V. The NO_x emissions data has been reduced to a 0% oxygen basis using the formula:

$$NO_x \ (0\% \ O_2) = [NO_x] / (1 - [O_2] / 0.21)$$

where

$\quad$ $[NO_x]$ $\quad$ = $\quad$ measured exhaust NO_x concentration in ppm

$\quad$ $[O_2]$ $\quad$ = $\quad$ measured O_2 mole fraction in exhaust

The combustion efficiency η_c was calculated using the formula:

$$\eta_c = 0.217 + \left(0.173 \ [CO_2] + 0.049 \ [CO] \right) N_{td}$$

where

$\quad$ $[CO_2]$ $\quad$ = $\quad$ measured exhaust CO_2 mole fraction

$\quad$ $[CO]$ $\quad$ = $\quad$ measured exhaust CO mole fraction

$\quad$ N_{td} $\quad$ = $\quad$ total number of moles in exhaust, dry basis

53

Table IV. Air Staging Data for Primary Dimensionless Air/Fuel Ratios of 0.9 and 0.8 for $\alpha_t > 1.00$.

Primary Air/Fuel Ratio α_1	Total Air/Fuel Ratio α_t	SPL (dB)	CO_2 (%)	O_2 (%)	NO_x (0% O_2) (ppm)	Combustion Efficiency
0.9	1.1	158.1	16.3	2.95	420	0.99
0.9	1.1	158.9	14.8	4.77	591	0.92
0.9	1.1	159.1	14.8	3.33	497	0.92
0.9	1.1	156.1	14.5	4.90	549	0.90
0.9	1.2	158.6	13.6	6.35	642	0.92
0.9	1.2	157.6	15.3	4.19	401	1.01
0.9	1.2	156.6	14.1	5.42	480	0.94
0.9	1.2	158.5	13.5	5.15	532	0.92
0.9	1.3	156.9	13.3	6.19	439	0.96
0.9	1.3	157.2	13.5	6.11	469	0.97
0.9	1.3	158.9	13.1	5.53	505	0.95
0.9	1.4	157.3	11.7	7.65	457	0.92
0.9	1.4	158.6	NA	6.55	489	NA
0.8	1.1	155.7	15.9	2.82	341	0.97
0.8	1.1	159.4	14.7	3.34	318	0.92
0.8	1.1	157.2	14.0	4.16	316	0.88
0.8	1.2	158.7	15.2	3.38	331	1.00
0.8	1.2	155.6	13.6	4.88	350	0.92
0.8	1.2	156.3	12.5	6.07	372	0.86
0.8	1.3	158.3	14.2	4.55	348	1.01
0.8	1.3	156.1	11.4	6.92	369	0.86
0.8	1.3	156.1	11.6	7.11	377	0.87
0.8	1.4	158.3	12.7	6.34	363	0.98
0.8	1.4	155.9	9.6	8.74	389	0.81

Table V. Air Staging Data for Primary Dimensionless Air/Fuel
Ratios of 0.7 and 0.6 for $\alpha_t > 1.00$.

Primary Air/Fuel Ratio α_1	Total Air/Fuel Ratio α_t	SPL (dB)	CO_2 (%)	O_2 (%)	NO_x (0% O_2) (ppm)	Combustion Efficiency
0.7	1.2	157.0	13.4	4.76	350	0.91
0.7	1.2	157.2	12.4	5.68	302	0.86
0.7	1.3	156.5	13.2	5.42	369	0.95
0.7	1.3	156.8	12.9	5.93	336	0.94
0.7	1.4	156.5	12.8	6.25	361	0.99
0.7	1.4	156.3	12.6	6.44	383	0.98
0.6	1.1	152.7	15.3	3.57	360	0.94
0.6	1.2	153.2	12.4	5.99	335	0.86
0.6	1.2	153.1	12.3	6.07	343	0.86
0.6	1.2	156.4	11.8	6.33	328	0.84
0.6	1.3	156.2	12.4	6.16	365	0.91
0.6	1.3	152.4	12.7	6.15	386	0.93
0.6	1.4	155.9	13.1	5.32	384	1.01
0.6	1.4	152.7	14.5	4.93	414	1.09

For given air staging parameters (i.e., α_1 and α_t) there were considerable variations in the efficiency of the overall combustion process as reflected in the variations in the exhaust concentrations of CO_2 and O_2. There were also significant variations in sound pressure levels and NO_x concentration for tests conducted with identical air staging parameters. The variations in the measured NO_x concentrations are best seen in Figure 30 where the individual time averaged test data are shown. The largest data scatter occurred for the primary dimensionless air/fuel ratio of 0.9, while the scatter was much smaller for the lower α_1 values. This graph readily shows that the NO_x emissions were significantly reduced as the primary
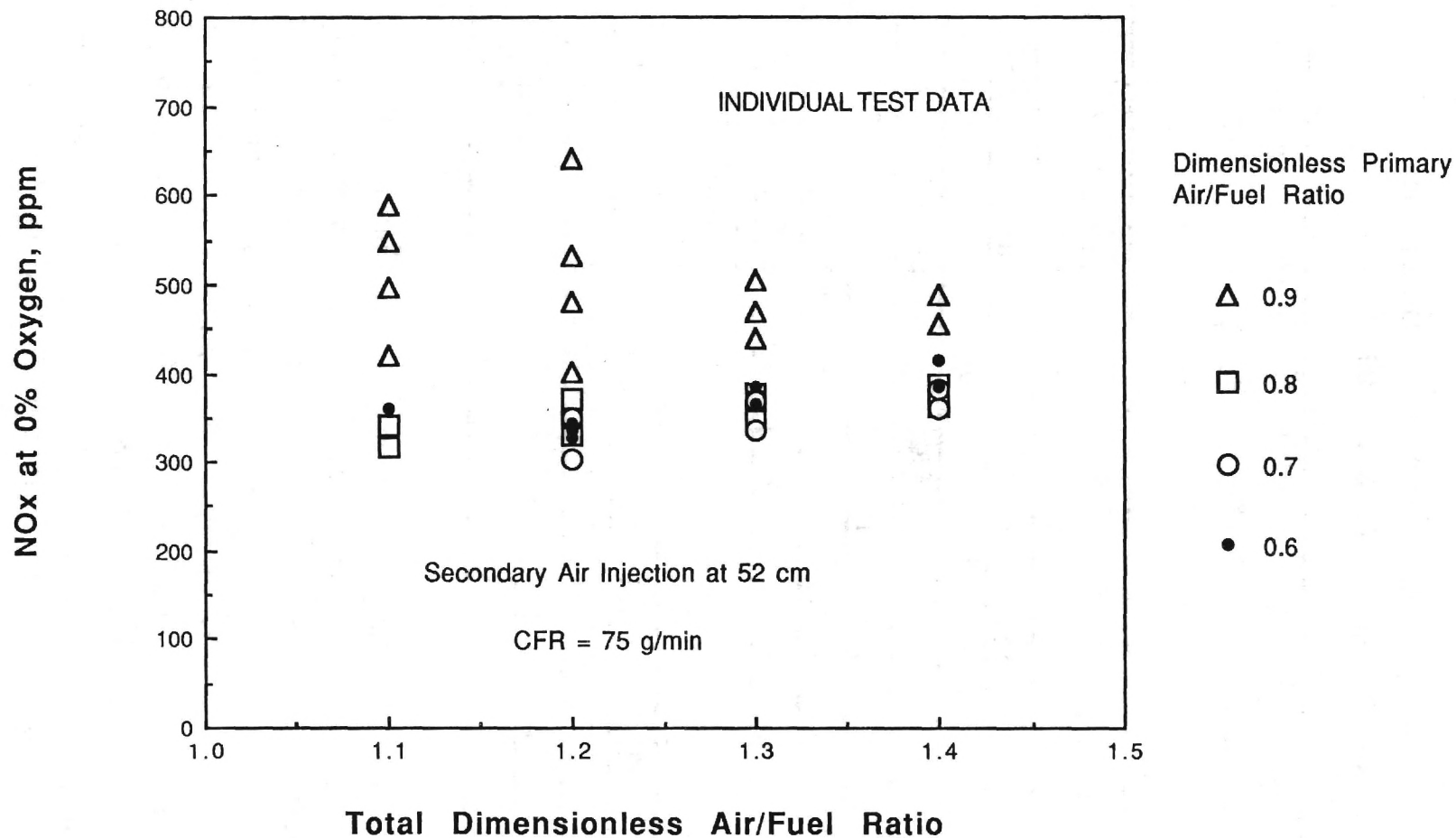
Figure 30. Individual Test Averages of Nitrogen Oxides Emissions for Air Staging Tests Showing the Effect of Total and Primary Air/Fuel Ratios.

dimensionless air/fuel ratio was decreased from 0.9 to 0.8, but only slight improvements were obtained by further decreases in the primary air/fuel ratio.

Mean values of sound pressure levels, combustion efficiencies and exhaust NO_x concentrations were also computed for each set of air staging parameters α_1 and α_t by taking the arithmetic average of the appropriate values shown in Tables IV and V. These mean values are given in Table VI.

Table VI. Averaged Air Staging Data for Experiments with $\alpha_t > 1.00$.

Primary Air/Fuel Ratio α_1	Total Air/Fuel Ratio α_t	Sound Pressure Level (dB)	Combustion Efficiency	NO_x (0% Oxygen) (ppm)
0.9	1.1	158.1	0.93	514
0.9	1.2	157.8	0.95	514
0.9	1.3	157.7	0.96	471
0.9	1.4	158.0	0.92	473
0.8	1.1	157.4	0.92	325
0.8	1.2	156.9	0.93	351
0.8	1.3	156.8	0.91	365
0.8	1.4	157.1	0.90	376
0.7	1.2	157.1	0.89	326
0.7	1.3	156.7	0.95	353
0.7	1.4	156.4	0.99	372
0.6	1.1	152.7	0.94	360
0.6	1.2	154.2	0.85	335
0.6	1.3	154.3	0.92	376
0.6	1.4	154.3	NA	399

The mean NO_x concentrations given in Table VI were plotted as a function of the total dimensionless air/fuel ratio, α_t, for each value of the primary dimensionless air/fuel ratio, α_1. These averaged NO_x

57

data are shown in Figure 31 along with the baseline NO_x concentrations obtained without air/staging. For the air staging data, a linear regression curve fit is shown for each primary air/fuel ratio, while a quadratic curve fit (nonlinear regression) is shown for the baseline data. Comparison of the air-staging curves with the baseline curve reveals that air staging yielded a very significant reduction in NO_x concentrations when expressed on a 0% oxygen basis. These reductions in NO_x emissions, which were small to modest for the lowest total air/fuel ratio (1.1), increased significantly as the total air/fuel ratio was increased. Extrapolation of the linear regression lines to $\alpha_t = 1.0$ shows that only small reductions or even increases ($\alpha_1 = 0.9$) in NO_x emissions occur with air staging to final stoichiometric conditions, which agrees with the results obtained in the first group of air staging experiments. The largest reductions in NO_x occurred when going from no air staging (baseline) to air staging with a primary dimensionless air/fuel ratio of 0.9. Significant further reductions in NO_x occurred with further reduction in the primary dimensionless air/fuel ratio to 0.8, but little additional reduction in NO_x emissions was obtained with lower primary air/fuel ratios. Close examination of Figure 31 shows that the optimum primary dimensionless air/fuel ratio for NO_x reduction is about 0.7. For this case the reduction in NO_x exhaust concentration due to air staging ranged from about 48 percent at $\alpha_t = 1.1$ to about 56 percent at $\alpha_t = 1.4$.

The averaged sound pressure levels from Table VI are plotted in Figure 32. For the air staging experiments with primary dimensionless air/fuel ratios of 0.7 to 0.9, sound pressure levels were generally about 2 to 4 decibels lower than those obtained without air staging (about 160 dB). This reduction in pulsation amplitude was expected since the combustion process no longer is completed at the optimum location in the Rijke tube (i. e., the point one fourth of the distance from the upstream end to the downstream end). With air staging, a significant fraction of the heat addition occurs in the region where the secondary air is injected, which is nearer to the midpoint of the tube. Even lower pulsation amplitudes,
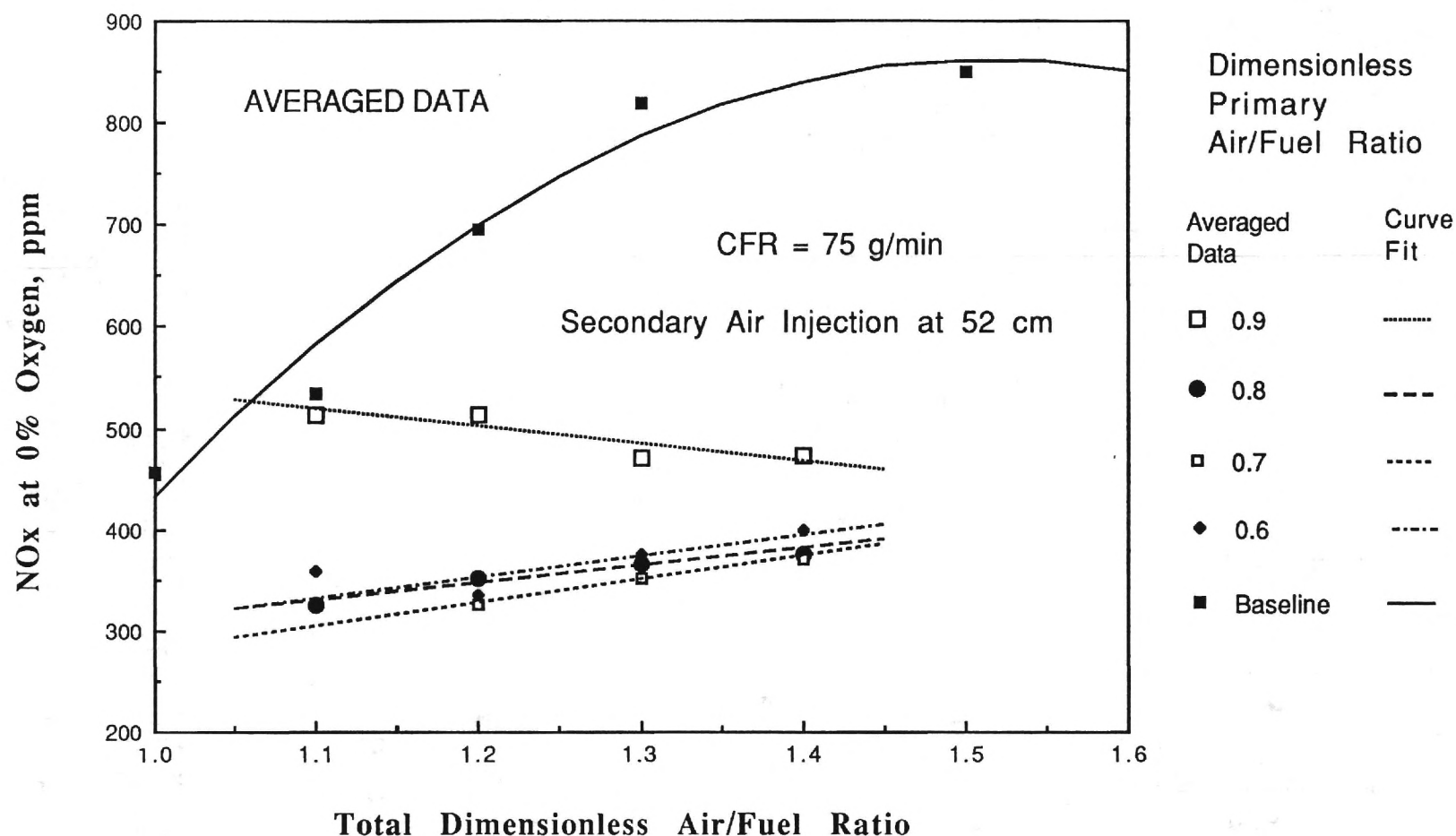
Figure 31. Comparison of Averaged Nitrogen Oxides Emissions for Air Staging Experiments with Baseline Experiments for Different Total and Primary Air/Fuel Ratios.
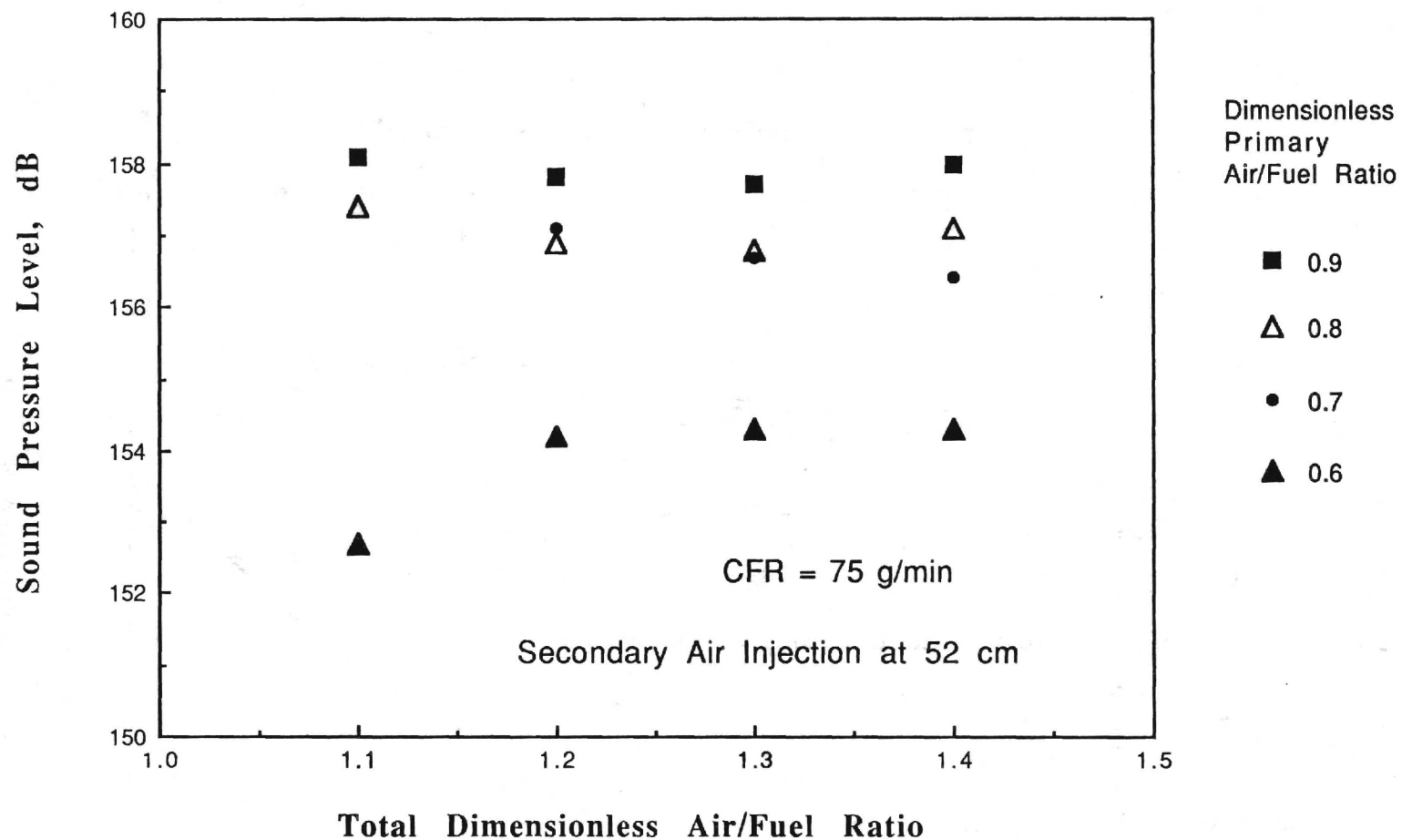
Figure 32.   Effect of Total Air/Fuel Ratio and Primary Air/Fuel Ratio on Sound Pressure Levels
for Air Staging Experiments.

from 6 to 7 decibels lower than baseline levels, were obtained when the primary air/fuel ratio was 0.6.

The averaged combustion efficiencies from Table VI are plotted in Figure 33. These efficiencies ranged from about 85 percent to 99 percent. Only for primary dimensionless air/fuel ratios of 0.9 and 0.8 is the combustion efficiency lower for the lower primary air/fuel ratio for all total air/fuel ratios tested. Thus the combustion efficiency is significantly influenced by factors other than the pulsation amplitude, since sound pressure levels generally decrease with decreasing primary dimensionless air/fuel ratio. One factor of considerable variability which influenced the combustion efficiency was the amount of unburned carbon in the refuse which fell through the rotating bed grid.

Gas temperatures were measured at the following eight stations above the coal bed: 7, 11, 15, 19, 23, 28, 62 and 107 cm. All of the thermocouples were positioned to measure the temperature at the axis of the combustor. Gas temperature profiles obtained during the experiments with secondary air injection at 52 cm above the bed are shown in Figures 34 and 35.

Figure 34 shows the temperature profiles for $\alpha_1 = 0.8$ and $\alpha_1 = 0.6$ for different dimensionless total air/fuel ratios (α_t). For $\alpha_1 = 0.8$ (upper graph) there is little effect of total air/fuel ratio on the temperature profiles, for which the gas temperature falls rapidly from about 1100 C at 7 cm above the bed to about 700 C at about 30 cm above the bed and decreases more gradually to about 500 C at about 110 cm above the bed. For $\alpha_1 = 0.6$ (lower graph) increasing the total air/fuel ratio from 1.2 to 1.4 increases the gas temperatures by about 100 C for all stations higher than 20 cm above the bed. This includes stations well below the secondary injection point, thus it is apparent that secondary air is being mixed with the incompletely burned gases above the bed by means of the acoustic velocity oscillations which produce reverse flow during part of each oscillation cycle. As a result of this mixing, further combustion occurs
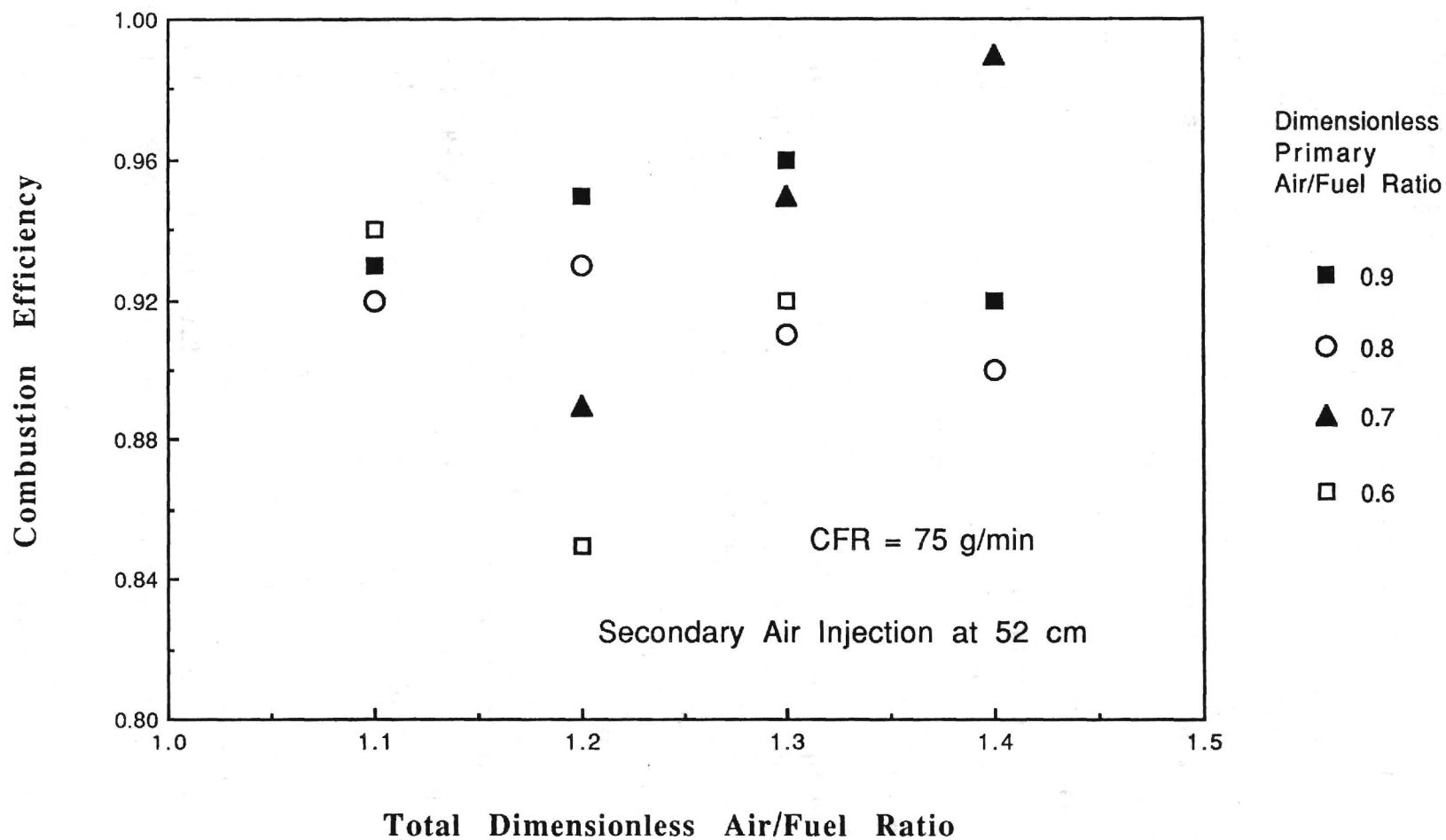
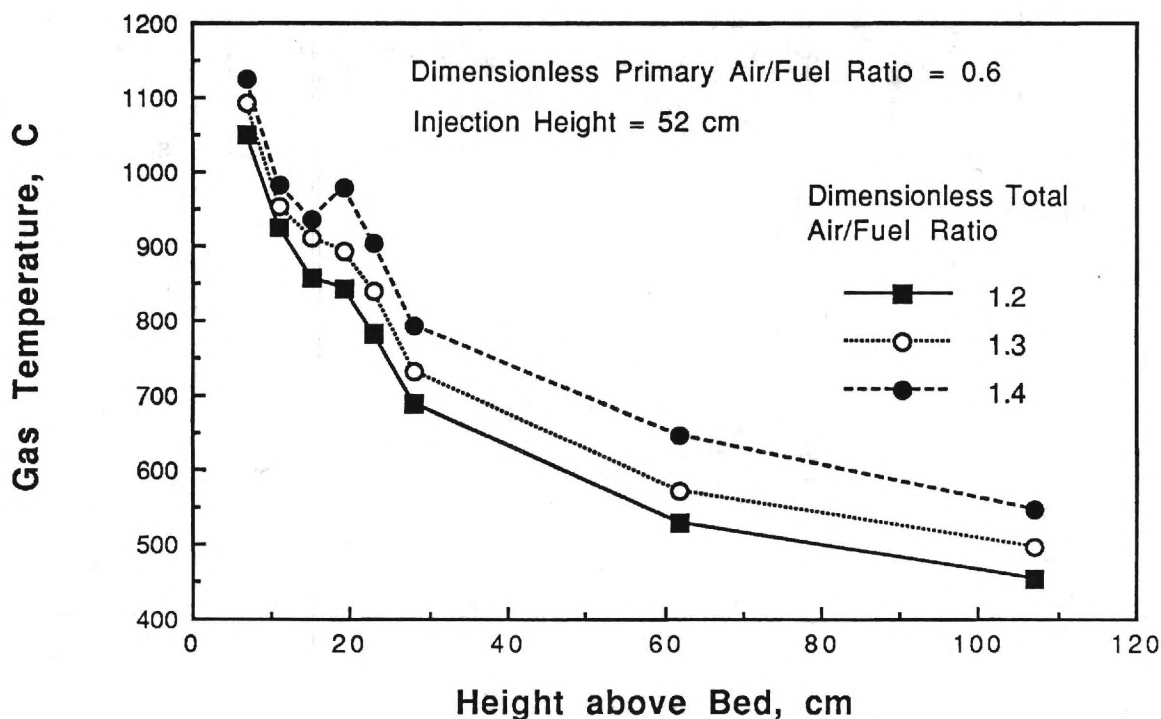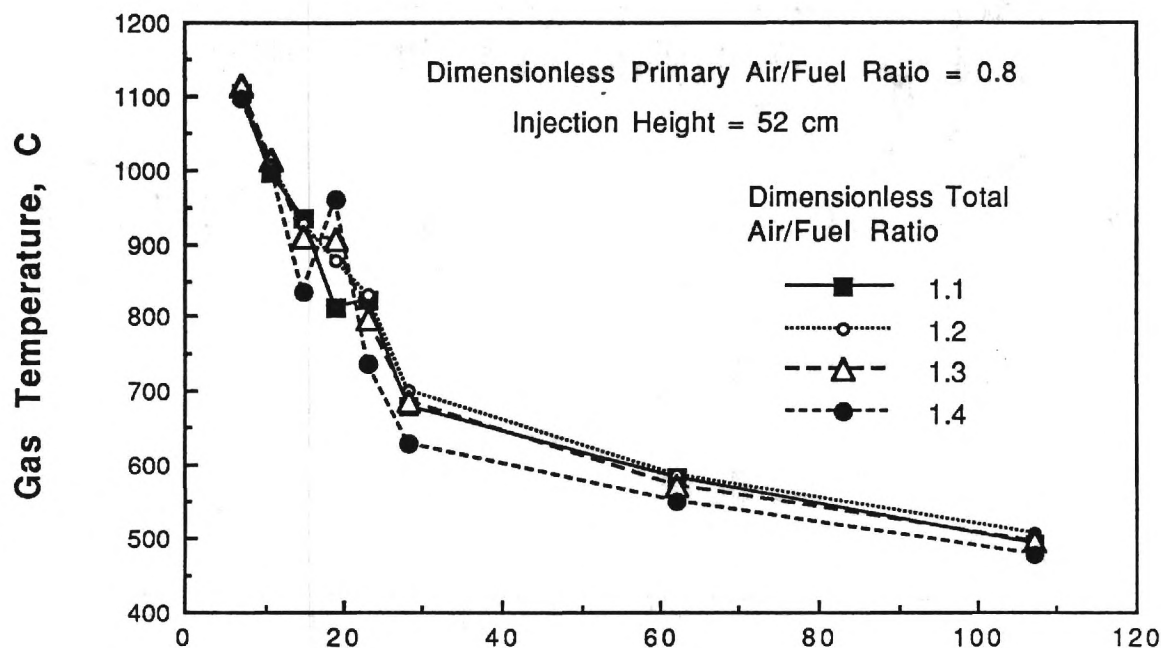Figure 33. Combustion Efficiencies for Air Staging Experiments.

Figure 34. Gas Temperature Profiles for Experiments with Secondary Air Injection at 52 cm for Primary Air/Fuel Ratios of 0.8 and 0.6.

63
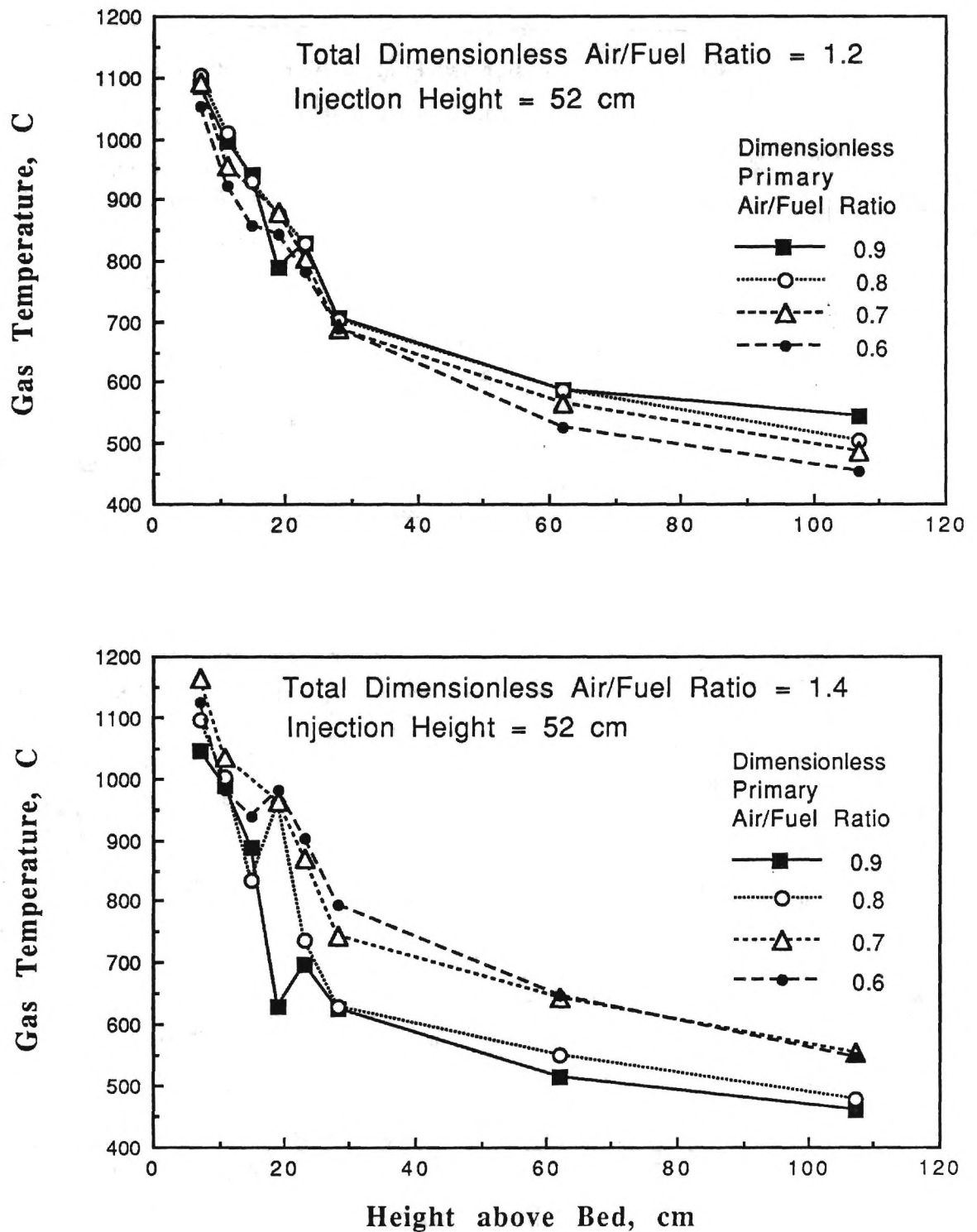
Figure 35. Gas Temperature Profiles for Experiments with Secondary Air Injection at 52 cm for Total Air/Fuel Ratios of 1.2 and 1.4.

in this region which accounts for the temperature rise. A somewhat smaller temperature rise with increasing α_t was obtained for $\alpha_1 = 0.7$ (not shown). For $\alpha_1 = 0.9$ (not shown) there was little effect of α_t on the temperature profiles for α_t between 1.1 and 1.3, and a temperature decrease was obtained with further increases in α_t to 1.4. For this highest primary air/fuel ratio, the amount of unburned combustible gases above the bed was small, so that the larger amounts of secondary air resulted in temperature decreases due to the dilution effect.

The temperature data can also be plotted for a fixed total dimensionless air/fuel ratio and different values of the dimensionless primary air/fuel ratio. Such plots for $\alpha_t = 1.2$ and $\alpha_t = 1.4$ are shown in Figure 35. For $\alpha_t = 1.2$ (upper graph) and below, decreasing the primary air/fuel ratio results in a moderate decrease in gas temperatures at stations higher than about 40 cm above the bed, while for $\alpha_t = 1.4$ (lower graph), decreasing the primary air/fuel ratio has the opposite effect on the gas temperatures over the same region. At the lower total air/fuel ratios, the amount of secondary air is insufficient to obtain complete combustion of the fuel (due to incomplete mixing) and temperature falls with decreasing primary air/fuel ratio. At the highest total air/fuel ratio, the secondary air is sufficient for nearly complete combustion and temperatures in the secondary combustion zone rise with decreasing primary air/fuel ratio. For $\alpha_t = 1.3$ (not shown) there is little effect of primary air/fuel ratio on gas temperatures.

NON-PULSATING EXPERIMENTS

A series of experiments was conducted under non-pulsating combustion conditions in order to determine the effect of pulsations on the performance of the combustor, particularly regarding NO_x and SO_2 emissions. Non-pulsating operation was obtained by partially opening the viewing window at the middle of the combustor, which forced the pressure perturbation to be zero where the pressure oscillations for the fundamental acoustic mode normally have their

maximum amplitude. To reduce the air leakage through this large opening, it was covered by a piece of cloth. A total of five non-pulsating experiments were conducted. Each experimental run was divided into four or five segments of about five minutes length. Most of the experiments were conducted without air staging, but in one of the experiments secondary air was injected 20 cm above the bed.

The results of the non-pulsating experiments without air staging are shown in Table VII and in Figures 36 through 39. The data shown are time-averaged values for the appropriate test segments. In Table VII, T_1 is the gas temperature measured on the axis of the combustor 18 cm above the bed. For test numbers 1-3, the coal feed rate was 75 g/min, while in test numbers 4 and 5, the coal feed rate was 40 g/min.

As shown in Table VII, there is considerable variation in the measured values from one experiment to another for the same dimensionless air/fuel ratio. This is due largely to the varying amounts of partially burned coal which fell through and around the periphery of the coal bed during the non-pulsating tests. Thus the effective air/fuel ratios varied considerably among each group of test segments with the same nominal dimensionless air/fuel ratio. Furthermore, the effective air/fuel ratios were always higher than the nominal values shown in Table VII. For this reason it was found to be more meaningful to plot the measured values of CO_2, CO, NO_x and SO_2 concentrations as a function of the O_2 concentration rather than the air/fuel ratio. The amount of residual oxygen remaining in the exhaust gases is a function of the both the nominal air/fuel ratio and the combustion efficiency. Plots of the concentrations of these four species as a function of residual oxygen concentration are shown in Figures 36 through 39.

The data shown in Figure 36 reveals that measured carbon dioxide concentrations for both pulsating and non-pulsating combustion are nearly linearly related to the residual oxygen concentration. For non-pulsating combustion, CO_2 concentrations

ranged from about 5 percent to about 11 percent, while the corresponding residual oxygen concentrations varied from about 15 percent to about 7 percent. Some of the scatter in the non-pulsating data results from differences in the dimensionless air/fuel ratios and coal feed rates for the different experiments. For the pulsating experiments, air/fuel ratios ranged from 0.6 to 1.5. The CO_2 concentrations for pulsating combustion were much higher with correspondingly lower residual O_2 concentrations. The pulsating experiments with the largest concentrations of residual oxygen corresponded to those with the largest amounts of excess air. These results show that the combustion efficiency is much lower under non-pulsating conditions, indicating incomplete combustion of the coal.

Table VII. Exhaust Gas Compositions and Above-Bed Temperatures for Non-Pulsating Tests Without Air Staging.

| Test Number	α	CO_2 (%)	CO (%)	NO_x (ppm)	SO_2 (ppm)	O_2 (%)	T_1 (C)
1	0.5	10.82	0.80	278	1412	6.50	994
2	0.5	10.10	1.01	199	1462	7.30	1082
3	0.5	5.15	0.35	114	831	14.77	1005
4	0.5	7.96	0.20	143	967	11.85	893
5	0.5	9.58	0.29	170	954	11.45	892
2	0.7	9.48	0.32	242	1064	8.76	1027
3	0.7	5.99	0.33	136	801	13.83	1034
4	0.7	6.83	0.10	125	1041	13.38	862
5	0.7	9.27	0.18	193	873	11.86	892
3	1.0	6.44	0.18	177	745	13.64	982
4	1.0	6.91	0.27	164	996	14.16	853
5	1.0	6.56	0.14	212	737	12.98	854
4	1.1	6.25	0.07	143	1043	15.15	860
5	1.1	NA	0.10	220	770	12.71	899
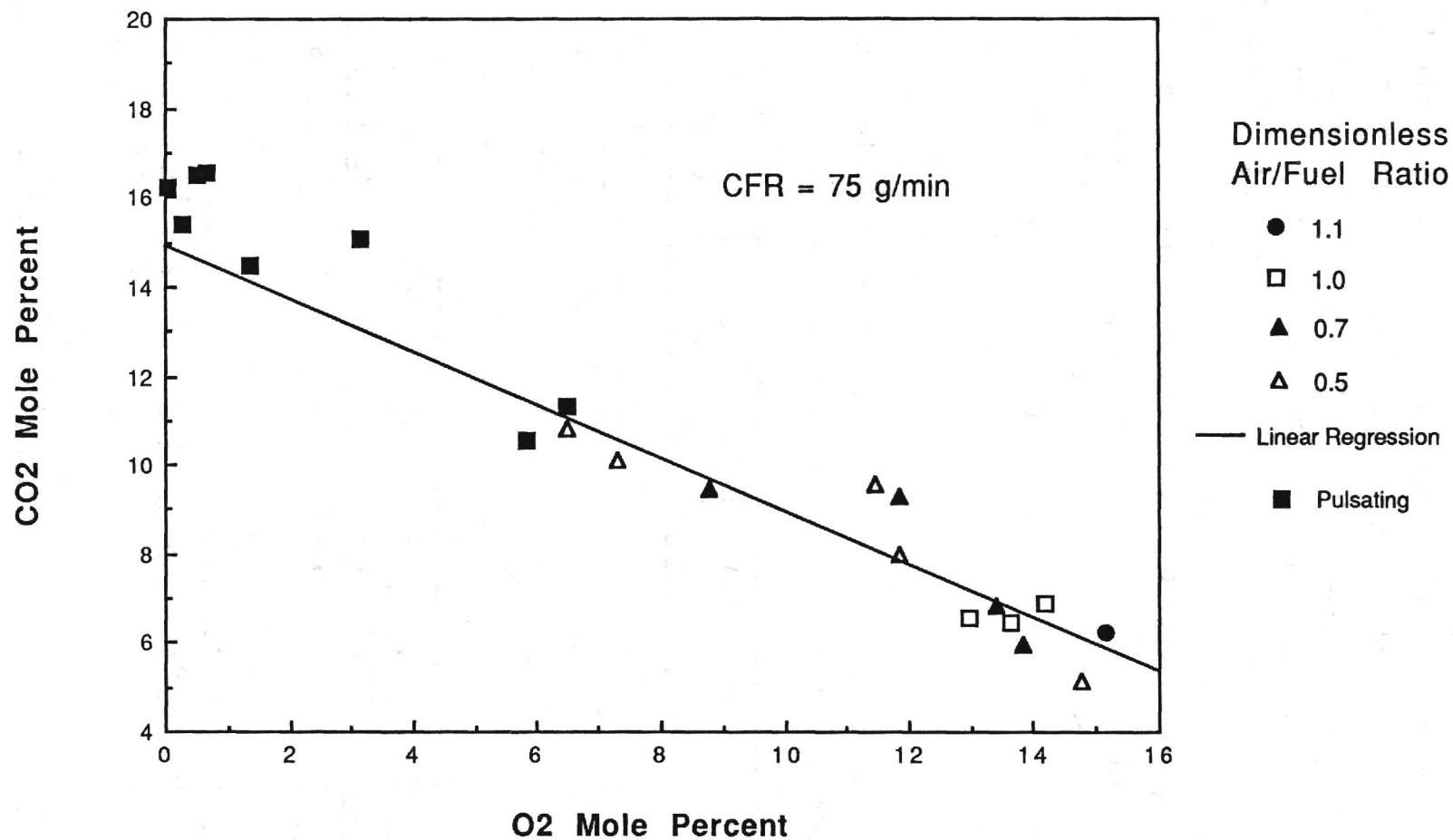
Figure 36. Comparison of Exhaust Carbon Dioxide Concentrations for Non-pulsating and Pulsating Combustion in the Rijke Combustor.

The carbon monoxide concentrations measured under non-pulsating combustion conditions are shown in Figure 37. Although there is considerable scatter in the CO data, there is a definite trend of decreasing CO concentration with increasing residual oxygen for the non-pulsating experiments. Similar results were obtained for pulsating combustion, but the corresponding residual oxygen levels were much lower due to the higher combustion efficiency. The decrease in CO concentration with increasing residual O_2 levels reflects the gas phase oxidation of CO to CO_2 in the region above the coal bed when ample oxygen is present.

The nitrogen oxides emissions measured under non-pulsating combustion conditions are shown in Figure 38. These data follow a definite trend of decreasing NO_x concentration with increasing O_2 concentration. Furthermore if a linear curve fit for the non-pulsating data is extended to very low residual oxygen levels, it agrees well with the pulsating combustion data for air/fuel ratios between 0.6 and 1.1, which is approximately the same range of α used in the non-pulsating experiments. For this range in α the residual oxygen levels are a good measure of combustion efficiency, since little or no excess air is present. It thus appears that as the combustion efficiency increases, as evidenced by the decrease in residual oxygen, the production of nitrogen oxides from fuel-bound nitrogen increases.

The non-pulsating data presented in Figure 38 also show a significant increase in NO_x production with increasing primary air/fuel ratio. For non-pulsating combustion under stoichiometric conditions and large residual O_2 levels (i.e., low combustion efficiency), NO_x concentrations averaged about 180 ppm, which decreased to about 115 ppm at an air/fuel ratio of about 0.5. The pulsating data for air/fuel ratios above 1.1 also exhibit this trend of increasing NO_x emissions with increases in excess air (Fig. 21). These results are consistent with the hypothesis that most of the NO_x is produced from fuel nitrogen and the amount produced is dependent on the availability of oxygen in the primary combustion zone. The
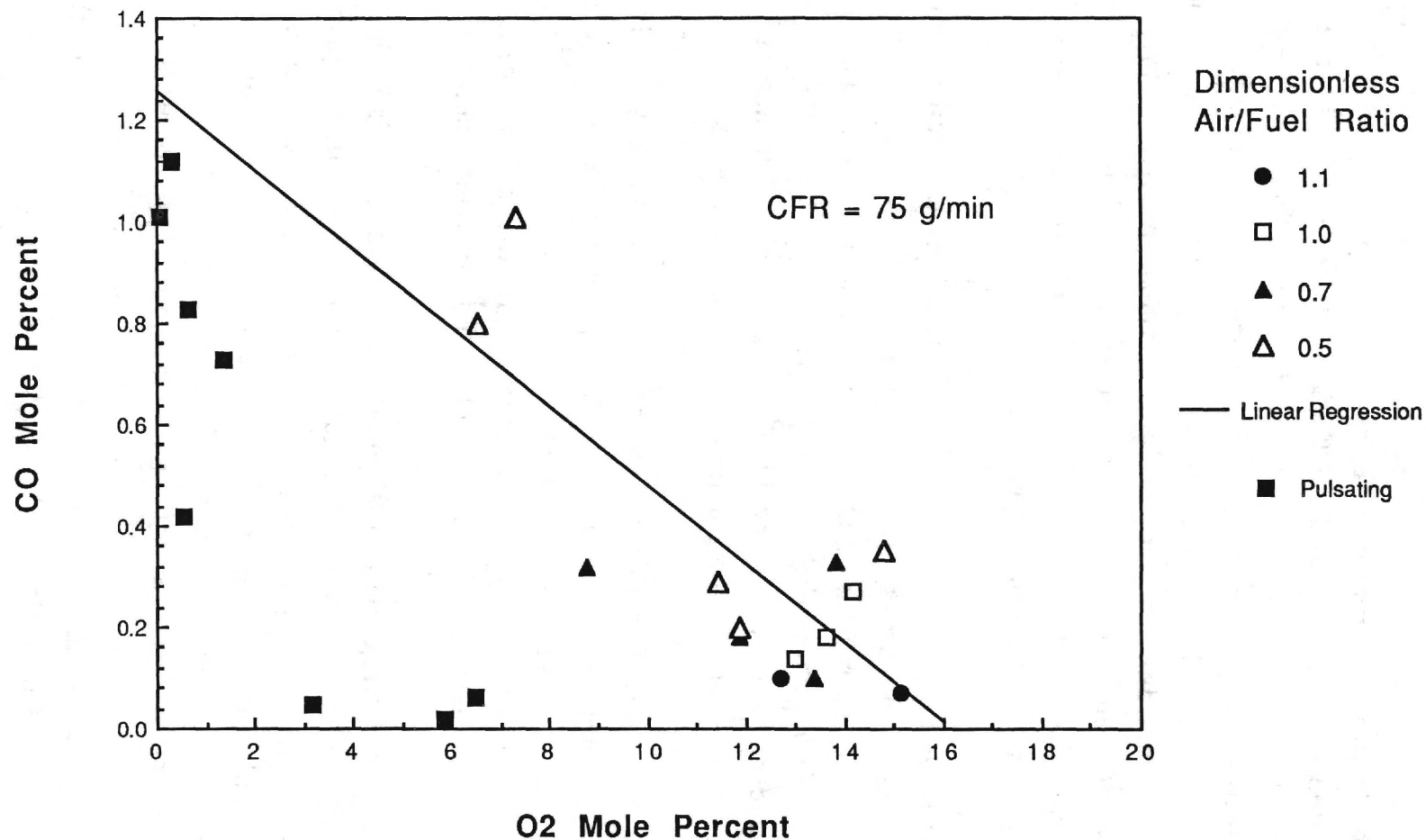
Figure 37. Comparison of Exhaust Carbon Monoxide Concentrations for Non-pulsating and Pulsating Combustion in the Rijke Pulse Combustor.
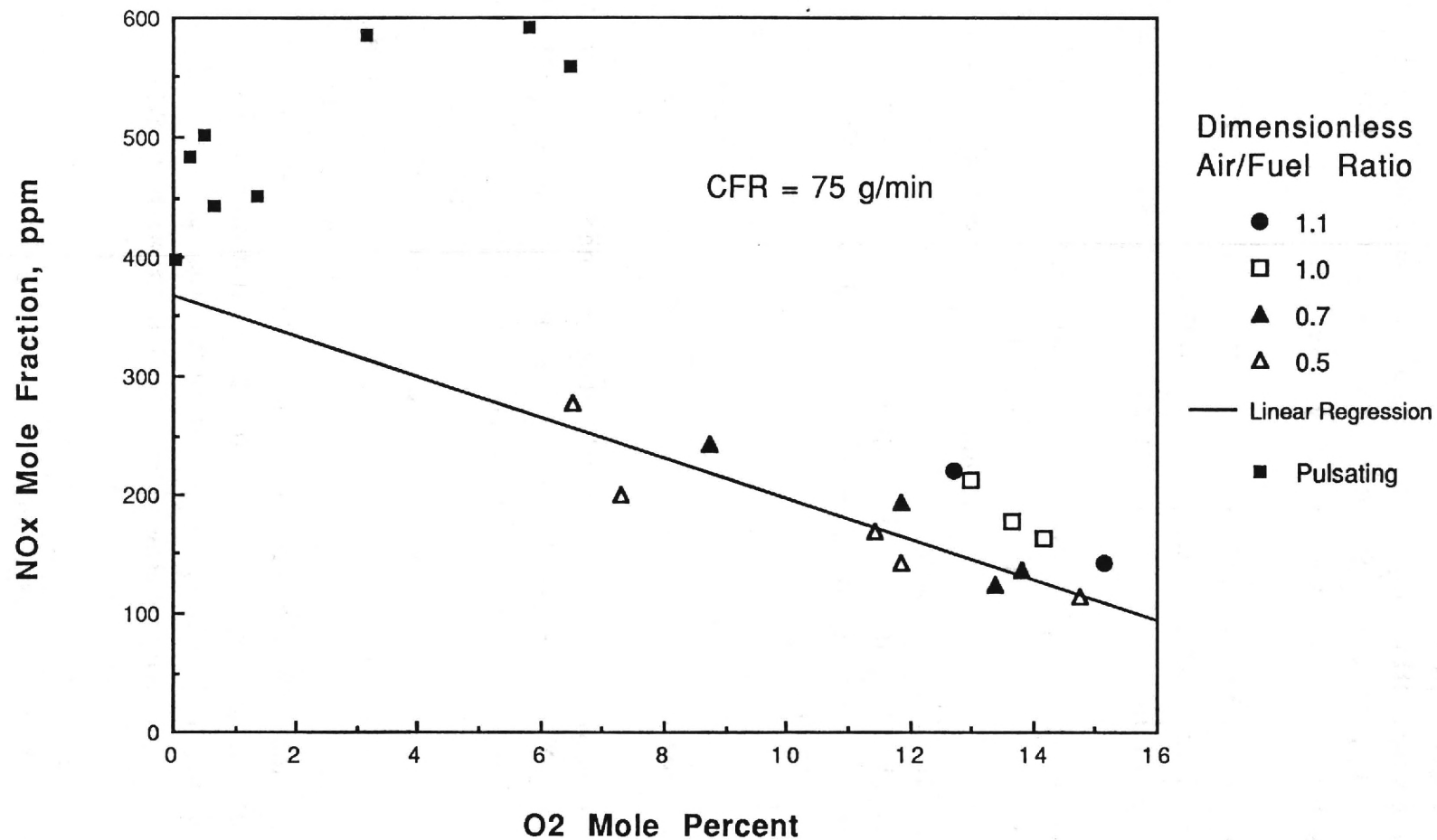
Figure 38. Comparison of Exhaust Nitrogen Oxides Concentrations for Non-pulsating and Pulsating Combustion in the Rijke Combustor.

NO_x concentrations under non-pulsating combustion at high residual O_2 (low combustion efficiency) were less than half (stoichiometric) to a fourth ($\alpha = 0.5$) of those produced under pulsating conditions with very low residual O_2 (high combustion efficiency).

Figure 39 shows the exhaust gas sulfur dioxide concentrations measured in both non-pulsating and pulsating experiments as a function of residual oxygen concentration. For substoichiometric burning in the primary combustion zone, there is a pronounced trend of decreasing SO_2 emissions with increasing residual O_2 concentrations (decreasing combustion efficiency). For the non-pulsating experiments under stoichiometric and excess air conditions, the scatter in the data is large, but the SO_2 emissions appear to be somewhat larger than in the corresponding substoichiometric tests. The SO_2 data for the pulsating tests, which follow closely a straight line curve fit, fall below the extension of the linear curve fit for the substoichiometric non-pulsating data. This is due partially to the fact that the largest SO_2 values shown in Figure 39 represent nearly complete conversion of the sulfur in the coal to sulfur dioxide.

For test number 3 in Table VII, two segments were run with air staging at 20 cm above the bed under non-pulsating combustion conditions. The first segment was conducted at a primary dimensionless air/fuel ratio of 0.7, while the second segment was conducted at $\alpha_1 = 0.5$. The results of these experiments showed that carbon dioxide and residual oxygen levels in the exhaust were not significantly affected by air staging under non-pulsating conditions. On the other hand carbon monoxide levels were drastically reduced by air staging, indicating that some of the combustion efficiency was recovered by nearly complete combustion of the CO formed in the primary combustion zone. However the CO apparently was only a small fraction of the coal which did not burn in the primary zone. It is suspected that most of the incompletely burned material under non-pulsating conditions was fixed carbon in the coal which was lost with the ash which fell through the bed. For non-pulsating experiments with air staging, the NO_x emissions were increased. For
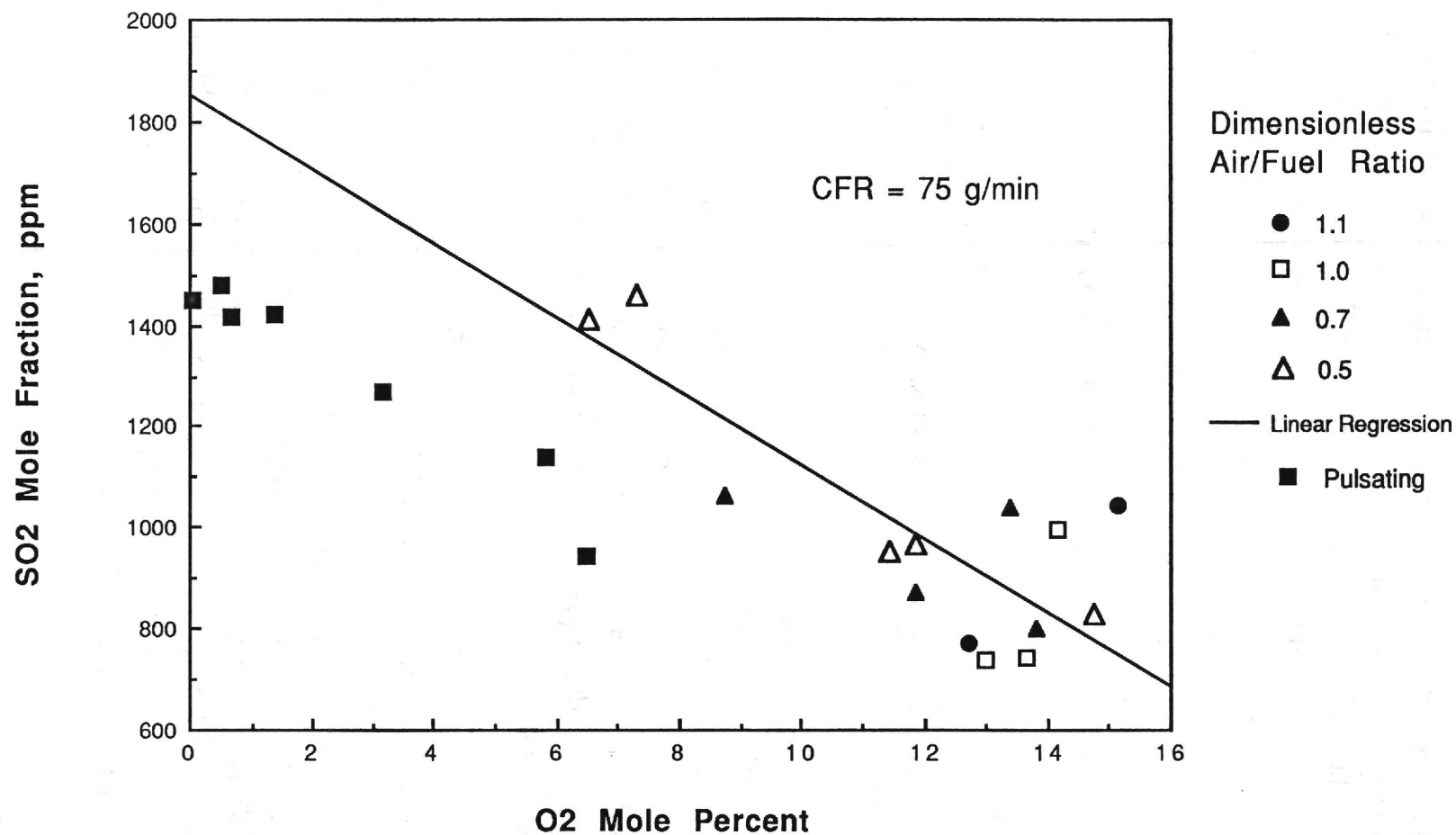
Figure 39. Comparison of Exhaust Sulfur Dioxide Concentrations for Non-pulsating and Pulsating Combustion in the Rijke Combustor.

example, at $\alpha = 0.7$, air staging increased the NO_x concentration from 135 ppm to 205 ppm, which was larger than that produced under stoichiometric conditions in the primary zone without air staging. A similar result was obtained for $\alpha = 0.5$. Since this increase occurred in the secondary combustion zone where fuel-bound nitrogen is not expected to be present, it was probably due to thermal NO_x production.

SORBENT ADDITION EXPERIMENTS

SORBENT MATERIALS

Two dolomitic limestone materials were obtained for use as sulfur capturing agents. Both are commercially available agricultural liming products used for reducing the acidity of soils. One of the materials is in a pelletized form with particle sizes between about 0.5 and 2 mm, while the other material is in a finely pulverized form with most of the particle sizes between 0.1 mm and 1.0 mm. The mass median diameter of the pulverized limestone is 0.4 mm. The pelletized dolomitic limestone contains about 24% calcium and 8% magnesium, while the pulverized material consists of 24% calcium and 6% magnesium.

The pelletized material is too coarse to pass through the auger feed and air entrainment system. This material is more suitable for mixing with the coal and introducing it into the combustor along with the coal using the coal feed system. On the other hand, the pulverized limestone was found to be unsuitable for directly mixing with the coal. Because the limestone particles are much smaller than the coal particles, they tend to settle to the bottom of the hopper by falling through the spaces between the coal particles. Thus uniform delivery of the limestone at a fixed Ca/S ratio is impossible by this method.

EXPERIMENTS WITH SORBENT INTRODUCED INTO COAL FEED SYSTEM

The first series of experiments with pulverized dolomitic limestone addition were conducted before the modifications of the air entrainment system were completed. The limestone auger was temporarily arranged to feed the limestone directly into the coal delivery tube. Thus the limestone and coal were fed together directly onto the coal bed grid during this series of experiments.

Each of these experimental runs was divided into two to five segments. In the first segment of a run, the combustor was operated in the pulsating mode for several minutes without sorbent addition. In subsequent run segments, dolomitic limestone was added at rates corresponding to Ca/S mole ratios ranging from 2.4 to 4.2. The coal feed rate was 75 g/min for all of these experiments. In most of the run segments, the dimensionless primary air/fuel ratio was 1.0 with no secondary air injection (air staging). In the remaining run segments the primary air/fuel ratio ranged from 1.1 to 1.6, again without air staging. The gas sampling and analysis system was used to determine sulfur dioxide concentrations in the exhaust gases. The results were reduced to a 0% oxygen basis in all cases.

The results of the these limestone addition experiments are shown in Figures 40 and 41. In Figure 40, sulfur dioxide concentrations are shown for all run segments with dimensionless air/fuel ratios of 1.0 and 1.2. The SO_2 concentrations obtained with sorbent addition can be compared with those obtained without sorbent addition (Ca/S = 0). For the cases with α = 1.0, there is no evidence in the data for significant SO_2 reduction when the pulverized dolomitic limestone was added. For the cases with α = 1.2, there appears to be a reduction of about 20% in SO_2 emissions when compared with the α = 1.0 case. In Figure 41, the effect of primary air/fuel ratio upon SO_2 concentrations are shown for a Ca/S mole ratio of 4.2. Here the individual data are plotted for
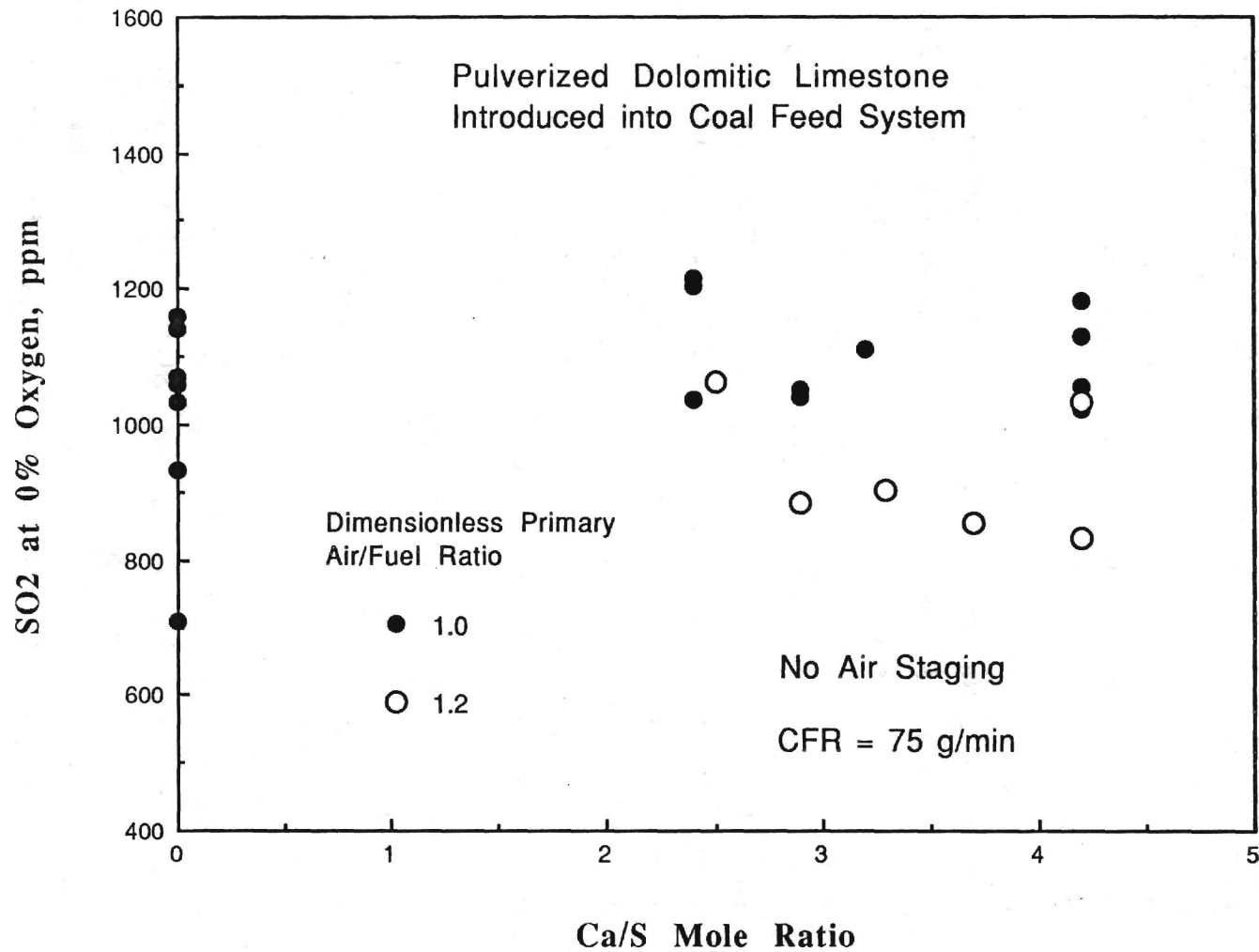
75

Figure 40. Effect of Ca/S Ratio on Sulfur Dioxide Emissions for Experiments with Sorbent Introduced into Coal Feed System.
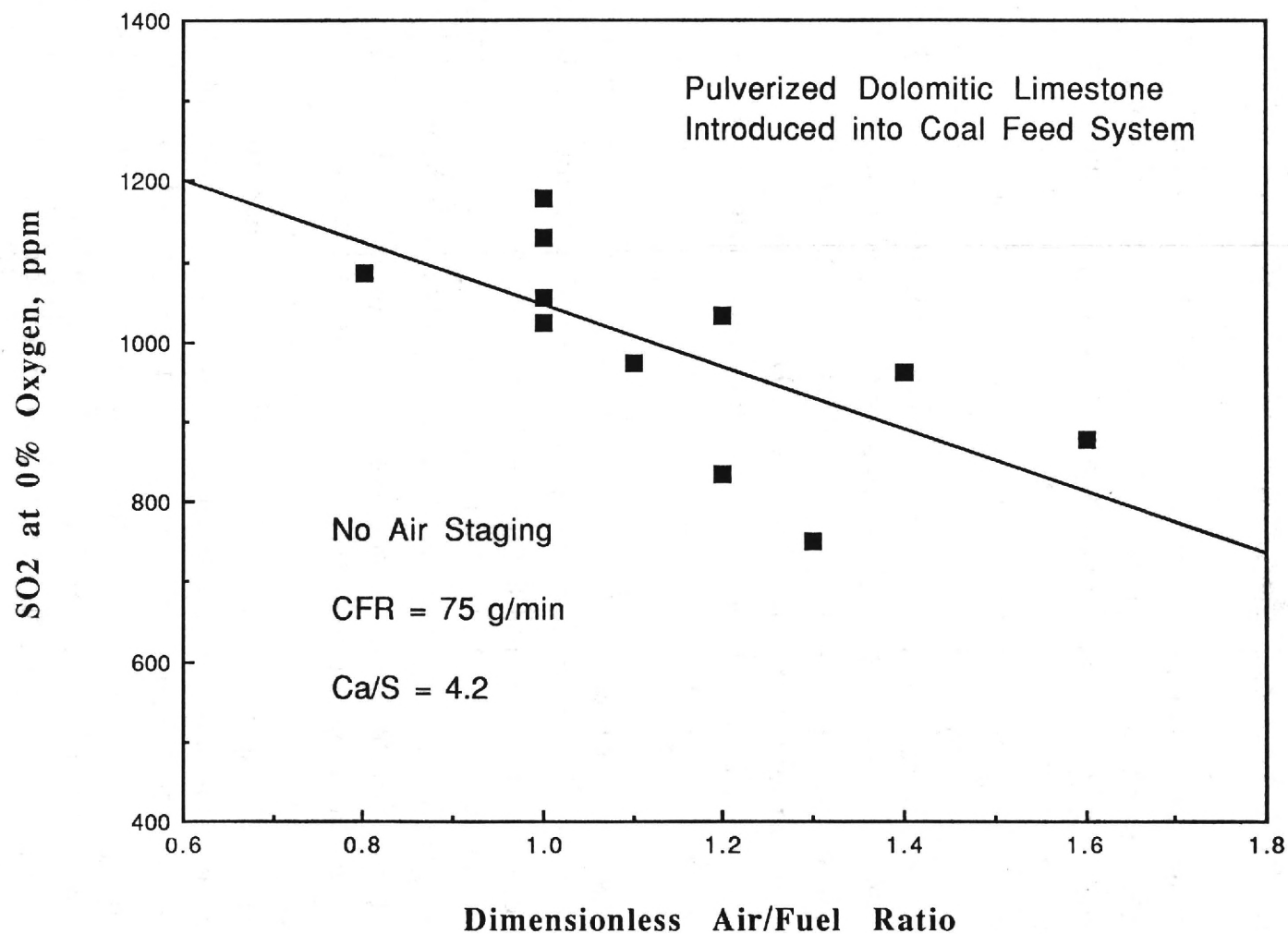
Figure 41. Effect of Air/Fuel Ratio on Sulfur Dioxide Emissions for Experiments with Sorbent Introduced into Coal Feed System.

all of these run segments along with a linear regression curve fit. This shows a definite trend of decreasing SO_2 emissions when the dimensionless air/fuel ratio is increased. This result can be explained by the fact that some residual oxygen is needed in order to complete the sulfur capture process; that is, to convert the SO_2 into $CaSO_4$.

Three additional experiments in this series were conducted, where the limestone was injected into the combustor using the air entrainment system. Each experiment was divided into three run segments, with the first segment being conducted without limestone addition. In the other run segments, limestone was added with Ca/S ratios ranging from 3.6 to 8.0. In the first two experiments the primary air/fuel ratio was 1.0, while a small amount of secondary air was needed for injection of the limestone. In the third experiment, the primary air/fuel ratio was 0.8. The coal feed rate was 75 g/min for all of the experiments. Measured SO_2 concentrations indicated that little or no reduction in SO_2 occurred as a result of the limestone injection even at the highest Ca/S ratio used.

There are three factors that are probably involved in the failure of the limestone addition to result in significant reduction in sulfur dioxide in this initial series of experiments: residence time, oxygen availablity, and reaction temperature. When the limestone was introduced through the coal delivery tube or through the air entrainment system, the larger limestone particles fell to the coal bed where the temperature was too high for effective sulfur dioxide capture, while the smallest particles were rapidly carried out with the flow of the exhaust gases. For adequate residence time for sulfur dioxide removal, the limestone particles should be of an intermediate size so that they neither fall to the bed nor are rapidly elutriated. Also the primary combustion zone should be provided with excess air to provide adequate residual oxygen needed for sulfur dioxide removal. Finally a means of temperature control in the region immediately above the bed is needed in order to maintain the gas temperature in the optimum range for sulfur dioxide capture.

EXPERIMENTAL RESULTS WITH PULVERIZED DOLOMITIC LIMESTONE

A more extensive series of experiments was conducted with modifications in the pulverized limestone addition procedure and operating parameters to determine if significant reductions in sulfur dioxide emissions can be obtained in the Rijke combustor. One of the modifications was the installation of a water cooled coil extending from about 5 cm below the limestone injector to about 15 cm above the injector. Some of these experiments were conducted with excess air in the primary combustion zone in order to provide adequate oxygen for sulfur dioxide removal. Finally, for some of the experiments, the limestone was further pulverized to reduce the size of the larger particles and sieved to remove the smaller particles in order to obtain particles of about 0.04 mm in diameter.

A total of 13 experiments were conducted in this series. Each experiment was divided into two to four segments. In the first segment, the combustor was operated in the pulsating mode for several minutes without sorbent addition. In subsequent segments, pulverized dolomitic limestone was introduced using the sorbent entrainment/injection system at rates corresponding to Ca/S mole ratios ranging from 1.8 to 8.0. The coal feed rate was 75 g/min for all of the experiments. In these experiments, the dimensionless primary air/fuel ratio was 1.0 or 1.1 with small amounts of secondary air injection (air staging) needed to deliver the sorbent material. Total dimensionless air/fuel ratios ranged from 1.05 to 1.30. Experiments were conducted at sorbent injection heights of 15 cm and 23 cm above the coal bed.

The gas sampling and analysis system was used to determine carbon dioxide, oxygen, and sulfur dioxide concentrations in the exhaust gases for all of these experiments. The measured sulfur dioxide concentrations were first corrected by subtracting a background reading to account for residual SO_2 in the sampling lines and the interfering effects of moisture. The corrected SO_2 concentrations were reduced to a 0% oxygen basis in all cases. In

addition, sound pressure levels and gas temperatures were measured for all of these experiments. The gas temperatures were obtained at heights of 10, 15, 20, 25, 30, 36, 157, and 272 cm above the coal bed.

Real time measurements of the exhaust concentrations of sulfur dioxide, carbon dioxide, and residual oxygen, and measured sound pressure levels are shown in Figures 42 through 44 for an experiment with sorbent injection at 23 cm above the bed. During the first nine minutes of this experiment, the combustor was operated in pulsating mode without sorbent injection (Ca/S = 0). The pulverized dolomitic limestone was then introduced through the air entrainment system at a Ca/S ratio of 3.3 for the remainder of the experiment. Figure 42 shows the sulfur dioxide concentrations as a function of time during this experiment. The SO_2 concentrations fluctuated about a mean value of about 860 ppm without sorbent addition. When the sorbent was introduced, exhaust SO_2 concentrations decreased steadily over the next seven minutes, reaching a steady state level of about 300 ppm during the last six minutes of the run. This represents about a 65 percent reduction in exhaust SO_2 concentration as a result of the limestone addition. The effect of limestone addition on the exhaust carbon dioxide and oxygen concentrations is shown in Figure 43. Although there appears to be a slight decrease in CO_2 and a corresponding increase in O_2 levels near the end of the experimental run, indicating a decrease in combustion efficiency, it does not appear to be associated with the sorbent injection process which began about ten minutes earlier. Measured sound pressure levels for this experiment are shown in Figure 44. Here the pulsation amplitude is not affected by the sorbent injection process, remaining constant at about 158 dB for most of the experimental run. The decrease in pulsation amplitude during the last four minutes of the run probably accounts for the decreased combustion efficiency noted above.

The results of the experiments with pulverized dolomitic limestone injection are summarized in Tables VIII and IX. Table VIII gives time averaged values of exhaust SO_2, O_2, CO_2 concentrations,

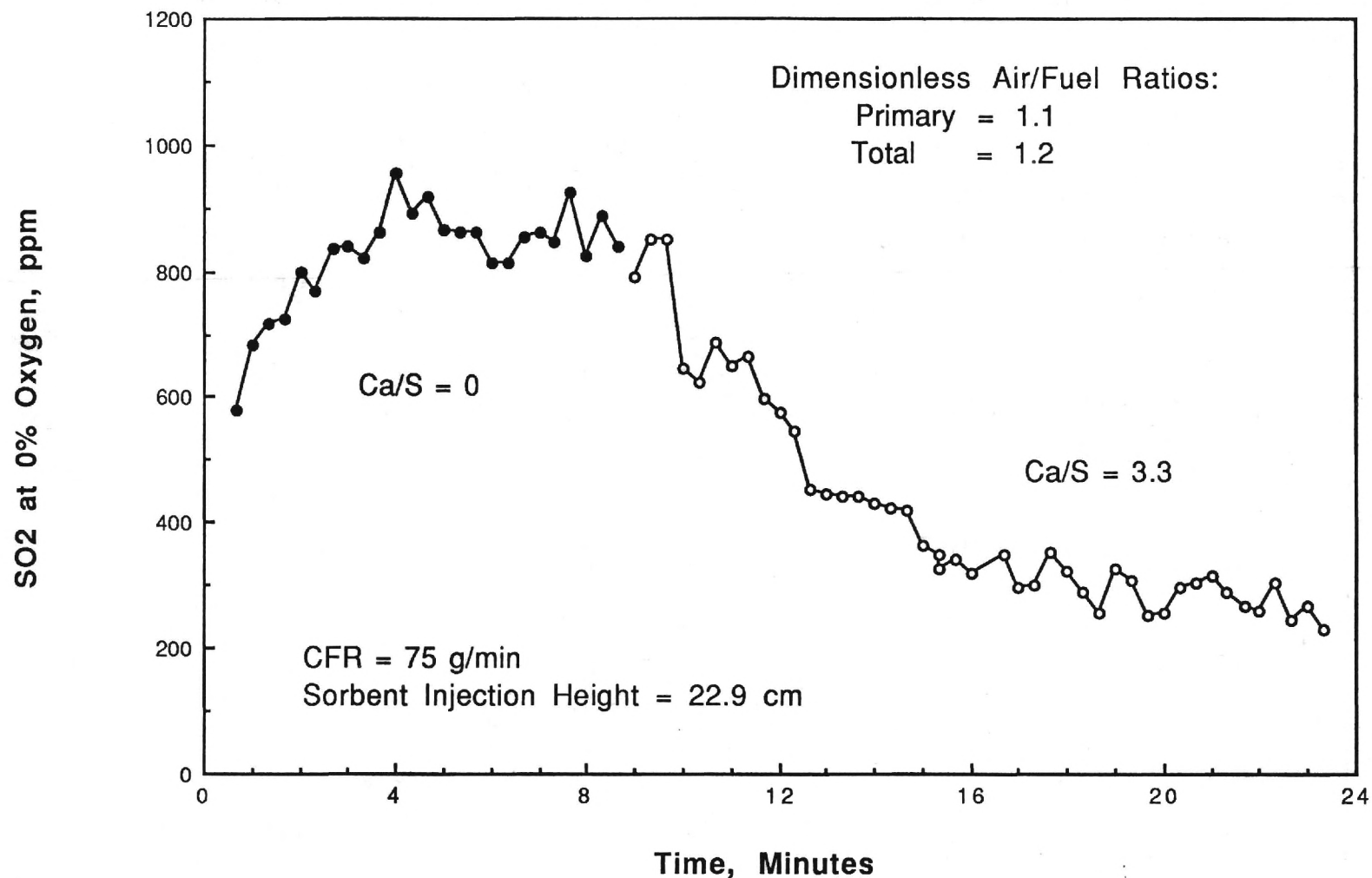Figure 42. Real Time Sulfur Dioxide Concentrations for a Typical Experiment with Pulverized Dolomitic Limestone Injection Above Bed.
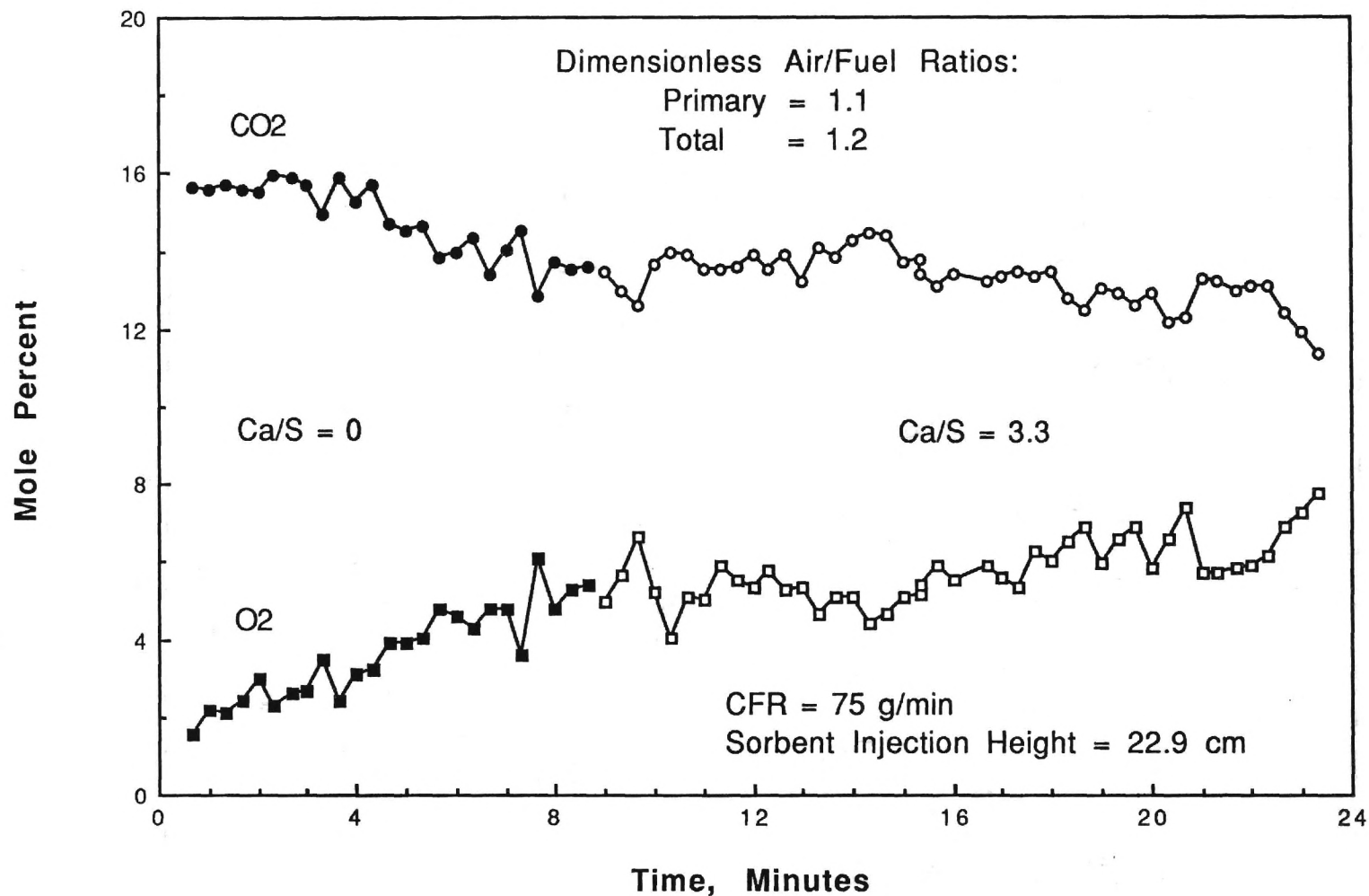
Figure 43. Real Time Carbon Dioxide and Oxygen Concentrations for a Typical Experiment with Pulverized Dolomitic Limestone Injection Above Bed.
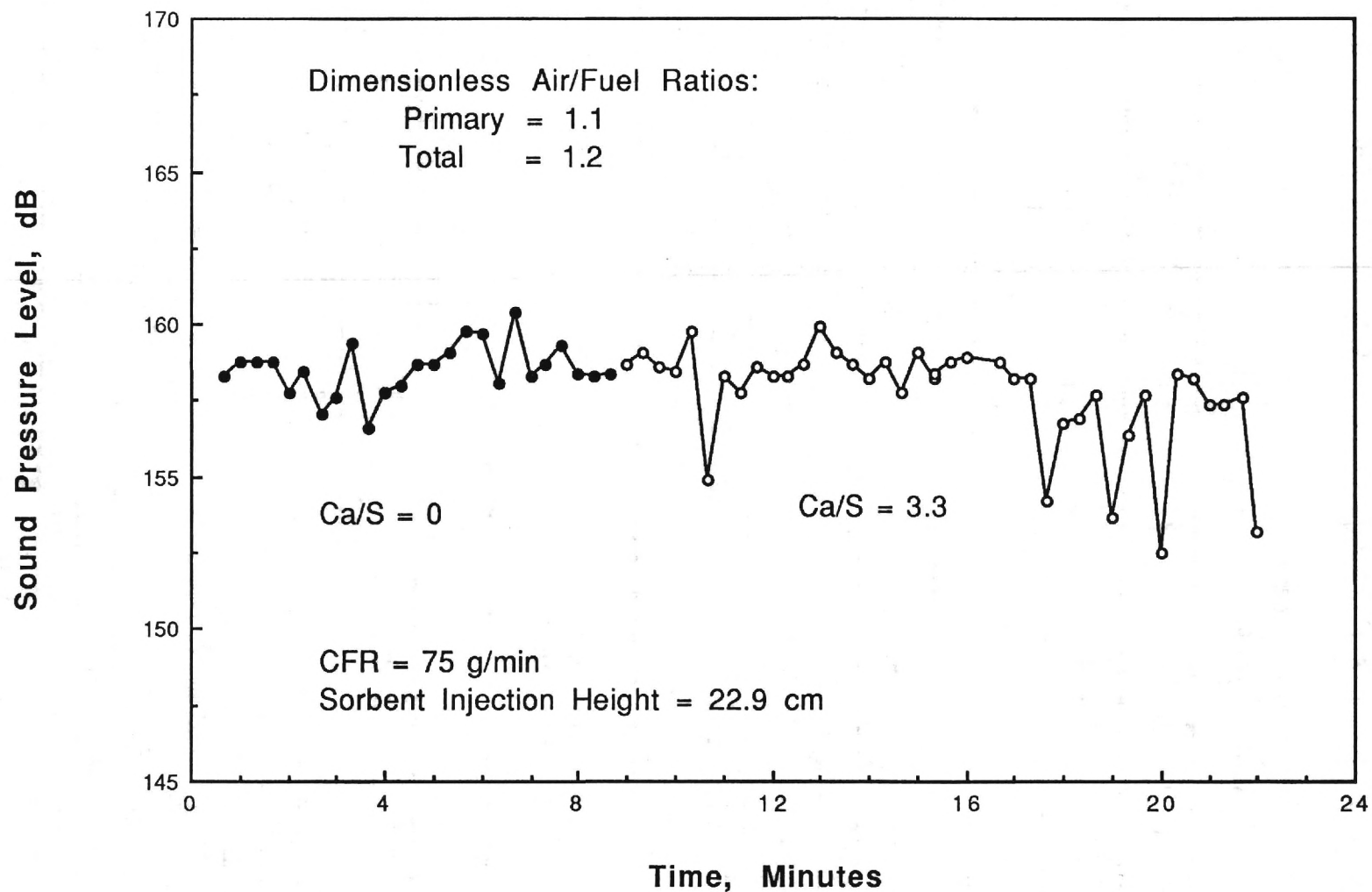
Figure 44. Real Time Sound Pressure Levels for a Typical Experiment with Pulverized Dolomitic Limestone Injection Above Bed.

sound pressure levels (SPL), and gas temperatures at 15 cm above the bed (T_2) for sorbent injection at 15 cm above the bed. Table IX gives the same data for sorbent injection at 23 cm above the bed.

Table VIII. Results of Sorbent Addition Experiments with Injection Height of 15 cm.

Run No.	Ca/S	α_1	α_t	SO$_2$ (ppm)	O$_2$ (%)	CO$_2$ (ppm)	SPL (dB)	T$_2$ (C)
3	0.0	1.1	1.2	894	6.45	12.01	155.0	1058
3	6.0	1.1	1.2	628	6.60	12.25	151.6	1076
4	0.0	1.1	1.2	1078	4.62	14.60	158.0	1132
4	4.0	1.1	1.2	654	5.90	14.31	156.8	1144
5	0.0	1.1	1.2	720	5.83	11.86	158.6	1040
6	0.0	1.1	1.2	945	5.37	14.42	158.9	1086
10	4.0	1.0	1.1	490	6.23	12.58	157.8	1035
10	5.5	1.0	1.1	298	6.90	12.01	157.6	1042
10	6.5	1.0	1.1	260	6.57	12.38	157.3	1058
11	0.0	1.0	1.2	900	5.50	12.98	157.6	1055
11	4.0	1.0	1.2	287	7.17	11.79	156.8	1015
12	1.8	1.0	1.1	402	6.39	12.59	156.9	987
13	2.4	1.1	1.05	155	5.82	13.48	156.0	1017

Table IX. Results of Sorbent Addition Experiments with Injection Height of 23 cm.

Run No.	Ca/S	α_1	α_t	SO$_2$ (ppm)	O$_2$ (%)	CO$_2$ (%)	SPL (dB)	T$_2$ (C)
1	0.0	1.1	1.3	1235	4.55	13.29	157.9	1091
1	6.0	1.1	1.3	998	7.39	11.02	158.0	1079
1	8.0	1.1	1.3	944	7.35	11.12	158.0	1078
2	0.0	1.1	1.3	1123	5.85	12.14	158.0	1077
2	6.0	1.1	1.3	548	6.63	11.97	157.4	1089
2	8.0	1.1	1.3	280	5.47	13.70	156.9	1135
7	0.0	1.0	1.2	859	4.40	14.21	158.7	1091
7	3.3	1.1	1.2	299	6.15	12.96	153.8	1109
8	3.3	1.0	1.1	572	5.67	14.77	157.1	1125
9	3.3	1.0	1.2	622	6.76	9.74	151.1	1023

Inspection of Tables VIII and IX reveals considerable variation in measured species concentrations for similar conditions. For example, exhaust SO_2 concentrations ranged from about 720 ppm to 1240 ppm for operation without limestone injection, and for limestone injection at 15 cm above the bed with a Ca/S ratio of 4.0, SO_2 concentrations varied from 290 ppm to 650 ppm. At an injection height of 23 cm and a Ca/S ratio of 3.3, SO_2 concentrations ranged from about 300 ppm to 620 ppm. It is unlikely that these variations are caused by the differences in the primary and total dimensionless air/fuel ratios (α_1 and α_t) for these experiments. It is more likely that some other factors, such as sorbent particle size distribution and gas temperature, which are difficult to control in these experiments, are causing these variations in SO_2 emissions. Carbon dioxide and oxygen concentrations exhibited smaller but significant variations, indicating variations in combustion efficiency. Over all of the experiments, CO_2 concentrations ranged between 9.7 and 14.8 percent, while O_2 concentrations varied from 4.4 to 7.4 percent. Sound pressure levels ranged from about 150 dB (case with lowest CO_2 concentration) to about 159 dB. Gas temperatures at 15 cm above the bed varied from about 990 C to about 1140 C.

The effect of Ca/S mole ratio on sulfur dioxide concentrations for this series of experiments is shown in Figure 45 for sorbent injection at 15 cm above the bed and in Figure 46 for a sorbent injection height of 23 cm. For the lower injection height (Figure 45), sorbent injection consistently resulted in lower SO_2 emissions than the baseline average of about 910 ppm, with the lowest emissions being obtained for the five experiments conducted with $\alpha_1 = 1.0$ and $\alpha_t = 1.1$. Only for this case, was there sufficient data to show a mild trend of decreasing SO_2 emissions with increasing Ca/S ratio. The greatest reduction in SO_2 concentration of about 83 percent occurred for the experiment conducted at Ca/S = 2.4 (#13). For this case and one conducted at a Ca/S ratio of 1.8 (#12), the sorbent particle size was the smallest, about 40 μm. For the highest primary and total air/fuel ratios ($\alpha_1 = 1.1$ and $\alpha_t = 1.2$), the reductions in SO_2 emissions were much smaller, averaging about 35 percent. For
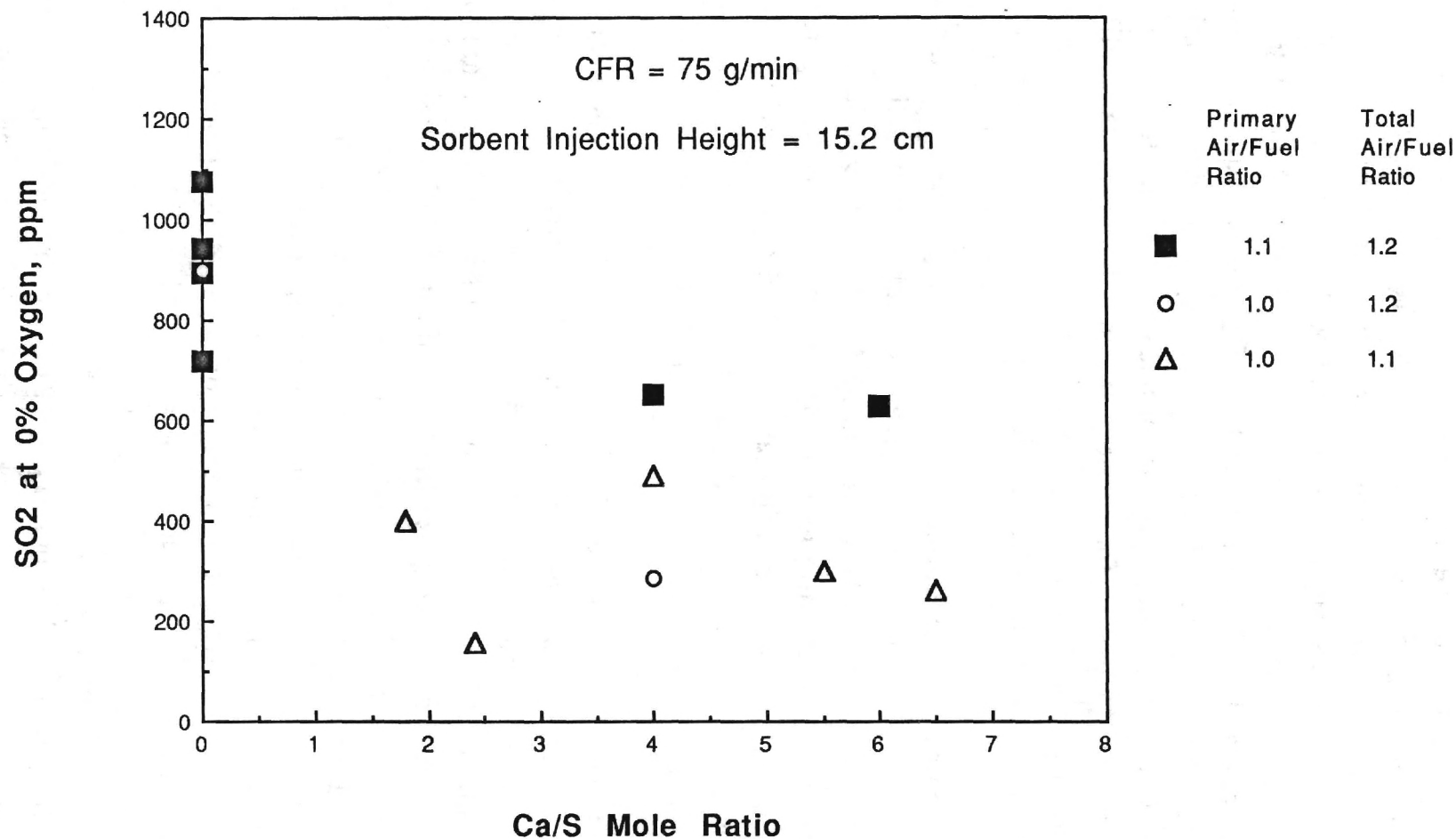
Figure 45. Effect of Ca/S Ratio upon Sulfur Dioxide Concentrations for Experiments with Pulverized Dolomitic Limestone Injection at 15 cm Above the Bed.
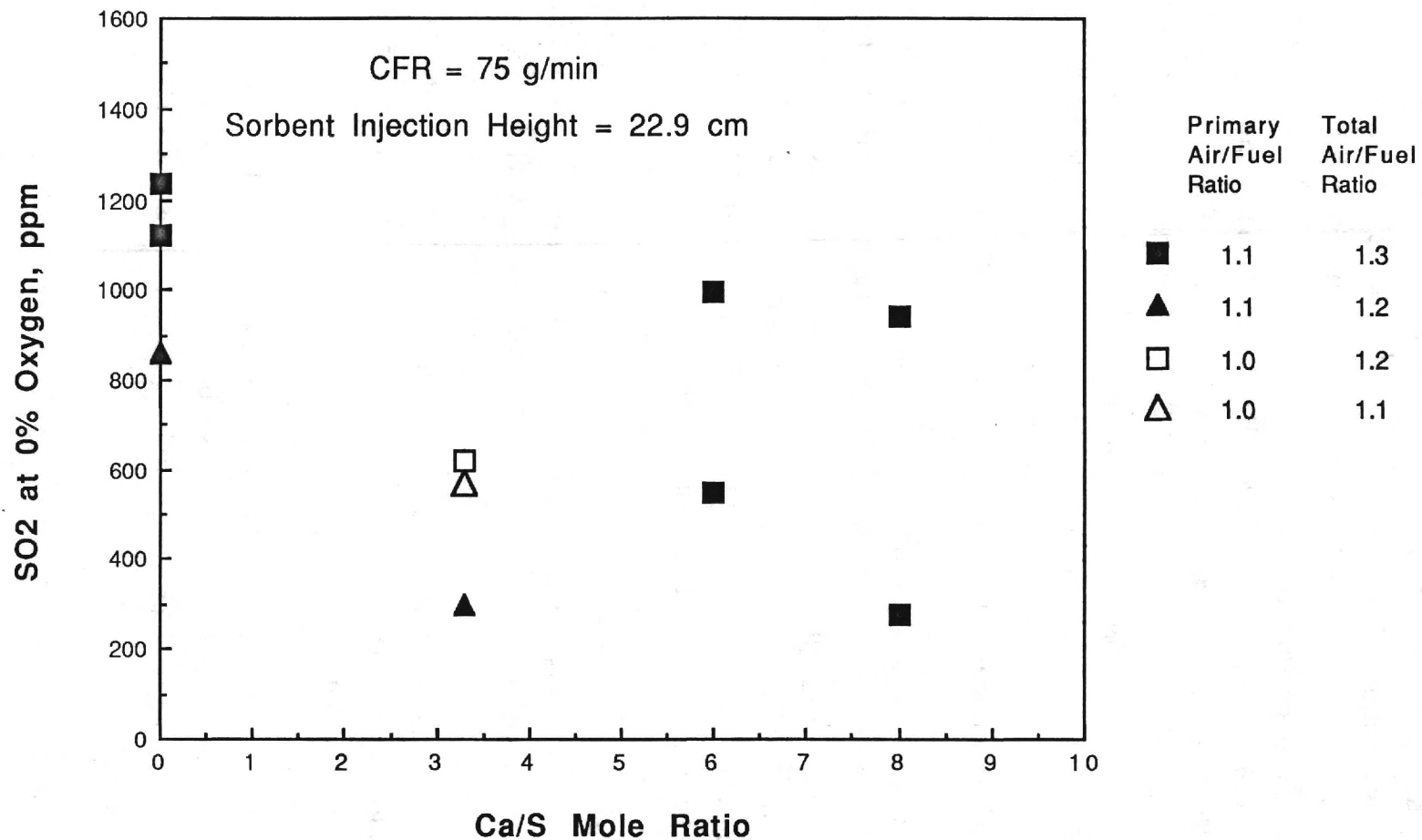
Figure 46. Effect of Ca/S Ratio upon Sulfur Dioxide Concentrations for Experiments with Pulverized Dolomitic Limestone Injection at 23 cm Above the Bed.

sorbent injection at 23 cm (Figure 46), most of the experiments were conducted with $\alpha_1 = 1.1$ and $\alpha_t = 1.3$. Here the average baseline SO_2 concentration was about 1180 ppm, and SO_2 reductions ranged from about 20 percent (#1 at Ca/S of 6) to about 75 percent (#2 at Ca/S = 8). Three experiments with a Ca/S ratio of 3.3 and different primary and total air/fuel ratios are also shown. Here increasing the primary air/fuel ratio for a fixed total air/fuel ratio ($\alpha_t = 1.2$) resulted in a significant reduction in SO_2 emissions, while changing the total air/fuel ratio for a fixed primary air/fuel ratio ($\alpha_1 = 1.0$) had little effect on SO_2 concentration. Comparison of the data shown in Figures 45 and 46 shows no clear effect of sorbent injection height upon the exhaust concentration of SO_2 for this series of experiments.

Due to the large amount of scatter in the graphs of SO_2 concentration versus Ca/S ratio, additional graphs were plotted in order to correlate SO_2 emission with other variables such as residual oxygen concentration and gas temperature. Since there was considerable variation in combustion efficiency among experiments for fixed primary and total air/fuel ratios, all of the SO_2 concentration data were plotted as a function of residual oxygen levels in the exhaust stream. The resulting graph is shown in Figure 47, where the data has been classified into five groups according to Ca/S ratio, but no distinction is made regarding sorbent injection height. Again there is a large amount of scatter in the data, indicating that there is no significant correlation between SO_2 and O_2 levels. Figure 47 shows, however, that except for two cases, all of the SO_2 concentrations measured with sorbent addition are lower than the SO_2 concentrations obtained without sorbent addition (Ca/S = 0.0). This graph also shows that residual oxygen levels tend to be significantly higher for cases with sorbent injection, which implies that injection of the limestone particles results in somewhat reduced combustion efficiency.

To determine the effect of gas temperature on the sulfur capture process, a graph was plotted of SO_2 concentration as a function of the gas temperature at a height of 15 cm above the bed.
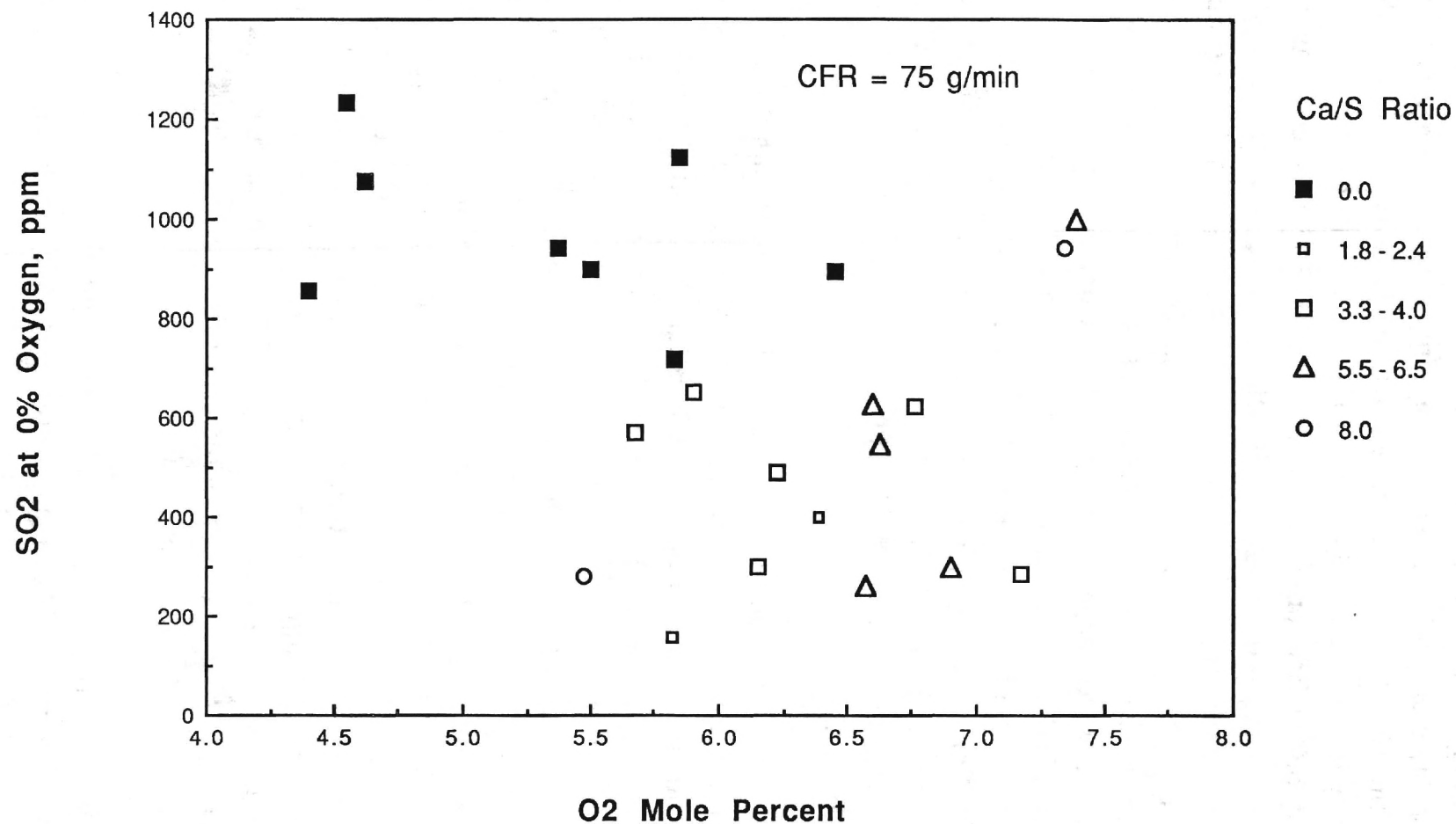
Figure 47. Correlation of Sulfur Dioxide Concentrations with Residual Oxygen Concentrations for Experiments with Pulverized Dolomitic Limestone Injection Above the Bed.

This corresponds to the temperature at the sorbent injection height for the lower injector position, and for a temperature 8 cm below the injection height for the upper injector position. Figure 48 shows this graph, again with the data classified into groups according to Ca/S ratio, but without indication of injection height. There is considerable scatter in this data, indicating no significant correlation of the SO_2 concentrations with the gas temperature. Although the optimum temperature for the sulfur capture process is known to be about 900 C [8], in seven cases large reductions in SO_2 emissions were obtained over a wide range of temperatures from just under 1000 C to nearly 1150 C. For six other cases, only moderate reductions in SO_2 emissions were obtained over a similar temperature range. As with the preceding figure, this graph shows, that with the exception of two cases, pulverized dolomitic limestone addition resulted in moderate to large reductions in sulfur dioxide emissions during pulsating combustion conditions.

The effect of the sorbent particles on pulsation amplitudes for these experiments is shown in Figure 49, where sound pressure levels are plotted as a function of Ca/S ratio. The plotted data points are distinguished only according to sorbent injection height. For most of these cases there is only a slight decrease in pulsation amplitude due to the damping effect of the sorbent particles. For no sorbent injection (Ca/S = 0), the average sound pressure level was 158.2 dB, excluding the lowest point. Particle damping resulted in a reduction of sound pressure level by a maximum of about 1.8 dB for Ca/S ratios of about 2, with an average loss of only about 0.6 dB for Ca/S ratios near 6. For four other cases, much larger losses in pulsation amplitude occurred, ranging from about 3 dB (Ca/S = 0) to about 7 dB. These larger losses in pulsation amplitude are probably due to other effects, such as bed nonuniformities, rather than to the damping effects of the limestone particles.

Finally, results of this study were compared with results presented in papers by Sheu, et al [8] and Wang, et al [9], who burned unpulverized coal in a similar Rijke type pulse combustor. In
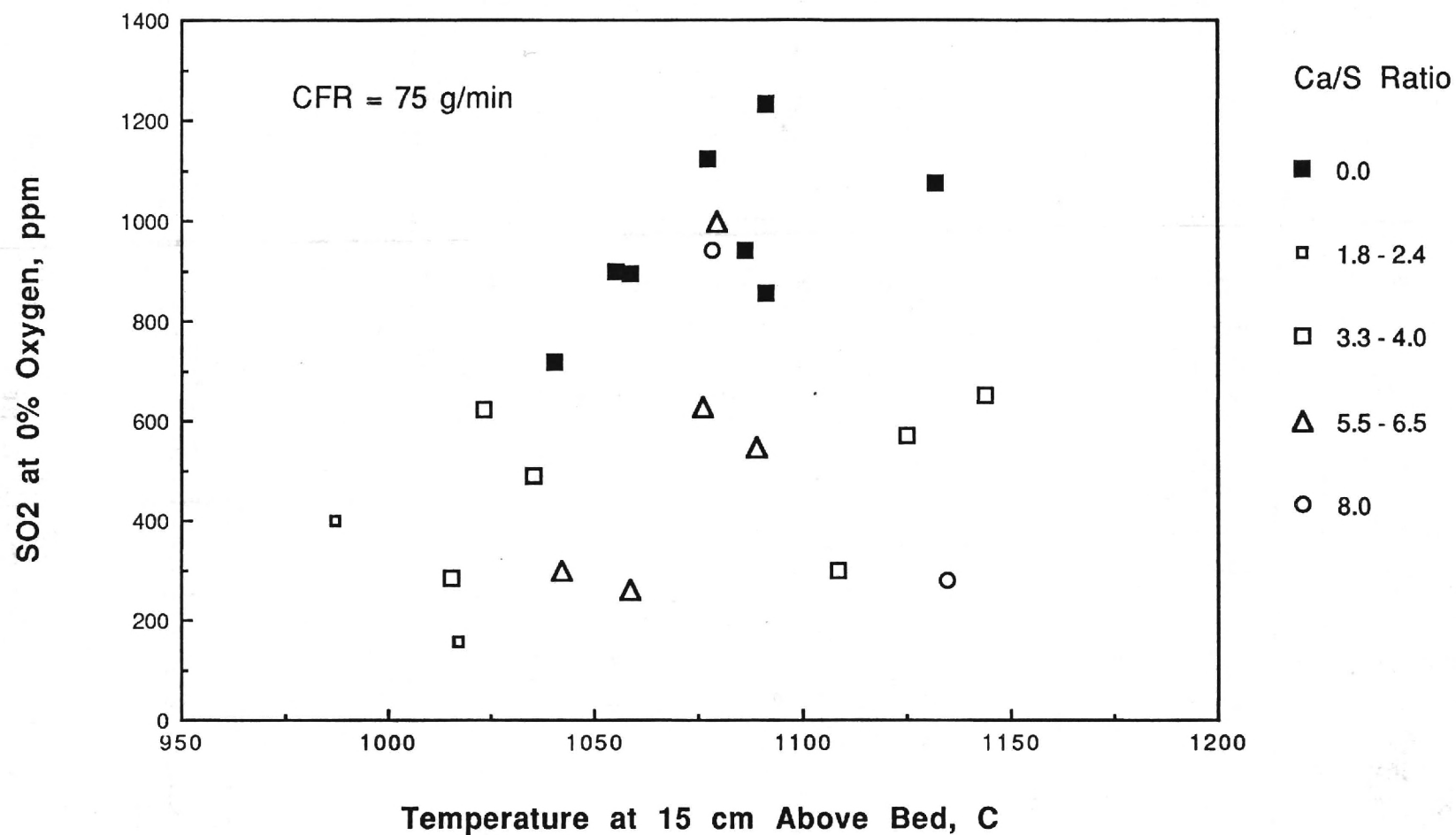
Figure 48. Correlation of Sulfur Dioxide Concentrations with Gas Temperatures for Experiments with Pulverized Dolomitic Limestone Injection Above the Bed.
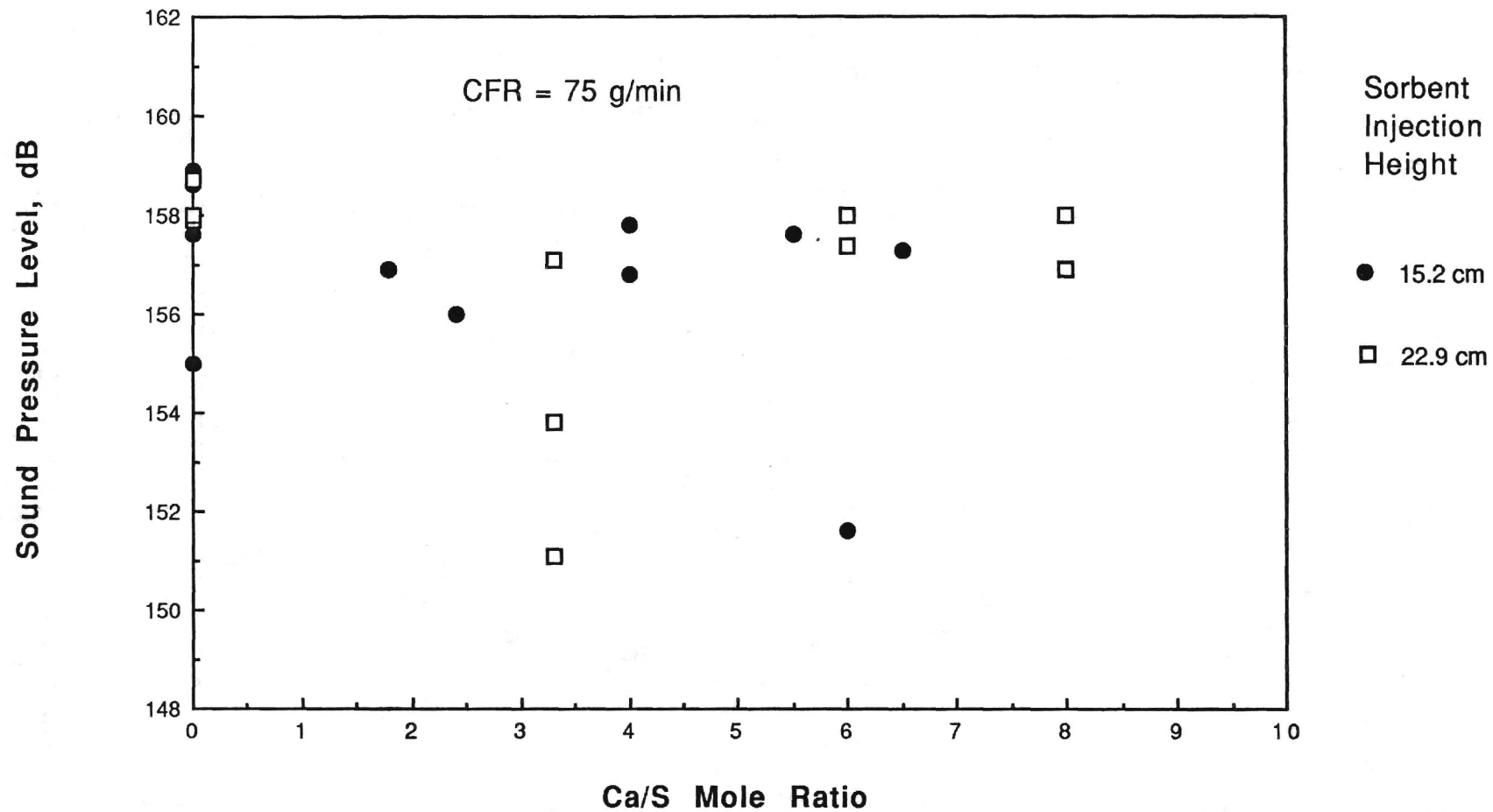
Figure 49.   Effect of Sorbent Particles upon Pulsation Amplitudes for Experiments with Pulverized Dolomitic Limestone Injection Above the Bed.

their studies, Sheu and Wang added the limestone or dolomite sorbents directly to the coal bed using a motor driven auger system. Like Sheu and Wang, the results of the present investigation show that the sulfur retention by dolomitic limestone was insensitive to the amount of excess air present. For dolomite, Sheu, et al, obtained a reduction of sulfur dioxide emissions of only 17 percent for a mean particle size of 2.75 mm at a Ca/S ratio of 3.0 [8]. Sulfur retention increased with decreasing particle size at the same Ca/S ratio, reaching 83 percent SO_2 reduction at a mean particle size of 0.5 mm. This latter result from Sheu compares favorably with an SO_2 reduction of 83 percent obtained in one of the experiments of the current investigation at a Ca/S ratio of 2.4 with dolomite particles of about 40 μm diameter. On the other hand, the results of Sheu, et al [8] indicated clear trends of increasing sulfur retention with increasing Ca/S ratio, a result which was not obtained in the present study. Also Sheu obtained maximum sulfur retention at a temperature of about 900 C, which was about 100 C lower than the lowest temperatures obtained in the present investigation. In their studies, Sheu and Wang obtained pulsation amplitudes slightly above 160 dB which agrees well with the amplitudes obtained in the current investigation.

SUMMARY AND CONCLUSIONS

In this investigation, a Rijke pulse combustor was constructed, in which unpulverized coal is burned on a rotating bed where the presence of acoustic velocity oscillations results in bed fluidization and intensification of the combustion process. The objectives of this investigation were to determine (1) if the nitrogen oxides emissions of the experimental Rijke pulse combustor could be reduced by air staging the combustion process and (2) if the sulfur dioxide emissions of this pulse combustor could be reduced by the addition of sorbent materials such as limestone to the coal bed or to the gas stream above the bed.

93

A series of experiments was conducted without air staging or sorbent addition in order to determine the baseline emissions of NO_x and SO_2. A bituminous coal with about 1.5 percent nitrogen and about 1.3 percent sulfur was burned in all of the experiments. Under pulsating combustion conditions at a sound pressure level of about 160 dB and a frequency of about 65 Hz, NO_x emissions (3% oxygen basis) ranged from about 250 ppm for extremely fuel rich combustion ($\alpha = 0.6$) to about 700 ppm for large excess air conditions ($\alpha = 1.5$). Peak SO_2 emissions of about 1400 ppm were measured at about 10 percent excess air, with minimum emissions of about 850 ppm for fuel rich combustion and somewhat less than peak emissions (about 1200 ppm) for large excess air conditions.

Two series of air staging experiments were conducted: (1) for total dimensionless air fuel ratios of 1.0 and (2) for total dimensionless air/fuel ratios ranging from 1.1 to 1.4. In both series of experiments, primary dimensionless air/fuel ratios ranged from 0.6 to 0.9. The results of this investigation showed that air staging is effective in reducing the nitrogen oxides emissions of coal burning Rijke type pulse combustors under the proper conditions. The largest reductions in NO_x emissions were obtained for primary dimensionless air/fuel ratios of about 0.7 with sufficient secondary air injection to yield total dimensionless air/fuel ratios between 1.1 and 1.4. For excess air values less than about 10 percent, air staging resulted in only small reductions in NO_x emissions. The injection point should be sufficiently high above the bed that the temperature is too low for significant thermal NO_x generation. Under these conditions NO_x emissions can be reduced by up to about 56 percent below the baseline concentrations obtained without air staging.

Two series of experiments were conducted using sorbent addition to reduce sulfur dioxide emissions. In the first series of experiments, pulverized dolomitic limestone was introduced along with the coal through the coal delivery tube just above the bed. In the second series of experiments, the dolomitic limestone was dispersed in an air stream and injected at 15 cm or 23 cm above the

coal bed. For sorbent introduced into the coal feed stream, sulfur dioxide reductions of only about 20 percent were obtained for pulsating combustion with about 20 percent excess air. For these experiments, there was a definite trend of decreasing SO_2 emissions with increases in excess air. Much higher SO_2 reductions were obtained when the sorbent was injected using the air entrainment system. There was much variation in the SO_2 reductions among the experiments in this series, even for the same Ca/S ratio, which was probably due to variations in combustion temperature or sorbent particle size. In many of these experiments, SO_2 reductions in excess of 50 percent were obtained. In one experiment, conducted at a Ca/S ratio of 2.4 with sorbent particles having a mean diameter of about 40 μm, an SO_2 reduction of 83 percent was obtained. From these experiments, it is concluded that injection of pulverized dolomitic limestone above the bed under pulsating combustion conditions can reduce sulfur dioxide emissions to acceptable levels.

REFERENCES

1. Zinn, B. T., Miller, N., Carvahlo, J. A. and Daniel, B. R., "Pulsating Combustion of Coal in a Rijke Type Combustor," Proceedings of the 19th Symposium (International) on Combustion, The Combustion Institute, pp. 1197-1203, 1982.

2. Carvahlo, J. A., Wang, M. R., Miller, N., Daniel, B. R. and Zinn, B. T., "Controlling Mechanisms and Performance of Coal Burning Rijke Type Pulsating Combustors, Proceedings of the 20th Symposium (International) on Combustion, The Combustion Institute, 1984.

3. Singer, J. G. (ed.), "Combustion-Fossil Power Systems," 3rd ed., Combustion Engineering, Inc., Windsor, CT, 1981.

4. Martin, G. D. and Bowen, Jr., J. S., "Control of Nitrogen Oxides from Combustion," in Proceedings of the 3rd Inter-Agency Conference on Energy and the Environment, Washington, DC, 1978.

5. Vogt, R. A. and Laurendeau, N. M., "NO$_x$ Formation from Coal Nitrogen: A Review and Model," Paper presented at the 1976 Spring Technical Meeting of the Central States Section of The Combustion Institute, Columbus, OH.

6. Vogel, G. J., Swift, W. M., Montagna, J. C., Lenc, J. F. and Jonke, A. A., <u>Fourth International Conference on Fluidized-Bed Combustion</u>, MITRE Corp., McLean, VA, 1975.

7. Locke, H. B., Lunn, H. G., Hoy, H. R. and Roberts, A. G., "Fluidized Combustion in Great Britain - Environmentally Clean Steam and Power Generation from Coal, Heavy Oil and Dirty Fuels," <u>Fourth International Conference on Fluidized-Bed Combustion</u>, MITRE Corp., McLean, VA, p. 69, 1975.

8. Sheu, K. C., Wang, M. R. and Chang, K. C., "Sulfur Retention in a Coal Burning Rijke Type Pulsating Combustor," Paper presented at the Western States Section of the Combustion Institute Spring Meeting, Salt Lake City, Utah, March 1988.

9. Wang, M. R., Chang, K. C., and Chang, W. C. "Experimental Study on Operating Conditions for SO$_2$ Removal in Pulsating Combustors," Paper presented at the Asian Conference on Fluidized Bed and Three-Phase Reactors," Tokyo, Japan, December 1988.